

Electronic Thesis and Dissertation Repository

4-17-2014 12:00 AM

Quantification of Axial Solids Mixing and Impacts of Internals in a Liquid-Solids Circulating Fluidized Bed Downer

Ha Doan

The University of Western Ontario

Supervisor

Jesse Zhu

The University of Western Ontario

Graduate Program in Chemical and Biochemical Engineering

A thesis submitted in partial fulfillment of the requirements for the degree in Master of Engineering Science

© Ha Doan 2014

Follow this and additional works at: <https://ir.lib.uwo.ca/etd>

 Part of the [Chemical Engineering Commons](#)

Recommended Citation

Doan, Ha, "Quantification of Axial Solids Mixing and Impacts of Internals in a Liquid-Solids Circulating Fluidized Bed Downer" (2014). *Electronic Thesis and Dissertation Repository*. 2029.

<https://ir.lib.uwo.ca/etd/2029>

This Dissertation/Thesis is brought to you for free and open access by Scholarship@Western. It has been accepted for inclusion in Electronic Thesis and Dissertation Repository by an authorized administrator of Scholarship@Western. For more information, please contact wlsadmin@uwo.ca.

QUANTIFICATION OF AXIAL SOLIDS MIXING AND IMPACTS OF INTERNALS IN
A LIQUID-SOLIDS CIRCULATING FLUIDIZED BED DOWNER

(Thesis format: Monograph Article)

by

Ha Doan

Graduate Program in Chemical and Biochemical Engineering

A thesis submitted in partial fulfillment
of the requirements for the degree of
Master of Engineering Science

The School of Graduate and Postdoctoral Studies
The University of Western Ontario
London, Ontario, Canada

© Ha Doan 2014

Abstract

Liquid solids circulating fluidized beds have great potential to be utilized in many chemical processes for their tremendous advantages. There are many studies about the riser but there is not any information on the downer as yet. This research is devoted to study the axial solids mixing in the downer. A new methodology was developed based on the concept of ion-exchanging ability of resins and the residence time distribution measurement. Resin particles were loaded with calcium ion as the tracer and Peclet number and the axial dispersion coefficient were determined for each set of operating conditions. Different designs of baffles were implemented in order to examine their effects on the axial solids dispersion. The results show that the baffles reduce the mixing substantially and their suppression effects increase with liquid velocity, except at very low liquid velocity where the presence of the baffle increases the mixing. Among the three designs – louver, mesh, and vertical plane, the louver has the most influence as it reduces the mixing coefficient by 60% when $U_1 = 3.86U_{mf}$. Under the same conditions, the mesh and vertical plane reduce the mixing coefficient by 46% and 32% respectively.

Keywords

Liquid-Solids Fluidization, Downer, Counter-Current, Axial Solids Mixing, Dispersion, Residence Time Distribution, Internals.

Acknowledgments

I would like to express the deepest appreciation to my supervisor, Dr. Zhu who is well-known for his knowledge as a researcher, and for his supportive attitude as a professor. He has set a bright example of a successful academic professional. I did not have him in my undergrad, and it is my honour to be his student now. Despite his busy schedule, my supervisor always makes himself available for weekly meetings with students. I am grateful for his time, for him always being smiling and positive, and giving me many insightful counsels. Without his encouragement and guidance, this thesis would not have been possible.

It is with immense gratitude that I acknowledge the support and help of my industrial partner, Renix Inc. and its president, Ms. Christine Haas. Ms. Haas and her colleagues have provided me many useful ideas and advices, and given me a chance to work in their facility and use their lab equipments. I am indebted to the colleagues who had helped me develop my methodology and repair the lab apparatus. I owe my deepest gratitude to Ms. Haas for her financial and intellectual supports to my research. This opportunity is an invaluable experience to me.

In addition, I would like to thank Dr. Gomaa for his valuable input which helped me find a way to interpret my experimental data. I thank Mr. Wen and Mr. Li – the technicians in Dr. Zhu's group, for their work getting the pilot scale unit ready. The financial support was provided by the University of Western Ontario, Renix Inc., MITACS and the Ontario Centres of Excellence.

Table of Contents

Abstract	ii
Acknowledgments.....	iii
Table of Contents	iv
List of Tables	vii
List of Figures	viii
List of Appendices	xiv
Chapter 1	1
1 Introduction	1
1.1 First Description of Fluidization.....	1
1.2 Objectives	4
Chapter 2.....	7
2 Literature Review.....	7
2.1 LSCFB System Details	7
2.2 Fluidization Regimes	9
2.3 Liquid-Solid Circulating Fluidized Bed Riser	17
2.3.1 Axial Hydrodynamic Behaviour	17
2.3.2 Radial Hydrodynamic Behaviour in LSCFB	22
2.3.3 Phase Mixing	31
2.4 Conventional Liquid-Solid Fluidized Bed	37
2.4.1 Bed Expansion	37
2.4.2 Axial Hydrodynamic Behaviour	41
2.4.3 Radial Hydrodynamic Behaviour	41
2.4.4 Phase Mixing	42

Chapter 3.....	54
3 Experimental Methods	54
3.1 Materials	54
3.2 Apparatus	55
3.3 Procedure	58
3.3.1 Tracers Preparation	58
3.3.2 Experiments in Lab Scale	60
3.3.3 Experiments in Pilot Scale	61
3.4 Analytical Methods and Calibration Curves.....	62
3.5 Mathematical Treatment	66
Chapter 4.....	69
4 Preliminary Results	69
4.1 Impact of Solids Superficial Velocity on Axial Solids Dispersion.....	69
4.2 Impact of Bed Height on Axial Solids Dispersion.....	71
4.3 Impact of Liquid Superficial Velocity on Axial Solids Dispersion.....	72
Chapter 5.....	74
5 Internals Design	74
5.1 Louver	74
5.2 Mesh.....	76
5.3 Vertical Plane.....	76
Chapter 6.....	79
6 Formal Results	79
6.1 Development of Methodology	79
6.1.1 Ion-exchange Resin.....	83
6.1.2 Procedure	84
6.1.3 Limitations	85

6.2 Operating at $U_1 = 1.45U_{mf}$	85
6.3 Operating at $U_1 = 2.66U_{mf}$	89
6.4 Operating at $U_1 = 3.86U_{mf}$	91
6.5 Repeatability of the Method.....	95
Chapter 7.....	97
7 Conclusions and Recommendations	97
7.1 Conclusions.....	97
7.2 Recommendations.....	97
Nomenclature	99
References.....	100
A. Appendices.....	105
B. Appendices: Lab Scale Testing Data	114
C. Appendices: Pilot Scale Testing Data	126

List of Tables

Table 2.1: The onset and critical transition velocities for different particles (Zheng & Zhu, 2001)	15
Table 2.2: Mixing parameters from solids RTD (Roy & Dudukovic, 2001).....	36
Table 2.3: Particles used in Tong and Sun's study (2001)	43
Table 2.4: Comparison of mixing coefficients in different expanded bed modes (Chang & Chase, 1996)	46
Table 2.5: Liquid distributor design parameters (Asif et al., 1991).....	46
Table 3.1: Properties of the resins.....	55
Table 4.1: Impact of solids superficial velocity on solids dispersion	69
Table 4.2: Impact on solids dispersion when bed height changes	71
Table 4.3: Impact on solids dispersion when liquid velocity changes.....	72
Table 6.1: Result summary ($U_1 = 1.45U_{mf}$).....	88
Table 6.2: Result summary ($U_1 = 2.66U_{mf}$).....	90
Table 6.3: Result summary ($U_1 = 3.86U_{mf}$).....	93
Table 6.4: Result summary for the repeated runs	96

List of Figures

Figure 1.1: Fluidized particles behave like liquid.....	2
Figure 2.1: Schematic diagram of a typical (G-)LSCFB system (Razzak et al., 2009).....	7
Figure 2.2: Schematic diagram of liquid distributors in a LSCFB a) riser (Razzak et al., 2009) b) downer	8
Figure 2.3: Variation of the axial liquid holdup distribution in the conventional and circulating regimes for 0.405mm glass beads (Liang et al., 1997).....	10
Figure 2.4: Circulation rate versus liquid velocity for three types of particles (Zheng et al., 1999).....	11
Figure 2.5: Determination of liquid transition velocity for the three types of particles (Zheng et al., 1999)	12
Figure 2.6: The effect of total solids inventory (expressed as the static bed height in the storage vessel before the start of solids circulation) on the critical transition velocity for plastic beads, glass bead I and steel shots (Zheng & Zhu, 2001)	13
Figure 2.7: Time required for all the particles to be entrained out of the bed, as a function of liquid velocity for glass beads I and plastic beads (Zheng & Zhu, 2001)	14
Figure 2.8: Flow regime map for liquid-solid circulating fluidized bed (Zhu et al., 2000)....	16
Figure 2.9: Variations of the solids circulation rate with the total liquid flowrate (Zheng et al., 1999).....	18
Figure 2.10: Variation of the axial solids holdup distribution with liquid velocity in the circulating fluidization regime for glass beads and steel shots (Zhu et al., 2000).....	19
Figure 2.11: Average solids holdup versus liquid velocity at different solids circulation rates for (a) plastic beads, (b) glass beads, and (c) steel shots (Zheng et al., 1999).....	20

Figure 2.12: Average solids holdup versus liquid velocity at a given solids circulation rate for all three types of particles (Zheng et al., 1999).....	21
Figure 2.13: Variation of solids holdup with the primary and auxiliary liquid velocities (Palani & Ramalingam, 2008)	21
Figure 2.14: Radial distribution of liquid velocity under $G_s = 5$ (a) and 10 (b) $\text{kg/m}^2\text{s}$ and different liquid velocities for glass beads (Zheng & Zhu, 2003).....	23
Figure 2.15: The radial distribution of the liquid velocity under different particle circulating rates (Zheng & Zhu, 2003).....	24
Figure 2.16: The radial distribution of solids holdup at four bed levels at (a) different superficial liquid and (b) solids velocities for glass beads (Zhu et al., 2000).....	25
Figure 2.17: Comparison of the radial solids holdup profiles for glass beads and plastic beads under the same cross-sectional average solids holdup ($\epsilon_s = 0.052$) at $H = 0.8\text{m}$ (Zheng et al., 2002)	26
Figure 2.18: Radial profiles of solids holdup at the level $H = 0.8\text{m}$ for different solids flowrates for (a) glass beads and (b) plastic beads at the same normalized liquid velocity, $UUt = 2.5$ (Zheng et al., 2002).....	27
Figure 2.19: The radial distributions of particle velocity at different superficial liquid velocities for glass beads averaged axially over the riser (Roy et al., 1997).....	29
Figure 2.20: Variation of superficial solid velocity with the superficial liquid velocities at different auxiliary liquid velocities for glass beads (500 and 1290 μm) (Razzek et al., 2009)	30
Figure 2.21: Radial distribution of solids holdups for glass beads (500 and 1290 μm) at axial location $h = 2.02$ m and $U_1 = 22.4$ cm/s (Razzak et al., 2009).....	31
Figure 2.22: Typical tracer concentration distribution profiles ($U_{10} = 0.072$ m/s, $\epsilon = 0.9$, $G_s = 7.5$ $\text{kg}^2\text{m}^{-1}\text{s}^{-1}$) (Chen et al., 2001).....	32
Figure 2.23: Effects of superficial liquid velocity on liquid axial mixing (Chen et al., 2001)	33

Figure 2.24: Effects of solid holdup on liquid axial mixing (Chen et al., 2001)	33
Figure 2.25: Effects of superficial liquid velocity on liquid radial mixing (Chen et al., 2001)	34
Figure 2.26: Effects of solid holdup on liquid radial mixing (Chen et al., 2001).....	35
Figure 2.27: Residence time distribution calculated from CARPT data ($U_1 = 20$ cm/s; $S/L = 0.10$) (Roy & Dudukovic, 2001).....	36
Figure 2.28: Pressure drop - velocity relationship (Couderc, 1985).....	38
Figure 2.29: Bed height - velocity relationship (Yang, 2003)	38
Figure 2.30: (a) Pressure drop and (b) bed expansion of resin bed as a function of vessel diameter. Water velocities (mm/s) 1) 0.5; 2) 1.2; 3) 1.9; 4) 5; 5) 6; 6) 9 (Nikitina et al., 1981)	39
Figure 2.31: Superficial velocity - bed voidage relationship (Chhabra, 2007).....	40
Figure 2.32: Radial particle holdup distribution under different operating conditions and at different bed sections for 0.405 mm glass beads. (●) $U_1 = 0.034$ m/s, $U_s = 0$; (Δ) $U_1 = 0.078$ m/s, $U_s = 0.0019$ m/s; (◇) $U_1 = 0.078$ m/s; $U_s = 0.0011$ m/s (Liang et al., 1997)	42
Figure 2.33: Effects of flow velocity on (a) the axial mixing coefficient and (b) the Bodenstein number (Tong & Sun, 2001).....	43
Figure 2.34: Axial mixing coefficient as a function of degree of bed expansion (Tong & Sun, 2001)	44
Figure 2.35: Effect of liquid viscosity on axial mixing coefficient: (○) NFBA-S / water; (●) NFBA-S / 10%(v/v) glycerol; (Δ) NFBA-L / water; (▲) NFBA-L / 10%(v/v) glycerol; (□) Streamline SP / water; (■) Streamline SP / 10% (v/v) glycerol (Tong & Sun, 2001)	45
Figure 2.36: Effect of distributors on the response of the liquid fluidized bed at different liquid velocities: a) $U_1 = 3.15$ cm/s; b) $U_1 = 1.46$ cm/s; c) $U_1 = 1.05$ cm/s (Asif et al., 1991)	47

Figure 2.37: Comparison of apparent dispersion coefficients D_a at different liquid superficial velocities (Asif et al., 1991).....	48
Figure 2.38: Effect of column size on (a) axial mean solids velocity, (b) dispersion coefficients (Limtrakul et al., 2005)	49
Figure 2.39: Effect of distributor type on (a) axial mean solids velocity, (b) dispersion coefficients (Limtrakul et al., 2005)	50
Figure 2.40: Effect of superficial liquid velocity on (a) axial mean solids velocity, (b) dispersion coefficients (Limtrakul et al., 2005).....	51
Figure 2.41: Effect of particle size at $U_1/U_{mf} = 1.7$ ($U_1 = 7$ cm/s for 0.003 m; $U_1 = 2.4$ cm/s for 0.001 m) on (a) axial solids velocity and (b) dispersion coefficients (Limtrakul et al., 2005).....	52
Figure 2.42: Effect of particle density at $U_1/U_{mf} = 1.7$ ($U_1 = 7$ cm/s for glass beads; $U_1 = 2.4$ cm/s for acetate) on (a) axial solids velocity and (b) dispersion coefficients (Limtrakul et al., 2005)	53
Figure 3.1: 5-cm column apparatus	56
Figure 3.2: Liquid distributor used in lab scale	57
Figure 3.3: Schematic diagram of the downer	58
Figure 3.4: Loading Ca^{2+} onto resin	59
Figure 3.5: Calibration curve for S 1668 resins	64
Figure 3.6: Calibration curve 1 for SGC 650 resins	65
Figure 3.7: Calibration curve 2 for SGC 650 resins	66
Figure 4.1: Comparing RTD at different solids velocities.....	70
Figure 4.2: Comparing RTD when bed height changes.....	71
Figure 4.3: Comparing RTD when liquid velocity changes	73

Figure 5.1: Louver baffles.....	75
Figure 5.2: Mesh baffle.....	76
Figure 5.3: Vertical plane	77
Figure 5.4: Positions of the baffles in the downer	78
Figure 6.1: Residence time distribution graph.....	79
Figure 6.2: Illustration of the phosphorescent tracer method (Wei & Zhu, 1996)	81
Figure 6.3: Particle velocity measurement by using two-fiber sensor (Nieuwland et al., 1996)	82
Figure 6.4: RTD graphs in baffle-free setup at $U_1 = 1.45U_{mf}$	86
Figure 6.5: RTD graphs in louver baffle setup at $U_1 = 1.45U_{mf}$	87
Figure 6.6: RTD graphs in mesh baffle setup at $U_1 = 1.45U_{mf}$	87
Figure 6.7: RTD graphs in vertical baffle setup at $U_1 = 1.45U_{mf}$	87
Figure 6.8: RTD graphs in baffle-free setup at $U_1 = 2.66U_{mf}$	89
Figure 6.9: RTD graphs in louver baffle setup at $U_1 = 2.66U_{mf}$	89
Figure 6.10: RTD graphs in mesh baffle setup at $U_1 = 2.66U_{mf}$	90
Figure 6.11: RTD graphs in vertical plane baffle setup at $U_1 = 2.66U_{mf}$	90
Figure 6.12: RTD graphs in baffle-free setup at $U_1 = 3.86U_{mf}$	92
Figure 6.13: RTD graphs in louver-baffled setup at $U_1 = 3.86U_{mf}$	92
Figure 6.14: RTD graphs in mesh-baffled setup at $U_1 = 3.86U_{mf}$	92
Figure 6.15: RTD graphs in vertical plane setup at $U_1 = 3.86U_{mf}$	93
Figure 6.16: Summary of experimental axial dispersion coefficients	95

Figure 6.17: RTD graphs Trial 1.....	96
Figure 6.18: RTD graphs Trial 2.....	96

List of Appendices

Appendix A-1: Maximum capacity of SGC 650 resins for calcium.....	105
Appendix A-2: Maximum capacity of S 1668 resins for calcium	107
Appendix A-3: Calculate mass rate of solids circulation.....	108
Appendix A-4: Mole ratio between sodium and calcium in a sample desorption	109
Appendix A-5: Calibration curve for S 1668 resins	110
Appendix A-6: Calibration curve for SGC 650 resins.....	111
Appendix A-7: Verification of calibration curve.....	113
Appendix B-1: Data for lab-scale run 1	114
Appendix B-2: Data for lab scale run 2	117
Appendix B-3: Data for lab scale run 3	119
Appendix B-4: Data for lab scale run 4	121
Appendix B-5: Data for lab scale run 5	124
Appendix C-1: Data for the baffle-free trial at $U_1 = 1.45U_{mf}$	126
Appendix C-2: Data for the louver trial at $U_1 = 1.45U_{mf}$	130
Appendix C-3: Data for the mesh trial at $U_1 = 1.45U_{mf}$	133
Appendix C-4: Data for the vertical plane trial at $U_1 = 1.45U_{mf}$	136
Appendix C-5: Data for the baffle-free trial at $U_1 = 2.66U_{mf}$ (Run #1).....	139
Appendix C-6: Data for the baffle-free trial at $U_1 = 2.66U_{mf}$ (Run #2).....	142
Appendix C-7: Data for the louver trial at $U_1 = 2.66U_{mf}$	145

Appendix C-8: Data for the mesh trial at $U_1 = 2.66U_{mf}$	148
Appendix C-9: Data for the vertical plane trial at $U_1 = 2.66U_{mf}$	151
Appendix C-10: Data for the baffle-free trial at $U_1 = 3.86U_{mf}$	154
Appendix C-11: Data for the louver trial at $U_1 = 3.86U_{mf}$	157
Appendix C-12: Data for the mesh trial at $U_1 = 3.86U_{mf}$	160
Appendix C-13: Data for the vertical plane trial at $U_1 = 3.86U_{mf}$	163

Chapter 1

1 Introduction

Fluidization is a process that involves contact of suspended solid phase with liquid and/or gas phase. The technology has been utilized in many various fields and becomes more and more important from industrial point of view.

1.1 First Description of Fluidization

When a bed of solid particles comes in contact with and is suspended in an upward fluid flow, the solid bed is said to be in fluidization and the fluid is called fluidizing fluid.

Fluidizing fluid could be either liquid, or gas, or combination of both. The reason for the name fluidization is that the solids bed gains a number of properties of liquid:

- Surface of a fluidized bed always maintains horizontal even if the bed is positioned on an inclined plane.
- Solids can be poured out of the vessel through an opening without requiring any mechanical device.
- A fluidized unit also exhibits a static pressure head due to gravity, given by $P = \rho_o gh$, where ρ_o is density of the bed.
- When a number of units are connected, particles in the one with higher bed level will flow to the more shallow one until the bed levels are the same, in order to equalize their static pressure heads.
- If the bed is constituted of two types of particles with different densities, the layer of the lighter particles floats on top while layer of the denser particles sinks at the bottom.

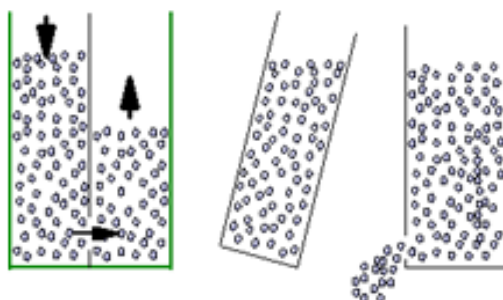


Figure 1.1: Fluidized particles behave like liquid

Depending on the phase of fluidizing fluid, fluidization is classified into three types: gas-solids, liquid-solids, and three phase gas-liquid-solids. Gas-solids was the first form of this technology, born in 1920s and found its first application in coal gasification by Winkler. The first large scale implementation was in 1940s in fluid catalytic cracking process (Anon, 1962). In 1950s was the emergence of liquid-solids fluidization. Over the decades, intensive studies have been done to understand the hydrodynamic behaviours of both gas-solids and liquid-solids fluidization systems due to their great advantages:

- Efficient interphase contact
- High mass transfer rate
- Even distribution of temperature
- Easy handling of large solids quantity

In some applications, particles lose their capacity over time as the process proceeds. For instance, solid catalysts become deactivated in metallurgical or petrochemical operations, or solid adsorbents are fully loaded in adsorption processes. As a result, they require a new batch of particles. In the past, to accommodate this demand, a number of vessels were built. When solids in a vessel became inactive after a period of time, a new unit took the position to continue the operation while the former one was being regenerated. Even though this method could provide a continuous process, batch operation still poses a number of disadvantages:

- Possible inconsistency in product grades from batch to batch
- High labour cost
- Low throughput
- Low productivity
- High back-mixing of phases

These limitations motivated the invention of an uninterrupted system: circulating fluidized beds. The inception of liquid – solids circulating fluidization in 1960s (Zhu et al., 2000) has become useful and been implemented in many areas. Some of them employ circulating fluidized units because their applications constantly require fresh particles like aforementioned examples. They need to have a continuous system to remove inactive solids and feed in the regenerated ones. Some others utilize this circulating fluidized bed technology because they operate liquid feed at high flowrate. The particles used are light and small, thus get entrained out of the column. Consequently, it is essential to keep feeding the particles into the column. With the advantages of the uninterrupted operation, liquid-solids circulating fluidization is widely used in many fields such as in food processing, water treatment, and metallurgical industries.

One example is the application of a liquid solids circulating fluidized bed (LSCFB) to recover proteins from waste streams which contains low protein concentration. The adsorption and desorption of proteins are accomplished separately in the two parallel columns: downer and riser, respectively. The solids used are ion-exchange resins which are circulated between these two columns. The feed broth is introduced from the bottom of the downer. The protein in the liquid phase is adsorbed onto the resins. While the deproteinized liquid stream is discarded from the top of the downer, the loaded particles exit the bottom of the downer to enter the riser. Desorption buffer is fed via a liquid distributor placed at the bottom of the riser, and carries the resins upward while desorbing protein out of the resins. After releasing the proteins, the resins are considered fresh, or regenerated. The regenerated particles are then separated from the buffer solution in a liquid-solids separator, they are returned to the downer and complete a

circulation cycle (Zhu et al., 2000; Zheng et al., 2002). (More details about system configurations can be found in Section 2.1)

The performance of an LSCFB relies on the two key factors: the chemistry aspect and the hydrodynamics aspect. The chemistry varies from application to application since it depends on the type of solids used, the treating liquid stream, and their reaction kinetics. As a result, this aspect cannot be generalized but needs to be considered for each individual case. In contrast, the hydrodynamics knowledge can be applied into design and scale-up in most cases. Even though this is an area of research since 1990s and becomes more and more popular over the years, some information is still incomplete. One of the missing pieces on this hydrodynamics picture is the longitudinal dispersion of solid phase in the downer.

1.2 Objectives

In order to properly design and scale up a LSCFB, it is important to understand the hydrodynamics behaviour of the system, such as phase holdups and their distributions, flow patterns and mixing levels of each phase (Limtrakul et al., 2005). A lot of studies have been reported for the riser exploring all the areas mentioned above. However, there is absolutely no available data on the downer. Often the fluid dynamics in the downer is presumed to be similar to conventional fluidized beds where there is no net flow of solid phase. This might be premature assumption for the downer at least about the mixing levels. In conventional fluidized beds, there is only upward flow of liquid whereas in downer the liquid and solids flow counter-currently, so that a conventional fluidized bed and a downer bed are incomparable. In other words, mixing levels in conventional fluidized beds cannot be representative for ones in downer. To avoid the same presumption, this project is designed to investigate mixing level of solid phase in the axial direction in the purpose of providing some insight about what is happening within the downer bed.

To conduct this study, a new method for particle tracking is developed since all other tracking techniques for solid phase are either inapplicable or unavailable. The new methodology is not expected to be perfect. In addition, it is not possible to validate the

method at this point because no data is reported in this area as yet. However, demonstration of the method can be performed within the scope of this study.

Longitudinal solids dispersion, also termed as back-mixing, is an important parameter to evaluate performance of a fluidized bed. It describes the random motion of particles in the axial direction and is driven by the diffusion force. In mixers, this type of motion is desirable since it promotes mixing. However, in fluidized beds, longitudinal dispersion of solids is better to be constrained. Large dispersion is an indication of broad distribution of solids residence time. On one side, some particles exit the system earlier than the expected time. In other words, the contact time between liquid and solid phases is not long enough, leading to part of their capacity is unused. On the other side, some particles exit the system much later than the designed contact time. This may cause two problems. One is if the process involves catalysts or adsorbents that are heat-sensitive and the reaction is exothermic, extended residence time may cause the damage to the solid particles. The other is when the catalysts are deactivated or when the adsorbents are fully adsorbed, their extra time residing in the bed does not results in a higher production but only means process delay. For these reasons, for the best interest, axial solids mixing should be minimized in the interest of obtaining the best performance.

Axial mixing of phases is often expressed as axial mixing coefficient, or Peclet number. In an ideal case where there is absolutely no axial dispersion, the particles exit a column in exact order as they have entered, the mixing coefficient would be zero and the Peclet number is infinity. The increasing of the mixing coefficient, or the decreasing of Peclet value indicates the distribution of particles is getting broader and the state of the fluidized bed is further away from the ideal plug flow. There are many factors effecting back-mixing of solids including but not limited to particle-particle collision, particle-wall collision, turbulence due to liquid flow, also not perfectly vertical column setup, non-ideal liquid distributor. The former three are infeasible to avoid as they are nature of phase interaction; the latter two are possible to be improved. Nevertheless, making an ideal distributor is extremely challenging because it has to provide equivalent hydraulic, which means equivalent flowrate, equivalent time of passage and equivalent pressure drop, to each exit, and be scalable. Not only designing is difficult but fabricating is also

limited. To achieve the goal of restricting axial solids mixing, one could attempt to make an ideal distributor facing those challenges and risking patent violation issues. In the same purpose, this project demonstrates an alternative to constrain the random motion of particles by inserting internals inside the downer fluidized bed. Different designs of internals are made and they show very promising results in solids mixing reduction.

Chapter 2

2 Literature Review

In this chapter available data on the liquid-solids fluidization will be presented. The first sections will cover the circulating fluidization hydrodynamics since the project is aimed to study the downer of a liquid-solids circulation system. The later sections cover the conventional fluidization hydrodynamics because no data is available for the downer as yet, and downer is in the same fluidization regime as conventional beds. The literature review for the circulating systems and the conventional systems are categorized into three topics: axial profiles, radial profiles and phase mixing. The focus of this project is on solids phase mixing, not liquid mixing or the axial and radial profiles, but all of them are essential to understand the dynamic behaviours of a particular system, therefore the discussion will be on all those topics.

2.1 LSCFB System Details

Figure 2.1 shows the schematic diagram of a typical (G-)LSCFB system.

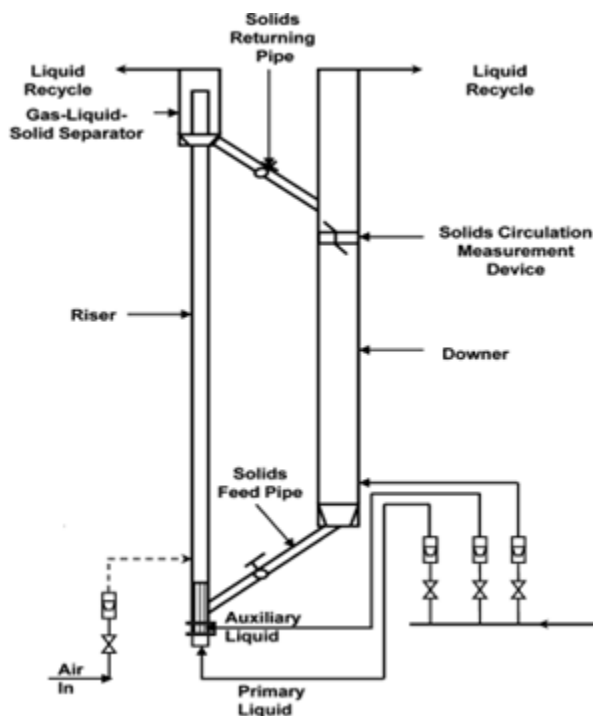


Figure 2.1: Schematic diagram of a typical (G-)LSCFB system (Razzak et al., 2009)

The setup consists of two main parallel cylindrical vessels called riser and downer. The processes taking place in these two reactors are often the reverse of each other, either adsorption / desorption processes or reaction / regeneration processes. Therefore, they are fluidized by two different fluidizing liquids. Liquid injected into the riser is divided into two streams: primary liquid and auxiliary liquid. There is distributor for each stream. The main liquid distributor is made of one or multiple stainless steel tubes, depending on the size of the vessel itself and the second liquid distributor is a porous plate. Both are placed at the base of the riser (Figure 2.2a). There is also a distributor at the conical bottom of the downer, which is a ring shape with multi-openings at different locations and in different angles (Figure 2.2b).

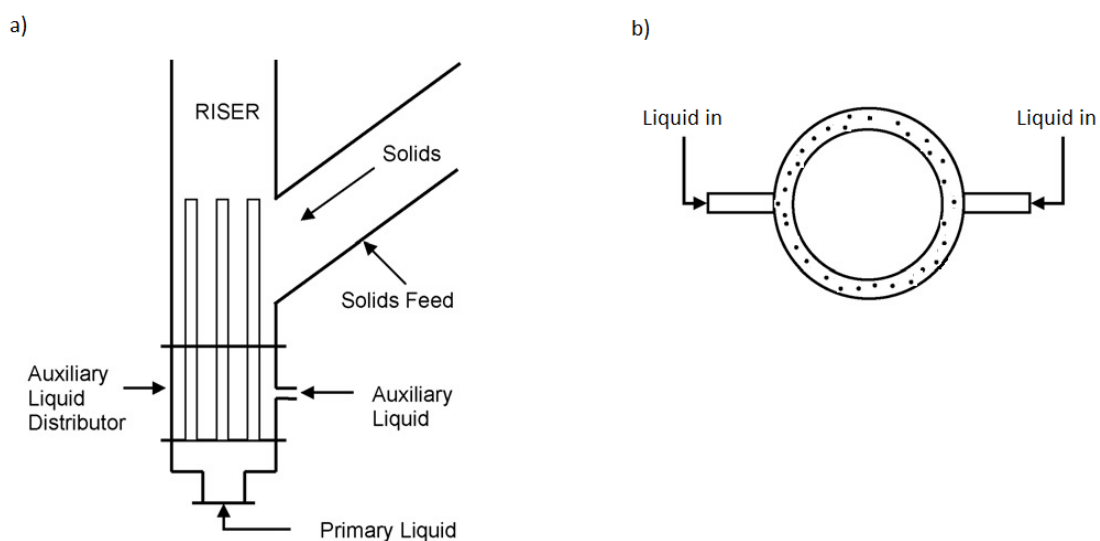


Figure 2.2: Schematic diagram of liquid distributors in a LSCFB a) riser (Razzak et al., 2009) b) downer

Particles are carried upward in the riser by conjunction of primary and auxiliary liquids. The existence of the auxiliary stream is to mobilize the solids as they exit the feeding pipe. In feeding pipe and returning pipe, solids travel like a packed bed. As they flow down from the feeding pipe, they come in contact with the secondary liquid, and are loosened up. The auxiliary stream works as a non-mechanical device to facilitate particles to enter the riser, therefore controls how much or how fast solids entrance is. The total liquid is the summation of these two liquid flows. By adjusting one of the two

liquid streams, solids circulation and total liquid velocity for the riser can be obtained independently.

Both solids and liquid phase flow upward in the riser, and enter the liquid-solids separator. The liquid-solids separator has conical bottom which allows solids to settle and form a packed bed more easily while the liquid floats on top and exits via the liquid outlet. The solids then return to the downer, passing through a solids circulation measurement device. The device is positioned slightly below the returning pipe, and is a vertical plate. It is divided by halves and equipped with two half butterfly valves at the ends of the plate. To measure solids circulation rate, these two butterfly valves are flipped to opposite direction for a short time interval, about a minute. As the top valve blocks one side, then particles come to the other side only; the lower valve blocks that side and captures the particles. By measuring the solids accumulation and knowing the time taken, solids circulation rate can be calculated.

Particles enter the downer from the top and travel counter-currently to the liquid flow which is upward. The downer has much higher solids concentration compared to the riser because they are in different fluidization regimes. Their fluidization regimes will be discussed in the following section of this chapter.

2.2 Fluidization Regimes

Fluidization of liquid-solids beds is controlled by superficial velocity of liquid. When liquid velocity is low, the solid particles remain static, and they are considered in the fixed state. When the fluid flowrate is high enough, the bed height starts to rise, and each individual particle becomes suspended in the fluid. The bed is now considered in the conventional fluidization regime. The value of liquid velocity that demarcates these two states is called the minimum fluidization velocity, U_{mf} , and can be calculated using Ergun equation:

$$\frac{150\mu_f(1 - \varepsilon)U_{mf}}{\varepsilon_{packed}^3 d_p^2} + \frac{1.75\rho_f U_{mf}^2}{\varepsilon_{packed}^3 d_p} - g(\rho_s - \rho_f) = 0 \quad (\text{Equation 2.1})$$

In both regimes, a clear boundary between the dense phase and freeboard phase is observed. When the liquid velocity is increasing, the dense phase continues to expand. Because the particles occupy a larger bed volume, the solids concentration becomes lower. With further increase of liquid flow, the boundary between the two phases becomes unclear. At sufficiently high liquid velocity, some particles start to get entrained out of the column, suggesting the transition of fluidized beds from the conventional regime to the circulating regime.

Figure 2.3 depicts dense phase, freeboard phase, and how dense phase expands with liquid velocity increase. Looking at the two curves whose velocities are the lowest ($U_1 = 0.90$ and 1.80 cm/s), which are the farthest left, all solids settle at the bottom of column. In this dense phase, it is noted that the voidage is the same at all axial locations. Above the dense phase, the voidage is 1.0, it means there is no solids in the higher region – freeboard phase. When liquid velocity increases to 2.50 cm/s, the dense phase expands. There is a dense zone up to bed height of 1.5 m, then dilute phase above that point. There is no longer a clear boundary between dense phase and freeboard. At liquid velocity of 3.61 cm/s or higher, it can be seen from the legend box that U_s is now above zero, indicating the formation of solids circulation. The bed is in the circulating regime, and there is only dilute zone. Bed voidage is constant along the bed height.

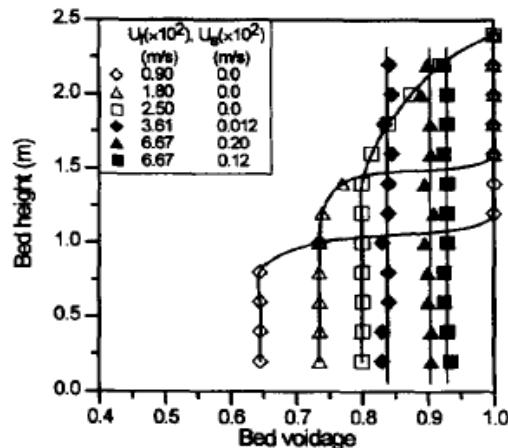


Figure 2.3: Variation of the axial liquid holdup distribution in the conventional and circulating regimes for 0.405mm glass beads (Liang et al., 1997)

The critical transition velocity

The point where particles start to get entrained out of the bed is termed as critical transition velocity, U_{cr} . Liang et al. (1997) established a way to determine this value by decreasing liquid velocity to the point where solids circulation stops and defined this point as U_{cr} . It is confirmed that the critical transition velocity and the transition state are affected by particle density. Shown in Figure 2.4, with increasing particle density, the value of U_{cr} is higher and the transition becomes gradual. For example, for plastic beads whose density is very low, solids circulation is formed at 0.01 m/s and the transition is sharp, almost at a single liquid velocity. Contrarily, for steel shots, which are very heavy particles, the transition starts much later at 0.21 m/s, and the range of liquid velocity for transition is widened.

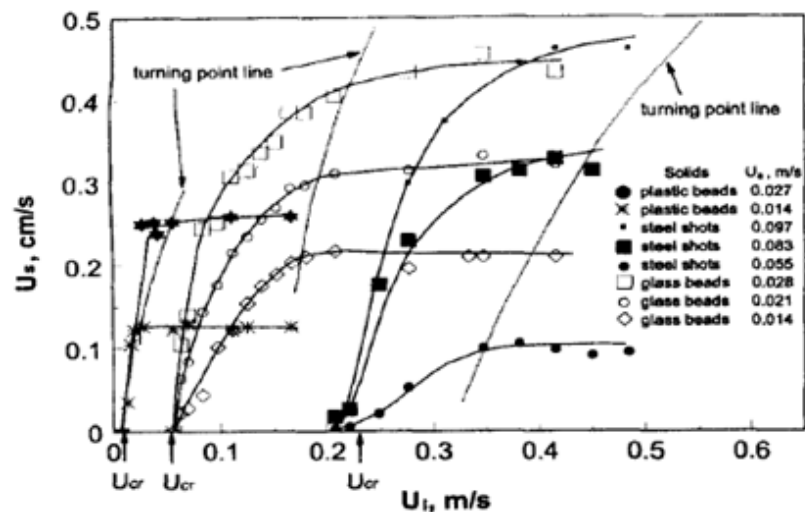


Figure 2.4: Circulation rate versus liquid velocity for three types of particles (Zheng et al., 1999)

Zheng et al. (1999) further found the relation of transition velocity with particle terminal velocity. Figure 2.5 shows that solids circulation stops as normalized liquid velocity U_l/U_t approaches values between 1.0 and 1.1 for all 3 types of particles. That means fluidization enters the circulating regime at transition velocity of equal or slightly higher than the terminal velocity of particles. This information is quite appreciable for system operation since solids terminal velocity can be calculated mathematically, and so the transition velocity can be accurately predicted while saving experimental time.

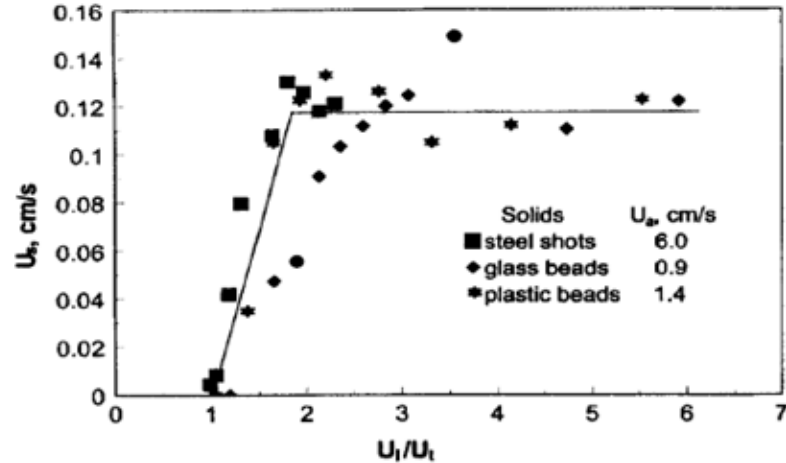


Figure 2.5: Determination of liquid transition velocity for the three types of particles (Zheng et al., 1999)

However, the critical transition velocity is found to be system operation dependent. Zheng and Zhu (2001) reported this lower boundary limit of circulating regime varies with the total solids inventory, which certainly affects the system pressure balance and the pressure difference across the solids feeding pipe particularly. When the bed height in the solids storage is increased, the pressure head at the base of the downer becomes higher, leading to the pressure difference across the non-mechanical valve is also higher. In turn, solids are fed to the riser faster. In other words, solids circulation increases at the same liquid velocities. It also means the same solids circulation rate can be achieved at lower liquid velocities when solids inventory is higher. Therefore, in identifying the critical transition velocity by reducing liquid velocity until the solids velocity reaches zero, one will find this velocity decreases with increasing height of solids storage bed.

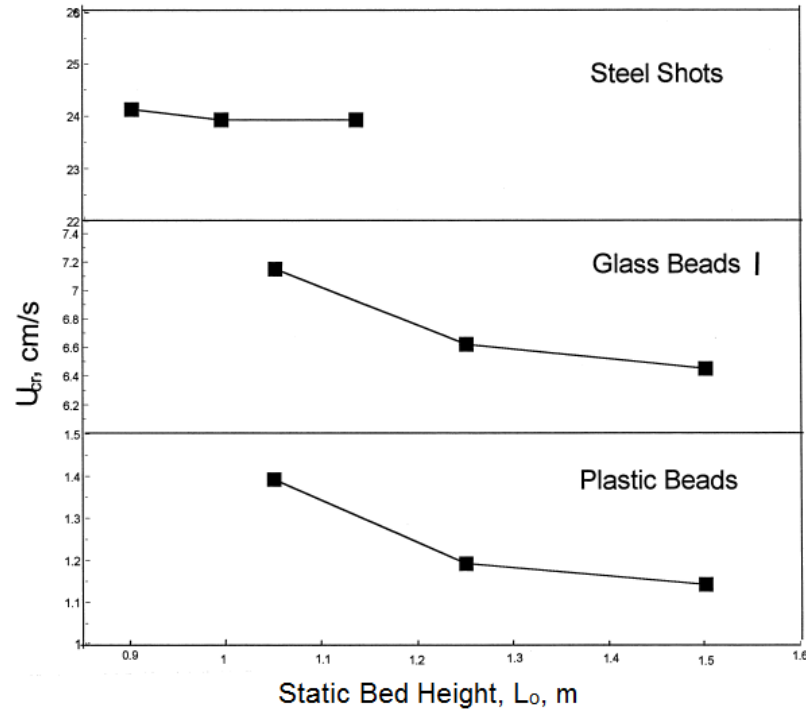


Figure 2.6: The effect of total solids inventory (expressed as the static bed height in the storage vessel before the start of solids circulation) on the critical transition velocity for plastic beads, glass bead I and steel shots (Zheng & Zhu, 2001)

The authors also noted how the critical transition velocity at first decreases drastically, then gradually when static bed height is increased. It is explained that when back pressure is high enough, the pressure distribution within the system has less influence on the transition velocity. This observation is more discernible in the case with lighter particles. The change in the transition velocity is hardly recognized in the steel shots system over the experimental range due to equipment limitation and high particle density. Overall, it is suggested to have a very high solids inventory when determining the value of the critical transition velocity in order to minimize the system configuration dependency and have the most accurate result.

The onset velocity

Since the critical transition velocity is intrinsically system dependent, it poses uncertainty in defining the lower boundary of circulating fluidization regime. Zheng and Zhu (2001) proposed a non-intrinsic method to determine the beginning of transition state. The

method is to measure how long it takes to empty a solids bed when there is no solids feed from the storage vessel at a particular fluidizing liquid velocity. When the liquid flowrate is slow, the time it takes for all particles to entrain out of the bed is very long. When the flowrate is higher, this process certainly takes less time. Zheng and Zhu observed that with increasing liquid velocity, the bed-emptying time is shortened drastically. Yet, to a certain point, further increase of liquid flow does not affect the emptying time as much. This turning point is marked as the onset velocity, U_{cf} . This phenomena is presented graphically in Figure 2.7. A steep line and a flatter line are seen and their intersection locates the onset velocity. The location of the onset velocity does not change with the initial bed volumes (486 and 811 cm^3). In addition, the method does not involve solids feeding. Therefore it is independent of solids storage volume and the configuration of the feeding system.

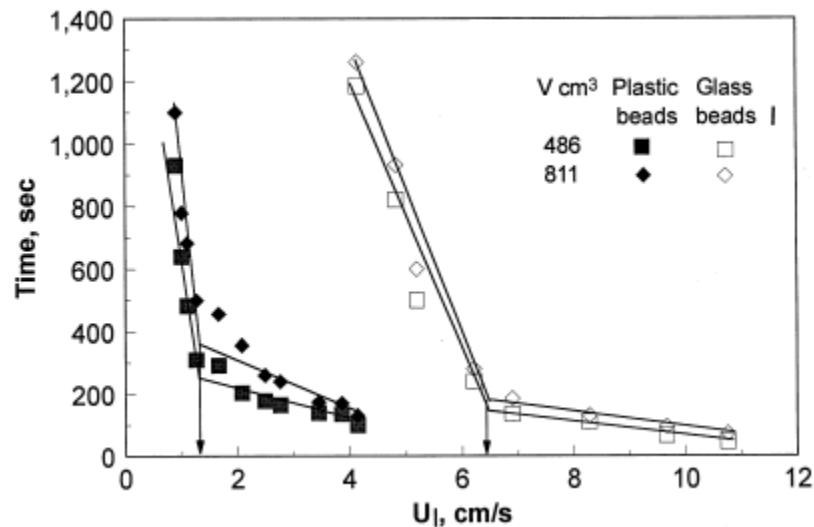


Figure 2.7: Time required for all the particles to be entrained out of the bed, as a function of liquid velocity for glass beads I and plastic beads (Zheng & Zhu, 2001)

Onset velocity versus critical transition velocity comparison

Table 1 shows the determined onset velocity and critical transition velocity for 4 types of particles, including their terminal velocity. Recalled from the previous discussion, the transition velocity decreases with bed height in the solids storage. When the storage bed

is high enough, this influence becomes less noticeable. That means the transition velocity determination is less varying when the storage static bed height is large. For the reason, the values presented in Table 1 are obtained under the highest bed height tested $L_0 = 1.5$ m.

Table 2.1: The onset and critical transition velocities for different particles (Zheng & Zhu, 2001)

	ρ_s (kg/m ³)	d_p (mm)	U_{cr}^a (cm/s)	U_{cf} (cm/s)	U_t (cm/s)	U_{cr}/U_t	U_{cf}/U_t
Plastic beads	1100	0.526	1.17	1.15	1.0	1.17	1.15
Glass beads I	2490	0.508	6.47	6.45	5.9	1.10	1.10
Glass beads II	2541	1.000	–	16.30	14.4	–	1.13
Steel shots	7000	0.580	24.84	23.70	21.6	1.15	1.10

^aObtained under highest L_0 .

The results show both the onset and the critical transition velocities are higher than the terminal velocity. It is reasonable since system has to operate at a liquid velocity higher than the particle terminal velocity in order to transport particles out of the bed. The onset is slightly lower than the critical velocity. Another note should be taken from the table above is that the ratios U_{cf}/U_t for various particle types are all about 1.1. Since U_{cf} is not affected by the geometrical conditions, it only depends on liquid and solids properties. Zheng and Zhu (2001) suggested a correlation for U_{cf} as following:

$$U_{cf} = aU_t \quad (\text{Equation 2.2})$$

where a is a function of liquid properties such as density and viscosity. Based on the experimental results, for tap water a is approximately 1.1 when operation is at room temperature.

To summarize, the critical velocity is the true value defining the transition from the conventional to the circulating fluidization regime and it varies with the operation setup. The onset velocity is the lowest U_{cr} and a convenient way to demarcate the two regimes independently from the geometry of the system. Therefore, it is accepted as the absolute lower boundary of the circulating fluidization regime.

Beyond the circulating fluidization regime is the transport/hydraulic regime. In this state, the particles continue to be carried out of the column. The only distinction between the circulating and the transport regime is the radial profile of solids holdup. In the circulating regime, solids concentration is higher near the wall and more dilute at the center; whereas in the transport regime, the radial solids holdup is uniform. The transition velocity between the two regimes is defined as U_{cv} (Liang et al., 1997). It is expected that U_{cv} would increase with solids circulation rate. When solids feed is fast, solids concentration is higher, leading to a solids concentration profile that is more non-uniform. As the result, it requires higher liquid input to "smooth" out this non-uniformity of radial solids profile, and enters the transport regime.

All fluidization regimes and transition velocities are summarized and presented in the regime map below. The axis are dimensionless liquid velocity U_l^* and dimensionless particle size d_p^*

$$U_l^* = \frac{U_l}{U_t} \text{ and } d_p^* = \frac{D_c}{d_p} \quad (\text{Equation 2.3})$$

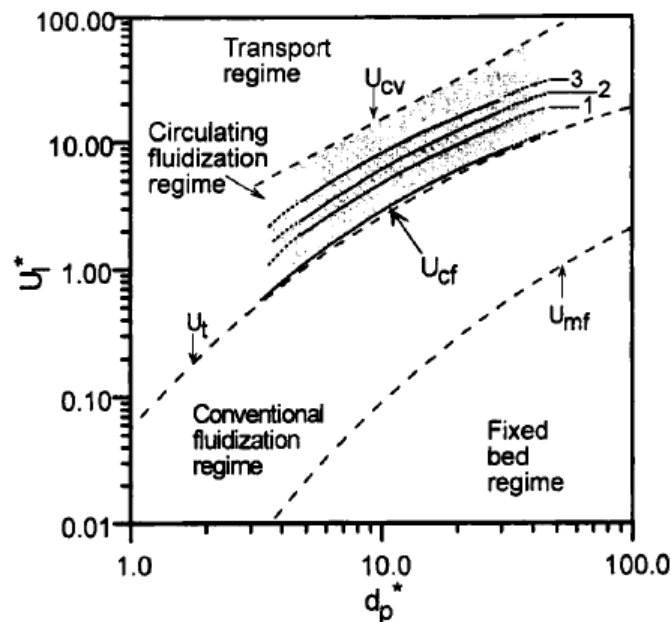


Figure 2.8: Flow regime map for liquid-solid circulating fluidized bed (Zhu et al., 2000)

2.3 Liquid-Solid Circulating Fluidized Bed Riser

The riser of a LSCFB system is fluidized by a fast flowing liquid. The liquid velocity is so high that it transports the solid particles out of the bed. The riser bed is in co-current circulating fluidization state.

2.3.1 Axial Hydrodynamic Behaviour

The Initial Zone and the Developed Zone

As liquid velocity reaches the transition velocity, U_{cr} , the fluidized bed enters the circulating regime. In this regime, there exists two zones: initial zone and developed zone. In the initial zone, solids circulation rate increases substantially with increase of total liquid velocity. Shown in Figure 2.9 below, the initial zone occurs in a very narrow range of liquid velocity to a point of being negligible for light particles such as plastic beads, but this range of liquid velocity becomes much widened as particle density increases. In the developed zone, the increase of liquid velocity affects solids circulation insignificantly for all particle densities. The liquid velocity that marks the transition from the initial circulating fluidized zone to the fully developed zone is the critical liquid velocity, U_{lc} (Palani & Ramalingam., 2008; Natarajan et al., 2007). Natarajan et al. (2007) proposed its value is 1.3 times the particle terminal velocity. It is suggested to operate a system at a lower liquid velocity than the critical velocity if high solids holdup is desired. Oppositely, liquid velocity should be higher than U_{cr} if a dilute phase and high solids circulation rate are more suitable.

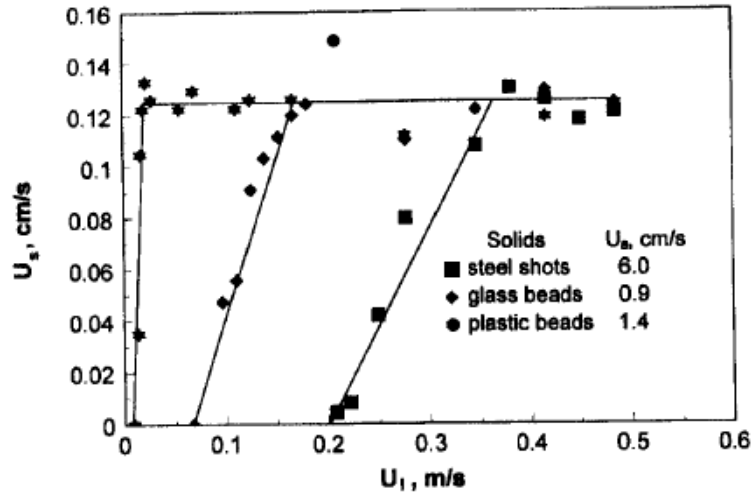


Figure 2.9: Variations of the solids circulation rate with the total liquid flowrate (Zheng et al., 1999)

For heavy particles, such as steel shots with density of 7000 kg/m^3 , the axial profile of solids holdup is not uniform in the initial circulation zone when the liquid velocity is low ($U_1 = 26$ and 28 cm/s). Recall from Table 1 the critical transition velocity of steel shots is 24.84 cm/s . When liquid velocity is 26 or 28 cm/s (Figure 2.10), it is the beginning of circulating fluidization. Solids entering the riser from the bottom are usually in downward or horizontal direction, they have zero or negative velocity. They need some time to accelerate; therefore solids holdup tends to be denser at the lower region than at the higher region. When particle density is low, the accelerating time is very short but for high density particles, their development is much slower, leading to longer accelerating distance. With further increase of liquid velocity ($U_1 = 35 \text{ cm/s}$), fluidization enters the developed zone and axial solids holdup is uniform throughout the column. For glass beads, the system is in developed circulating fluidization zone at lower liquid velocity (10 cm/s) and axial distribution of solids holdup remains uniform.

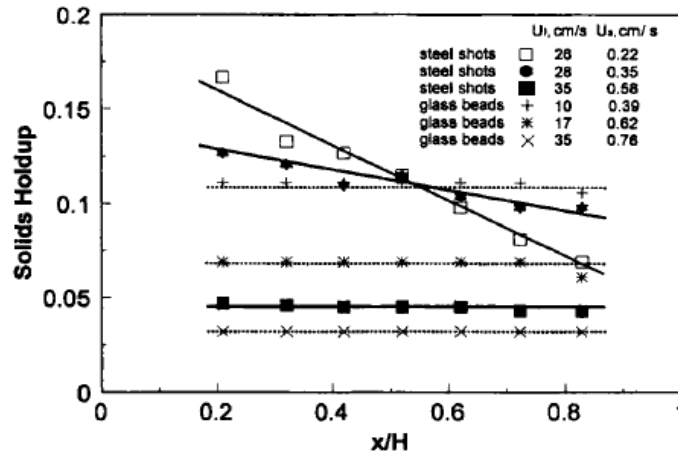


Figure 2.10: Variation of the axial solids holdup distribution with liquid velocity in the circulating fluidization regime for glass beads and steel shots (Zhu et al., 2000)

The initial zone and developed zone are distinct from one another not only in terms of the variation of solids circulation (Figure 2.9) and axial solids distribution (Figure 2.10) with change in liquid velocity, but also in term of average solids holdup. Figure 2.11 expresses how average solids holdup changes with total liquid velocity. The graphs show different trends in the initial zone and developed zone. In the initial zone, the graphs are very steeply downward for all three types of particles. The indication is that the average solids holdup decreases drastically with increasing liquid velocity. This is because when liquid flows fast, it carries solids out of the riser quickly. Consequently, solids residence time is shortened, leading to less solids holdup. In contrast, the graphs show a plateau in the developed zone. Solids holdup is reduced much more slowly in this zone. It can be explained that at a certain point, the increase in liquid velocity does not affect solids circulation rate, as seen in Figure 2.9. As the result, the decrease of average solids holdup with liquid velocity becomes less noticeable. Also seen in Figure 2.11, when solids circulation rate increases, more solids are fed into the column, hence solids holdup increases.

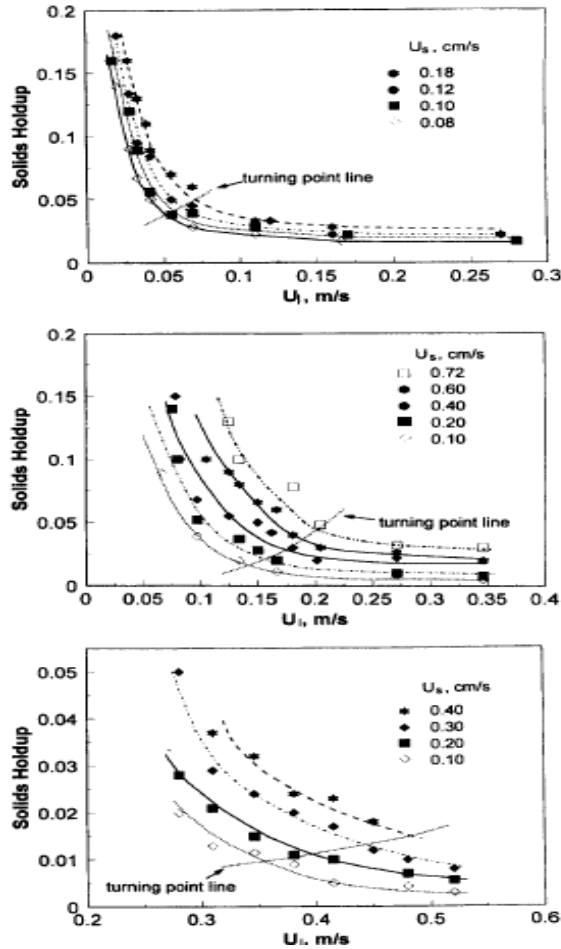


Figure 2.11: Average solids holdup versus liquid velocity at different solids circulation rates for (a) plastic beads, (b) glass beads, and (c) steel shots (Zheng et al., 1999)

Another note taken from Figure 2.11 is that particles density has strong influence on hydrodynamic behaviour in the initial and developed zone. For light particle (plastic beads), solids holdup decreases quickly, from 0.15 to 0.05. For heavy particle (steel shots), solids holdup decreases very slowly, from 0.04 to 0.01. Yet, when fluidization is fully developed, solids holdup profile reaches the same value 0.01 for all three types of particles if under the same solids circulation rate (Figure 2.12). Therefore, hydrodynamics in the initial zone varies by particle density, sharp for light particles and gradual for heavy particles. When it reaches full development, they all experience the same trend, same solids distribution profile.

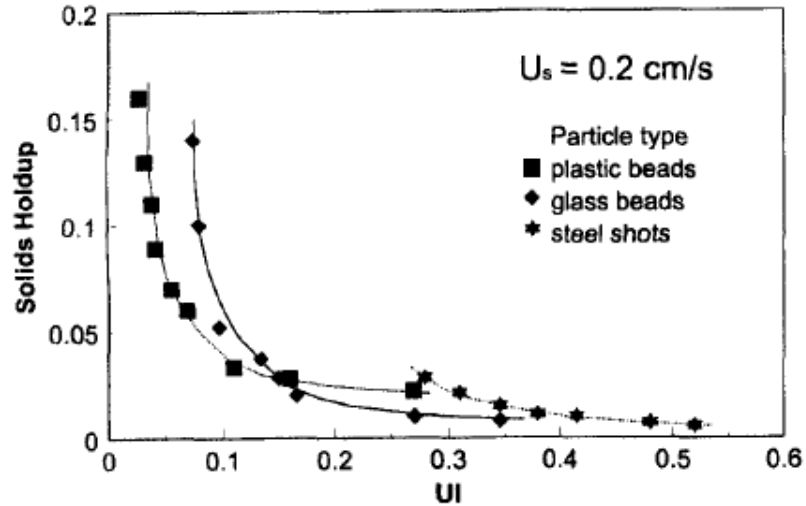


Figure 2.12: Average solids holdup versus liquid velocity at a given solids circulation rate for all three types of particles (Zheng et al., 1999)

Variation of Solids Holdups with Liquid Velocities

Palani and Ramalingam (2008) conducted their experiments to relate solids holdup with liquid velocity. In their study, they used sand whose diameter is $550 \mu\text{m}$ and the result is shown in the graph below.

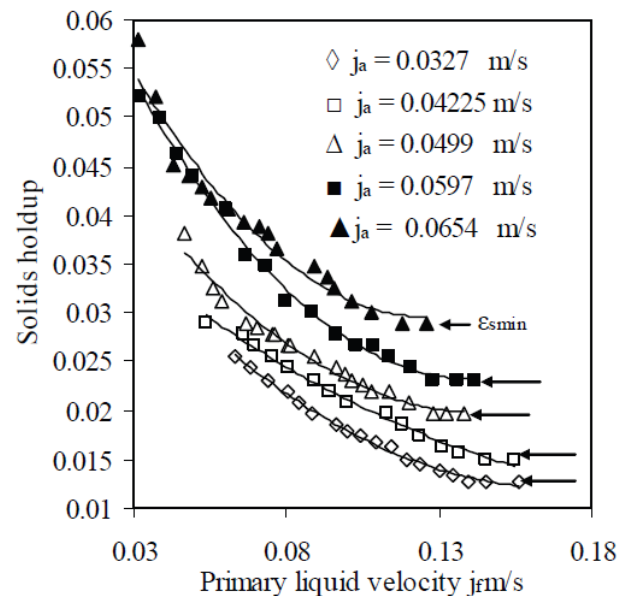


Figure 2.13: Variation of solids holdup with the primary and auxiliary liquid velocities (Palani & Ramalingam, 2008)

It is seen that when fixing the auxiliary velocity and turning up the primary liquid velocity, the solids holdup is decreased. When liquid is fed into the riser at a faster rate, more particles are transported out, as a result, less particles are present inside the column. Oppositely, if one looks vertically, across the drawn lines, the data points show how solids holdup in the riser changes when the primary is constant and the auxiliary varies. The solids holdup increases with the auxiliary velocity. This can be explained by the function of the auxiliary stream to loosen up the plug flow in the returning pipe and to mobilize the particles as they are emerging the flow in the unit. In conclusion, the main liquid stream is to carry the solid particles upward and entrain them out of the riser; whereas the secondary stream is to aid the solids feeding system. Therefore the solids holdup in the riser increases with increase of the secondary stream but with decrease of the main stream. The knowledge of this variation is definitely beneficial for optimizing operating conditions.

2.3.2 Radial Hydrodynamic Behaviour in LSCFB

Unlike conventional fluidization regime and transport regime, radial profiles of liquid velocity, solids velocity and solids holdup in liquid - solids circulating regime are non-uniform. The non-uniformity may have negative effects on the productivity of fluidized beds since it causes uneven interphase contact. Therefore, understanding radial flow structure is crucial to design reactors and to optimize processes.

Radial Distribution of Liquid Velocity

The radial distribution of liquid velocity presented in Figure 2.14 is at solids circulation flux of 5 and 10 kg/m²s and different liquid velocities. The liquid velocity profile under conventional fluidization regime, which means no solids circulation $G_s = 0$, is also plotted for comparison.

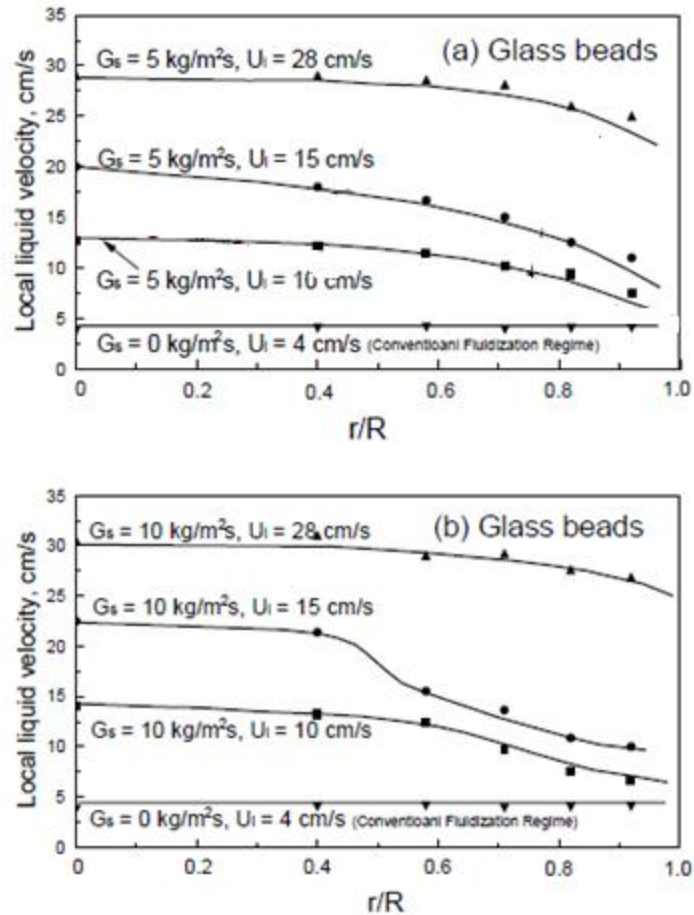


Figure 2.14: Radial distribution of liquid velocity under $G_s = 5$ (a) and 10 (b) $\text{kg/m}^2\text{s}$ and different liquid velocities for glass beads (Zheng & Zhu, 2003)

When fluidization is in the conventional regime, the radial profile of liquid velocity is uniform. The profile becomes non-uniform once solids circulation starts. Higher liquid velocity occurs at the center ($r/R = 0$) and lower velocity is near the wall ($r/R = 1.0$). This non-uniformity increases when liquid flows faster. For example, when $G_s = 10 \text{ kg/m}^2\text{s}$, graph is steeper when liquid velocity changes from 10 to 15 cm/s. With further increase of liquid velocity ($U_l = 28 \text{ cm/s}$), the graph flattens out, indicating the transition from the circulating regime to the transport regime. In the dilute transport regime, solids concentration is very low, thus the impact of solids presence on liquid profile is small. In addition, when liquid velocity is quite high, liquid profile tends to distribute more uniformly.

The effect of change in solids circulation on liquid velocity profile is also studied by Zheng and Zhu (2003). At a fixed liquid velocity ($U_1 = 15 \text{ cm/s}$), the radial distribution graph is steeper, means more non-uniformity, as solids circulation flux increases. A possible explanation for this phenomenon is that when more solids are fed into the riser, solids accumulation near the wall is greater than at the center. To accommodate this variation, liquid flows more slowly near the wall than at the center.

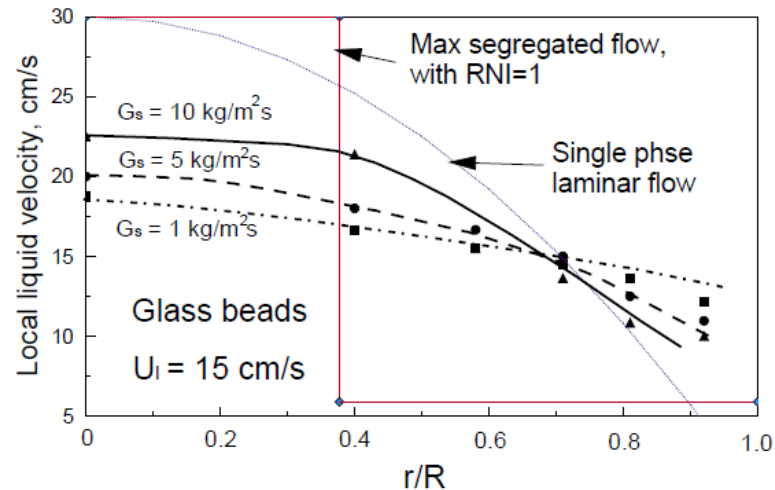


Figure 2.15: The radial distribution of the liquid velocity under different particle circulating rates (Zheng & Zhu, 2003)

Radial Solids Holdup Distribution

A typical radial distribution of solids holdup is plotted in Figure 2.16. It is seen that the profile is not uniform. The solids concentration is higher at the wall ($r/R = 1$) than at the center ($r/R = 0$). Measurements were done at 4 different heights along the riser: one in the lower region ($h = 0.3 \text{ m}$), two at the middle region ($h = 0.8$ and 1.2 m) and one at the upper region ($h = 1.7 \text{ m}$). The data points at the same radial position are very close to each other. It again proves that in liquid - solids circulating fluidization, the axial solids holdup is uniform.

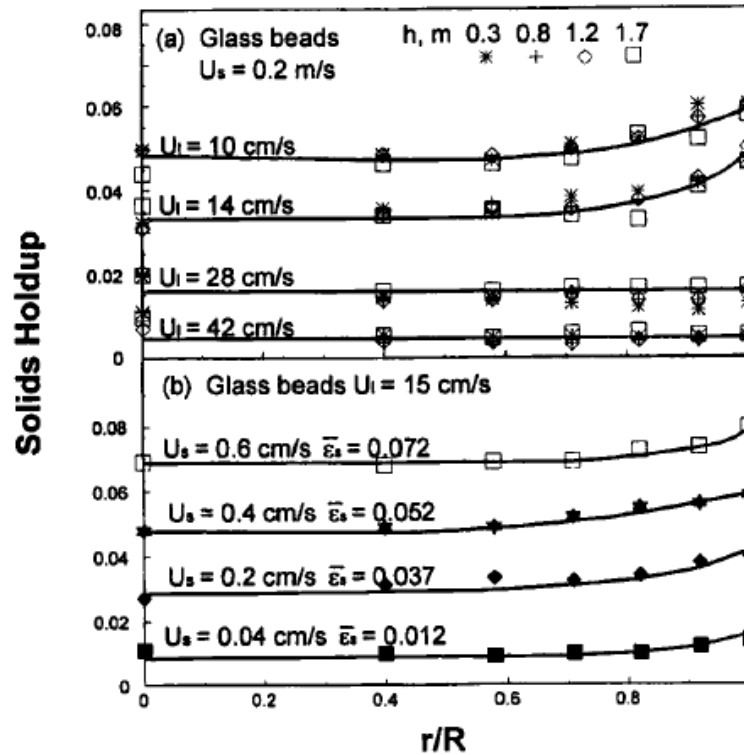


Figure 2.16: The radial distribution of solids holdup at four bed levels at (a) different superficial liquid and (b) solids velocities for glass beads (Zhu et al., 2000)

With an increase in liquid velocity from $U_1 = 10$ to $U_1 = 14 \text{ cm/s}$ (Figure 2.16a), the graph gets steeper near the wall, indicating an increase in non-uniformity. As a natural phenomenon, liquid flowing in a cylindrical pipe tends to flow faster at the center than at the wall due to wall friction. Faster moving fluid at the center carries solids out more, consequently makes solids holdup less at the core. When liquid velocity increases further to 28 or 42 cm/s, the graphs flatten out. In other words, solids holdup is distributed uniformly in the radial direction, indicating the transition to the transport regime. In addition, a liquid velocity increase shifts the graph down, means solids holdup is reduced at all radial positions. When liquid travels fast inside the riser, it entrains solids more quickly, hence shortens solids retention time. As the result, solids holdup is overall less at high liquid flowrate.

In Figure 2.16b, liquid velocity is fixed while solids velocity varies. It shows that when solids circulation rate, which is expressed as solids velocity, increases, average solids holdup also increases. This is absolutely understandable since when liquid flowrate is

unchanged, the more solids are fed, the more solids are present in the column. Therefore, solids holdup increases. In a denser zone, solids tend to accumulate at the wall even more, leading to the difference in solids concentration at the wall and centre is widened. This explains how the non-uniformity increases with solids velocity.

Non-uniformity in radial distribution of solids holdup is also affected by particle density. The statement is demonstrated in the Figure 2.17 where the radial profiles of solids holdup for glass beads and plastic beads are plotted. The two types of particles have similar size and are fluidized in operating conditions that give the same average solids holdup ($\bar{\epsilon}_s = 0.052$). The profiles for each type of particles under two different operating conditions almost coincide with each other when the cross-sectional average solids holdups are the same. Comparing the profiles of the two particles types, the lighter particles (plastic beads) have more uniform distribution, giving flatter parabolic curve. This phenomenon is possibly due to the lower value of the ratio ρ_s/ρ_l . When the density ratio is large, solids have a tendency to agglomerate at the wall more. For example in gas - solids fluidization, the density ratio is very high, and significant cluster agglomeration is seen. A conclusion that may be drawn here is that high density ratio ρ_s/ρ_l worsens uniformity in radial solids holdup distribution.

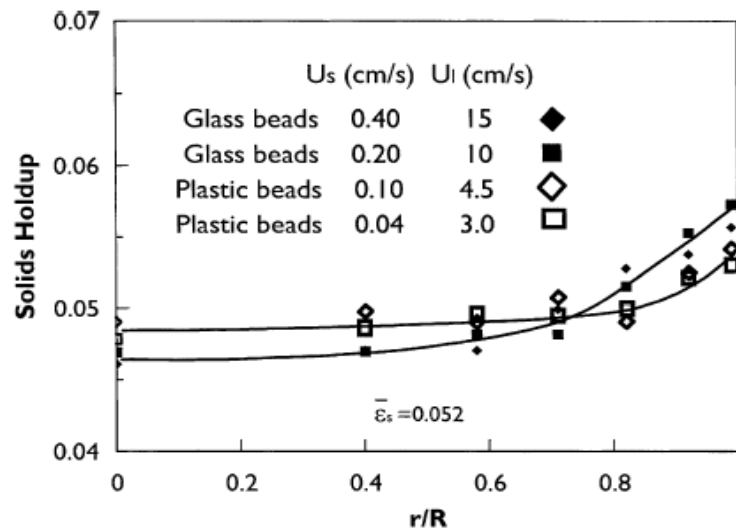


Figure 2.17: Comparison of the radial solids holdup profiles for glass beads and plastic beads under the same cross-sectional average solids holdup ($\epsilon_s = 0.052$) at $H = 0.8\text{m}$ (Zheng et al., 2002)

In the previous case, the average solids holdup is kept constant. In the following study, the normalized liquid velocity remains unchanged and the impact of particle density on solids holdup is investigated. Figure 2.18 presents radial profiles of solids holdup for glass beads and plastic beads under different solids circulation rates. For light particles (plastic beads), small increment of solids velocity, from 0.04 to 0.14 cm/s, increases average solids holdup substantially. In contrary, for heavier particle an increment of solids velocity, for instance from 0.04 to 0.2 cm/s, does not affect average solids concentration greatly. Additionally, at the same solids velocity ($U_s = 0.04 \text{ cm/s}$), plastic beads experience more solids holdup non-uniformity compared glass beads. Again, this is because a higher concentration of solids always leads to more uneven distribution.

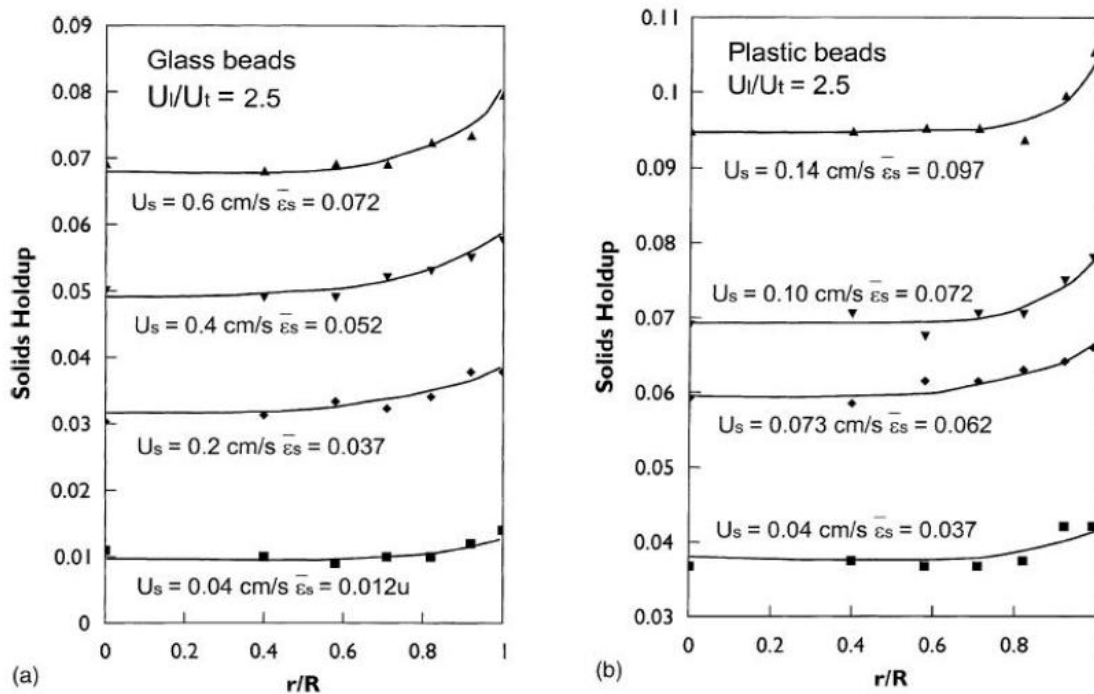


Figure 2.18: Radial profiles of solids holdup at the level $H = 0.8\text{m}$ for different solids flowrates for (a) glass beads and (b) plastic beads at the same normalized liquid velocity, $U_l/U_t = 2.5$ (Zheng et al., 2002)

Solids Acceleration

When solids enter the column from the returning pipe, they have velocity of zero or even negative due to their direction either horizontal or downward at the entrance. They need to be accelerated by the drag force that the liquid exerts on them. After this point, their velocity is constant. Therefore there exist two regions: initial region, where particles accelerate, located at the bottom of riser, and fully developed region, where particle velocity is unchanged.

The length of the developing region, also called acceleration length, depends on liquid and solids velocity and also density ratio. When liquid velocity is high, this length is shortened because the drag force is higher. In opposite, an increase of solids circulation rate makes this region extend longer since the same drag force supports a heavier mass. Another factor impacting the acceleration length is the ratio ρ_s/ρ_l . The larger the ratio is, the longer the length is. For example, in gas - solids fluidized beds, the density ratio ρ_s/ρ_g is very high. For this reason, the developing region extends and could even takes up the entire column, leading to non-uniformity in axial direction throughout the column in gas-solids fluidization. For liquid - solids fluidization, the density ratio ρ_s/ρ_l is much smaller, especially for light particles for which the density ratio is close to unity. Consequently, the developing region sometimes does not seem to exist.

Radial Distribution of Particle Velocity

There is limited study on radial distribution of particle velocity in liquid - solids fluidized beds. Roy et al. (1997) employed large and dense particles ($d_p = 2.5$ cm and $\rho_s = 2500$ kg/m³) to conduct their experiments measuring local solids velocity. Figure 2.19 shows that increasing liquid velocity steepens the parabolic curve of particle velocity profile. It was also found that there is no significant difference in local particle velocities at different axial locations. Noticeably, the profile for particle velocity is more non-uniform than for liquid velocity. Perhaps it is because the friction force between solids and wall is higher than the one between liquid and wall. The friction force makes movement of solids at wall more stagnant.

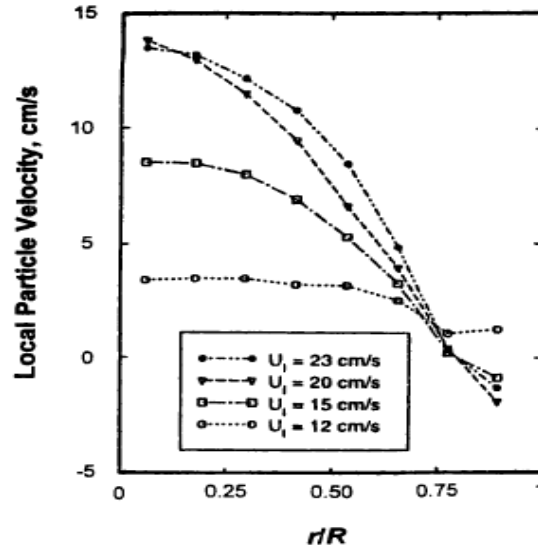


Figure 2.19: The radial distributions of particle velocity at different superficial liquid velocities for glass beads averaged axially over the riser (Roy et al., 1997)

Particle Size Effects

A study of effects of particle size on hydrodynamics of LSCFB was done by Razzak group (2009). They conducted experiments using two types of glass beads with diameters of 500 μm (GB-500) and 1290 μm (GB-1290), both having the same density of 2500 kg/m^3 . Figure 2.20 shows the variation of solids circulation rate, expressed as solids velocity, with the change in superficial liquid velocity for the two types of glass beads. It is clearly seen that under the same auxiliary liquid velocity and total liquid velocity, the smaller particles (GB-500) have higher solids circulation rate. Recall that particles are fluidized by exertion of drag force and buoyant force which are calculated as following:

Buoyant force: $F_B = V_p \rho_l g$

$$\rightarrow \frac{F_B}{V_p} = \rho_l g \quad (\text{Equation 2.4})$$

Drag force: $F_D = \frac{1}{2} \rho_l v^2 C_D A$

$$\rightarrow \frac{F_D}{V_p} = \frac{1/2 \rho_l v^2 C_D A}{V_p} = \frac{1/2 \rho_l v^2 C_D (\pi/4 d_p^2)}{\pi/6 d_p^3} = \frac{3 \rho_l v^2 C_D}{4 d_p} \quad (\text{Equation 2.5})$$

It is seen from equations (4) and (5) that buoyant force per volume is independent of particle size. Yet, drag force per volume is inversely proportional to particle diameter. Consequently, the larger beads have less drag force per volume than the smaller beads. It leads to slower solids velocity for GB-1290 when being fluidized by the same amount of liquid compared to GB-500.

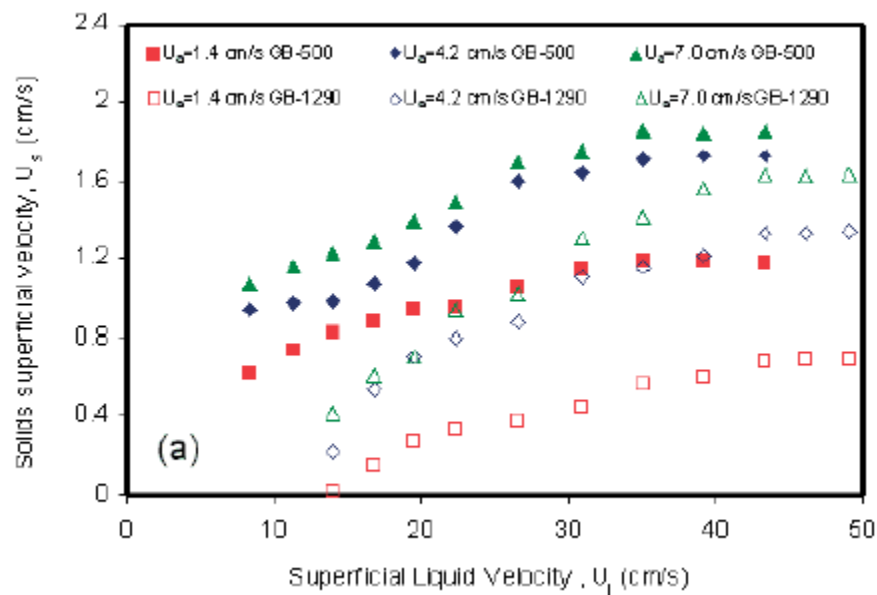


Figure 2.20: Variation of superficial solid velocity with the superficial liquid velocities at different auxiliary liquid velocities for glass beads (500 and 1290 μm) (Razzek et al., 2009)

Studies have also been done to examine the impacts of particle size on the radial distribution of solids holdup. Under the same operating conditions, e.g. same superficial liquid velocity – 22.4 cm/s, same superficial solids velocity – 0.95 cm/s, measurements were taken at different radial locations at the elevation $H = 2.02$ m (Figure 2.21). Radial non-uniformity and local solids concentration for the smaller particles are consistently higher than for the larger particles. This phenomenon can be explained by two reasons. First, under the same operation, Reynold number increases with particle diameter,

resulting in a lower drag coefficient. Second, larger particles also have higher settling velocity, therefore lower slip velocity. For these two reasons, although the projected area of GB-1290 is larger, the effects of drag coefficient and slip velocity are more prominent, resulting in a lower drag force for the larger glass beads. That is why solids holdups for GB-1290 is less compared to the GB-500 at a constant solids velocity.

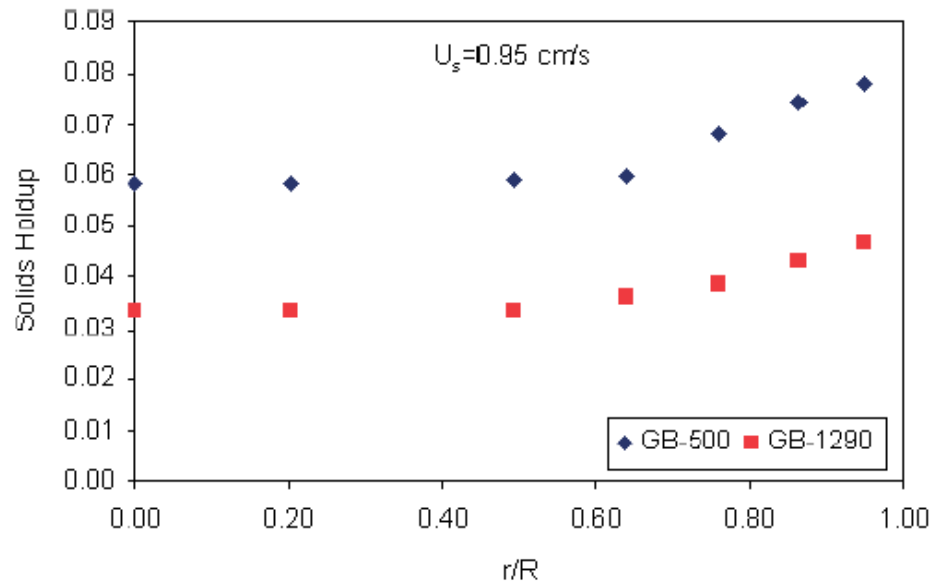


Figure 2.21: Radial distribution of solids holdups for glass beads (500 and 1290 μm) at axial location $h = 2.02$ m and $U_1 = 22.4$ cm/s (Razzak et al., 2009)

2.3.3 Phase Mixing

In the previous sections, phase holdups, their distribution and flow patterns of both solids and liquid phase have been presented. The following discussion will cover mixing levels of the two phases.

Liquid Mixing

The liquid mixing study commonly utilizes the pulse response technique and saturated solution such as KCl or NaCl as tracer. The concentration of tracer in downstream at different radial positions is recorded. A typical tracer concentration profile as shown in Figure 2.22 below.

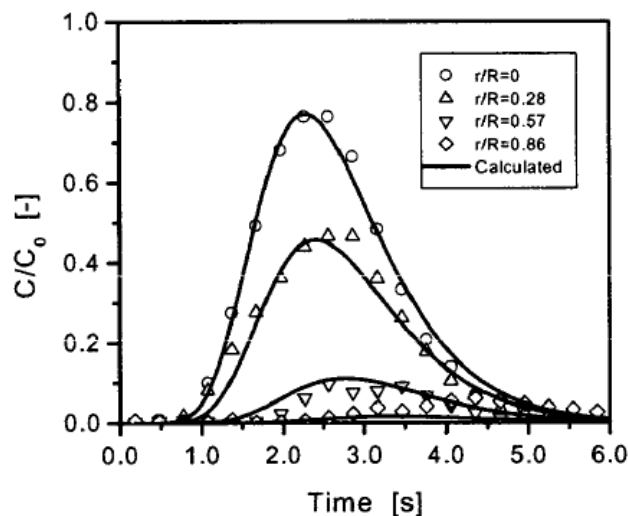


Figure 2.22: Typical tracer concentration distribution profiles ($U_{10} = 0.072$ m/s, $\varepsilon = 0.9$, $G_s = 7.5$ kg²m⁻¹s⁻¹) (Chen et al., 2001)

When tracer is injected at the center of the riser, it is reasonable to expect the highest reading at $r/R = 0$. The bell-shaped profiles indicate the spreading of particles over time, which is caused by dispersion in the longitudinal direction. Additionally, tracer is detected at other radial locations as well, indicating the radial dispersion of liquid molecules. Chen et. al. (2001) successfully measured the extension of liquid mixing in both axial and radial directions. They further investigated the impacts of superficial liquid velocity and solids holdup on the mixing. Recall that radial distribution of liquid velocity is non-uniform. Liquid flows faster at the center and slower near the wall. The profile non-uniformity becomes more pronounced when superficial liquid velocity increases, or solids circulation rate increases, which is accompanied with denser solids concentration. Since superficial liquid velocity and solids holdup have impacts on the distribution of local liquid velocity, they are expected to influence liquid mixing as well. Understanding the effects of these parameters on liquid mixing is definitely advantageous in optimizing operation of LSCFBs.

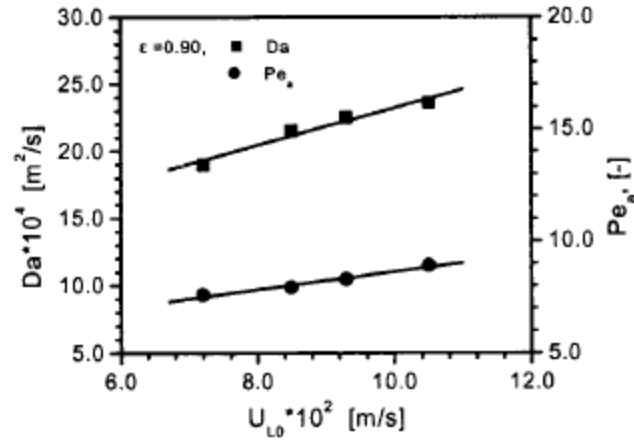


Figure 2.23: Effects of superficial liquid velocity on liquid axial mixing (Chen et al., 2001)

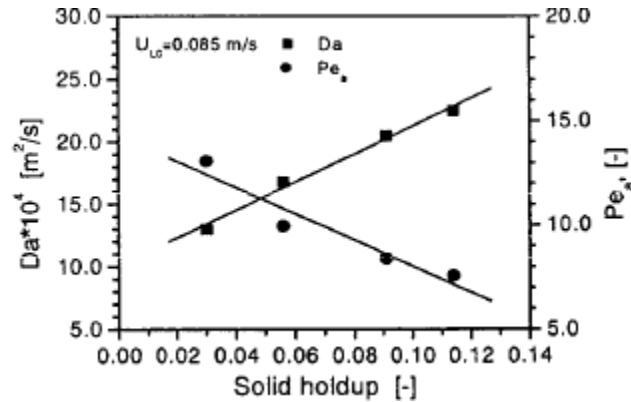


Figure 2.24: Effects of solid holdup on liquid axial mixing (Chen et al., 2001)

Figure 2.23 shows how the axial mixing coefficient, D_a , and dimensionless Peclet number, Pe_a change when liquid velocity increases, yet the bed voidage is maintained at 0.90. Peclet number is defined as:

$$Pe_a = \frac{U_L L}{D_a} \quad (\text{Equation 2.6})$$

Both mixing coefficient and Peclet number are in proportional relation with liquid velocity. The increase of mixing coefficient can be explained that when liquid flows more rapidly, it creates more turbulence diffusion inside the bed (Chen et al., 2001). The same trend is found in Zheng's study (Zheng et al., 2001). According to the definition,

Peclet number is inversely proportional to mixing coefficient. Therefore, when D_a increases, Peclet number should decrease. However, Peclet number increases with liquid velocity, also from its definition. This increase compensates for the decrease due to mixing coefficient, leading to the overall increment of Pe_a .

Following, effects of solid holdup on liquid axial mixing are also considered (Chen et al., 2001). While the liquid velocity is kept constant at 0.085 m/s, solids circulation rate is adjusted to obtain different solids concentration. The trend of D_a increasing with solid holdup are depicted in Figure 2.24. This agrees well with the results shown on Zheng's paper (Zheng et al, 2001). In this case, the liquid velocity is unchanged, hence Pe_a is simply inversely proportional to D_a . The fluidized bed experiences more mixing when denser because high solids concentration promotes non-uniform distribution of radial local liquid velocity, in turns enhances axial back-mixing of liquid.

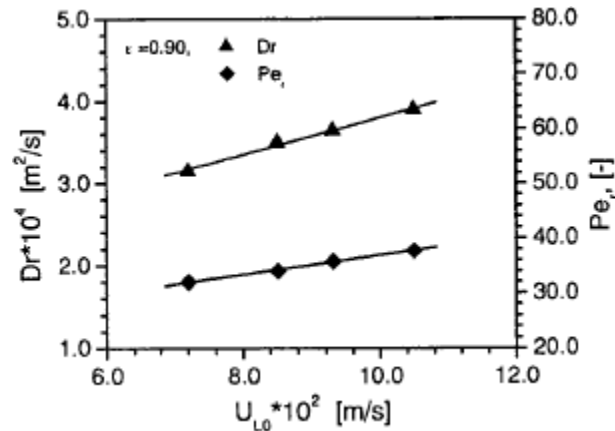


Figure 2.25: Effects of superficial liquid velocity on liquid radial mixing (Chen et al., 2001)

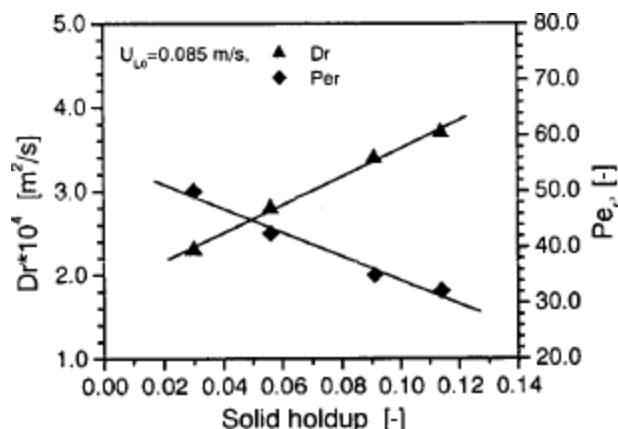


Figure 2.26: Effects of solid holdup on liquid radial mixing (Chen et al., 2001)

The effects of superficial liquid velocity and solid holdup on the radial mixing of liquid phase are presented in Figure 2.25 and Figure 2.26. The trends observed are the same as for the axial mixing. Additionally, it should be noted that radial mixing is less than axial mixing by an order of magnitude.

Solids Mixing

Solid phase exhibits severe mixing, especially in the axial direction compared to the liquid phase as it is being fluidized upward by the liquid. The liquid eddies containing energy catch some particles and carry them up for some distance. The interactions between liquid-solid, solid-solid, and solid-wall extract the energy from the eddies, resulting in the shedding of particles. The particles fall downward until they meet other liquid eddies with sufficient energy. This mechanism may happen for several times until the particles exit the riser to the separator. For these reasons, solids undergo very intense back-mixing even if the liquid is close to ideal flow (Roy & Dudukovic, 2001).

To track the trajectory of the tracer particle, the computer-automated radioactive particle tracking (CARPT) technique is used. The tracer encapsulates radioactive Sc-46 which allows it to emit gamma radiation. Multiple detectors are positioned along the riser. When the detector near the solids feeding pipe realizes the entrance of the tracer, it sends signals to the rest of the detectors to start data acquisition. They record the positions of the tracer. When the detector at the exit signals that the particle has passed it, the time

difference from the entrance to the exit is the residence time of a typical particle inside riser bed. At a set of operation conditions (fixed liquid velocity and fixed solid to liquid ratio), massive number of trajectories are recorded. The fraction of trajectories that fall under the same range of residence time is called frequency. A typical residence time distribution is shown below:

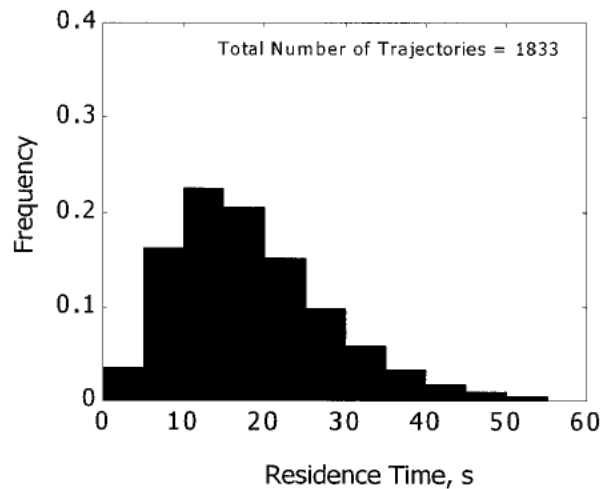


Figure 2.27: Residence time distribution calculated from CARPT data ($U_1 = 20$ cm/s; $S/L = 0.10$) (Roy & Dudukovic, 2001)

From the residence time distribution, Roy and Dudukovic calculated the time average, variance, equivalent number of tanks, and axial Peclet number. Table 2.2 lists those values obtained at different solid to liquid ratios while U_1 is kept constant.

Table 2.2: Mixing parameters from solids RTD (Roy & Dudukovic, 2001)

S/L	Solids mean residence time (s)	Variance (s^2)	Dimensionless variance	Equivalent number of tanks in series	Axial Peclet number	D_{ax} (cm^2/s)
0.10	19.3	108	0.29	4	6.9	245
0.15	13.2	67.9	0.39	3	5.1	444
0.20	12.5	95.3	0.61	2	3.3	564

Beside mixing coefficient and Peclet number, equivalent number of tanks in series, N , is also a measurement of phase mixing. Like Peclet number, it is more favorable to have high equivalent number of tanks, which indicates less back-mixing. N can be determined

using equation (7) and is related to Peclet number as shown by equation (8) (Menkhaus & Glatz, 2005):

$$N = \frac{\bar{t}^2}{\delta^2} \quad (\text{Equation 2.7})$$

$$Pe = 2N \quad (\text{Equation 2.8})$$

It is seen in Table 2.2 that solid back-mixing increases when S/L increases. Fixing the liquid flowrate and increasing solids circulation, or fixing solids circulation and reducing liquid flowrate result in a denser bed. When solids concentration is higher, there are more solid-solid collisions, more particle shedding, and more particles flowing downward, resulting in more solids axial dispersion.

Similar with the finding established in liquid mixing study is that solids radial mixing is also 1 order of magnitude smaller than the axial mixing (Roy et al., 2005; Roy & Dedukovic, 2001). In addition, in both directions, the mixing of solids is 1 order of magnitude larger than mixing of liquid phase ($D_{a,l} = 10\text{-}25 \text{ cm}^2/\text{s}$, $D_{r,l} = 3\text{-}4 \text{ cm}^2/\text{s}$ in Chen's study (Chen et al., 2001)).

2.4 Conventional Liquid-Solid Fluidized Bed

Liquid-solid fluidized beds (LSFBs) operate in the conventional fluidization regime, or sometimes the fixed regime. In this case the liquid velocity is much lower than the particle terminal velocity and there is no particle entrainment. The information available for LSFBs is often used to predict the hydrodynamic behaviour in a downer simply because they are in the same fluidization regime, and up to date there is no available information on the hydrodynamic properties of the downer. Therefore, before presenting research on downer, review on LSFBs is necessary.

2.4.1 Bed Expansion

In LSFBs, when the superficial liquid velocity is lower than the minimum fluidization velocity, U_{mf} , the bed does not expand and keeps its static bed height. When the liquid velocity exceeds U_{mf} , the bed height starts to rise. Figure 2.28 and 2.29 show the

variations of pressure drop and bed height with respect to change of liquid velocity. When fluid flows through a particle bed for the first time, the bed initially remains very densely packed. However, with increasing velocity, the pressure drop increases and overshoots the fluidized bed pressure slightly to escape from the dense packing. Once the velocity reaches U_{mf} , pressure drop is constant despite further increase of liquid flowrate. The trend of the bed height is opposite. At first, bed height is unchanged with increasing of U_1 . Beyond the minimum fluidization value, particles start to mobilize. The top surface is then flattened and remains horizontal. The bed height continues to rise with increase of U_1 . To determine minimum fluidization experimentally, the method of decreasing liquid velocity to avoid the initial densely packed bed situation gives more accurate result, as seen in both Figure 2.28 and 2.29.

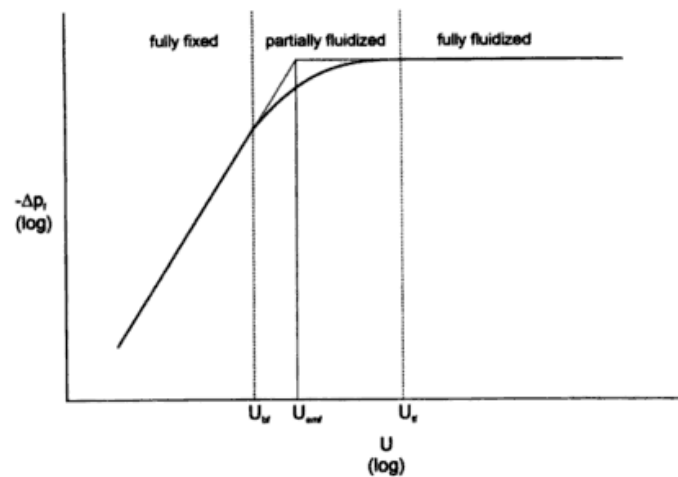


Figure 2.28: Pressure drop - velocity relationship (Couderc, 1985)

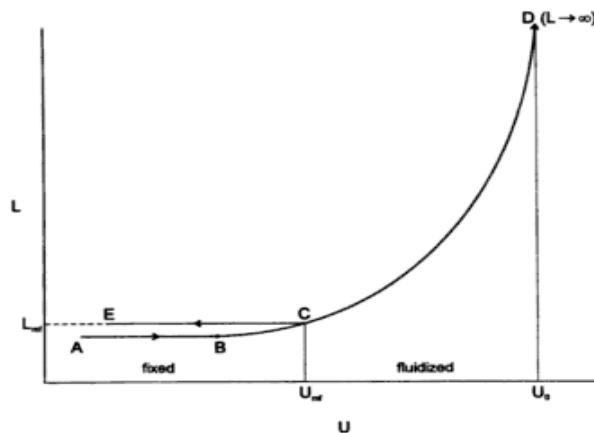


Figure 2.29: Bed height - velocity relationship (Yang, 2003)

Vessel diameter has profound impact on bed expansion and pressure drop as well, especially with smaller size particles. Nikitina et.al. (1981) measured these two parameters in variation of column diameter for two types of particles of the same density. One is KU-2 resin with average diameter of 0.68 mm; and the other is large granule KU-2 resin whose average diameter is 2.6 mm. The settled bed height is kept the same, 300 mm.

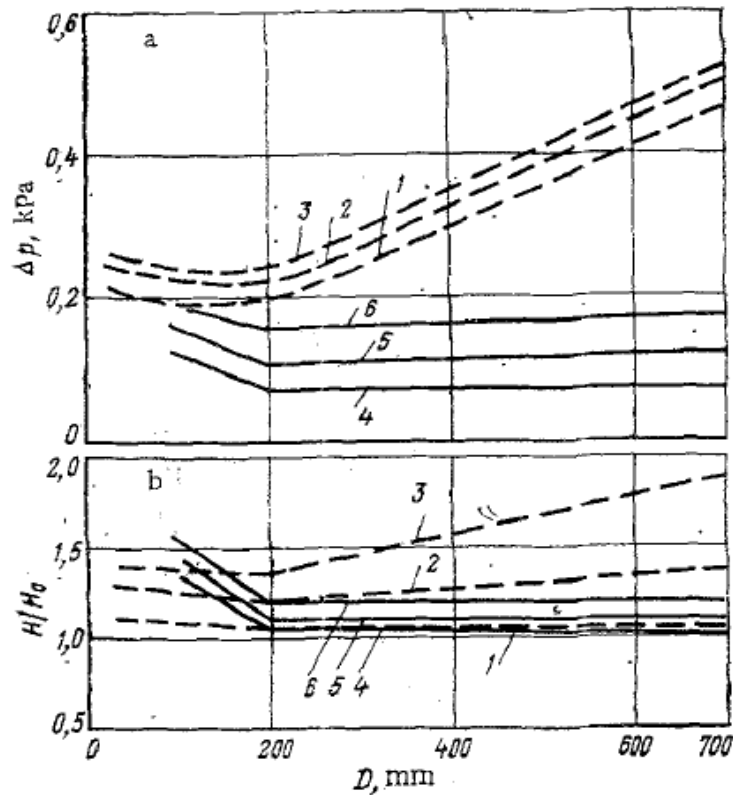


Figure 2.30: (a) Pressure drop and (b) bed expansion of resin bed as a function of vessel diameter. Water velocities (mm/s) 1) 0.5; 2) 1.2; 3) 1.9; 4) 5; 5) 6; 6) 9 (Nikitina et al., 1981)

In Figure 2.30, dashed curves are for KU-2 resin; continuous curves are for large-granule KU-2 resin. Nikitina et. al. found that pressure drop and bed expansion of a small-particles bed are not affected by vessel size significantly when the vessel diameter is in the range 30 - 200 mm. When vessel diameter is larger 200 mm, then bed expands with much higher degree even though liquid velocity was constant. The observation is different for larger resins, where bed expansion was less for column diameter in the range

30 - 200 mm. Beyond this range, D_c almost had no effects on pressure drop and bed expansion. They concluded model vessel should be 200-300 mm for large particles systems, and should be no smaller than 500-700 mm for small particles systems (Nikitina et al., 1981).

As the bed height rises, the voidage is increased. Many researchers suggested mathematical models to calculate the voidage. A simple way is to use pressure drop, ΔP , across a segment of bed height, h .

$$\Delta P = \rho_o g h = [\rho_l \varepsilon + \rho_s (1 - \varepsilon)] g h \quad (\text{Equation 2.9})$$

Garside and Al-Dibouni (1979) proposed a relationship between liquid velocity and the voidage as following:

$$\frac{U_l}{U_t} = \varepsilon^z \quad (\text{Equation 2.10})$$

where z is a function of terminal Reynolds number, and given by:

$$z = \frac{5.09 + 0.2839 Re_t^{0.877}}{1 + 0.104 Re_t^{0.87}}; \quad 10^{-3} \leq Re_t \leq 10^4 \quad (\text{Equation 2.11})$$

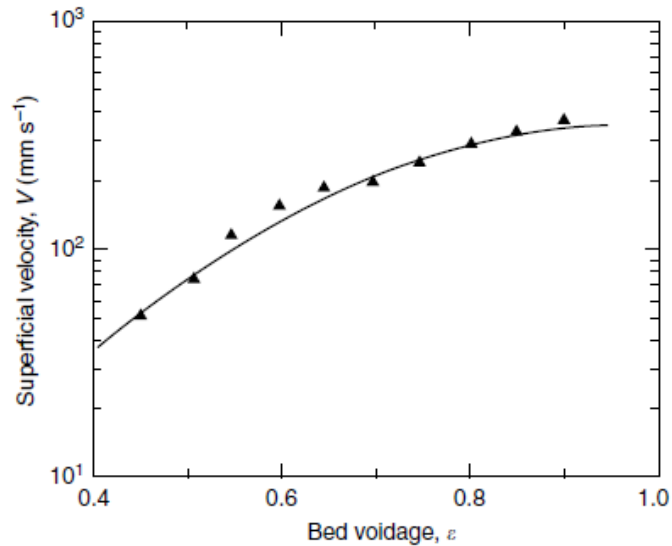


Figure 2.31: Superficial velocity - bed voidage relationship (Chhabra, 2007)

From the Equation (10) and the Figure 2.31, it can be expected that the voidage of liquid fluidized bed is in a logarithm relationship with liquid velocity. It is definitely useful to be able to predict how the particles distribute within the bed when liquid flowrate changes.

2.4.2 Axial Hydrodynamic Behaviour

When a bed of particles is in the fixed regime or the conventional regime, all particles are suspended at the base of the column. Figure 2.3 (in Section 2.2) demonstrates a uniform distribution of particle concentration. When there are only a dense phase and a freeboard phase, the solids holdup is constant in the axial direction in the region which the particles occupy (Liang et al., 1997).

2.4.3 Radial Hydrodynamic Behaviour

Radial Profile of Local Liquid Velocity

Zheng and Zhu (2003) studied the profile of liquid velocity in the radial direction for circulating fluidized bed but their data also cover a condition where there is no solids circulation, and the fluidization is in the conventional regime (refer to Figure 2.14). It is shown that in this regime, the liquid velocity is quite low, $U_1 = 4$ cm/s, therefore laminar. Without presence of solids, liquid velocity profile would have parabolic shape. However, the existence of dense solids phase smoothens and flattens the profile. Therefore a uniform distribution of local liquid velocity in radial direction is observed. It agrees well with the finding of Liang et al. (1997).

Radial Profile of Solids Holdup

The radial distribution of the solids holdup is non-uniform in the circulating regime but it is uniform in the fixed and conventional regime, thus the distribution of solids holdup is strongly related to liquid velocity. In a region, if liquid flows fast, it carries the solids with it, leading to a more dilute region. Oppositely, if liquid flows more slowly, less particles are carried up, in turn that region is more dense. In the conventional fluidization regime, liquid flow is evenly distributed over the cross-sectional area. It explains the fact that the solids holdup is uniform as well. Figure 2.32 presents radial profile of particle

concentration under different operating conditions. One of them, symbolized as ●, is when $U_l = 0.034$ m/s and $U_s = 0$. The liquid velocity is just below the transition velocity, and the solids bed is expanded. As shown in the Figure 2.32, the particle holdup profile is flat, and the same for all 4 elevations. It demonstrates the homogeneity of particles in a conventional fluidized bed – uniform in both axial and radial directions.

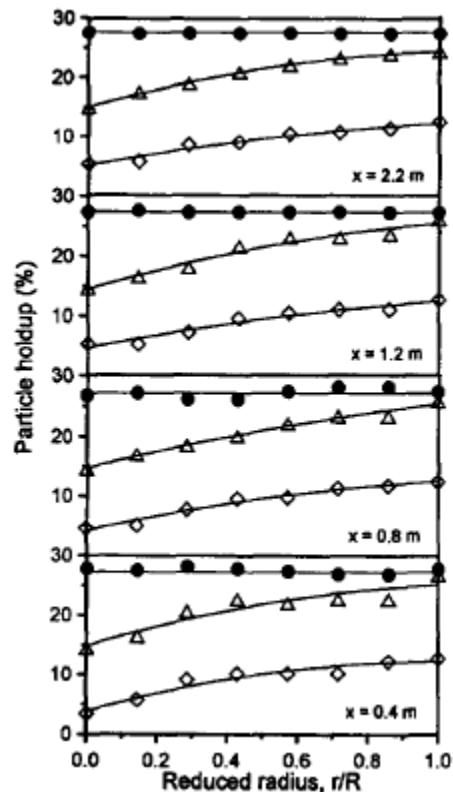


Figure 2.32: Radial particle holdup distribution under different operating conditions and at different bed sections for 0.405 mm glass beads. (●) $U_l = 0.034$ m/s, $U_s = 0$; (▲) $U_l = 0.078$ m/s, $U_s = 0.0019$ m/s; (◇) $U_l = 0.078$ m/s; $U_s = 0.0011$ m/s (Liang et al., 1997)

2.4.4 Phase Mixing

Liquid Mixing

Flow pattern of liquid phase has strong dependency on solid type, liquid velocity and viscosity, column dimensions, and distributor design (Tong & Sun, 2001). Tong and Sun

(2001) employed 3 different types of particles in their experiments. Their properties are listed in the table below.

Table 2.3: Particles used in Tong and Sun's study (2001)

Name	Symbol	Size range (μm)	Average size (μm)	Density (kg/m^3)	Terminal velocity (mm/s)	Terminal velocity (cm/h)
NFBA-S	o	50 – 165	102	1880	4.18	1504
NFBA-L	Δ	140 – 300	215	2040	14.3	5148
StreamlineSP	\square	100 – 300		1184	4.38	1577

They examined the effects of superficial liquid velocity, bed expansion, static bed height, and liquid viscosity on the axial liquid mixing coefficient and the Bodenstein number, defined the same as Peclet number, equal to uL/D . First, presented here are the effects of liquid velocity (Figure 2.33).

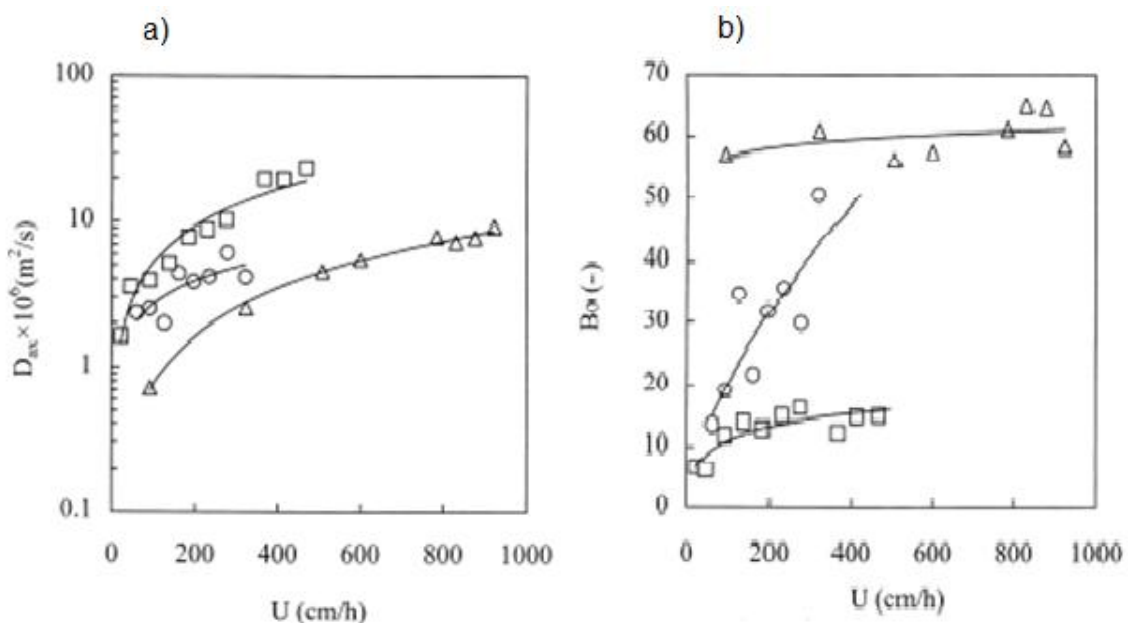


Figure 2.33: Effects of flow velocity on (a) the axial mixing coefficient and (b) the Bodenstein number (Tong & Sun, 2001)

The graphs show that when liquid flow increases, the mixing also increases, as shown by increasing axial mixing coefficient and Bodenstein number. This mixing increase is due to the turbulence added to the bed at higher inlet liquid velocity. Among the three types of particles, NFBA-L is the heaviest and largest, and has much higher terminal velocity

compared to the other two particles. At the same flowrate, the heavier particles expand less, and are less mobile than the lighter ones, explaining the fact that NFBA-L consistently has the lowest axial mixing rate.

Even though Bodenstein number and the mixing coefficient are inversely proportional, it does not necessarily mean when D_{ax} increases, Bo decreases. Figure 2.33b shows an increase of Bodenstein number with velocity as well. As previously discussed, this is because the effect of liquid velocity increase on Bodenstein determination dominates the effect of D_{ax} . Therefore, Bodenstein number increases with the increase of liquid flow as well.

It is worth noting that the impact of liquid flow on heavy particles is less substantial than on light particles. Particularly, for NFBA-L, as liquid velocity increases from roughly 100 to 900 cm/h, the mixing coefficient increases from 0.7 to 8 mm²/s. The liquid velocity, U_l , and the mixing coefficient, D_a , both increase by almost the same factor, leading to the plateau curve of Bo . The curve representing NFBA-S particles looks the steepest, and is much steeper than the one that represents StreamlineSP. There is no explicit explanation for this observation but Tong & Sun concluded NFBA adsorbents are promising for the use in expanded bed adsorption due to their higher Bo numbers.

The mixing coefficients for the three adsorbents are then shown as a function of bed expansion.

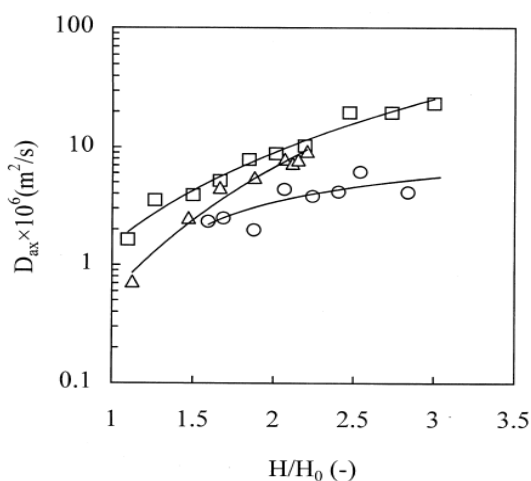


Figure 2.34: Axial mixing coefficient as a function of degree of bed expansion (Tong & Sun, 2001)

As previously noted, bed expansion depends on not only liquid velocity (liquid viscosity will be discussed later), but also the size and density of particles. Therefore, to have a fair comparison, it is reasonable to adjust the liquid flow in order to have the same degree of expansion for all types of particles. In this case, their difference in mixing is shown to be no longer significant.

The effect of liquid viscosity was also investigated. Glycerol was added to distilled water at 10% volume fraction, to provide a fluidizing liquid with viscosity of 1.39×10^{-3} Pa·s.

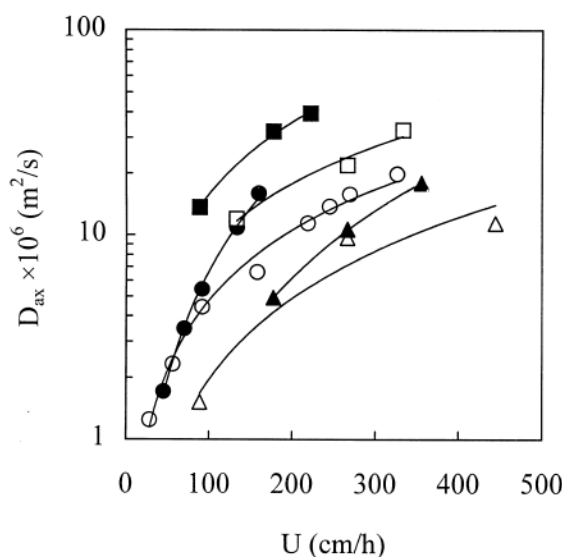


Figure 2.35: Effect of liquid viscosity on axial mixing coefficient: (o) NFBA-S / water; (●) NFBA-S / 10%(v/v) glycerol; (Δ) NFBA-L / water; (▲) NFBA-L / 10%(v/v) glycerol; (□) Streamline SP / water; (■) Streamline SP / 10% (v/v) glycerol (Tong & Sun, 2001)

For all three types of particles, it is seen that increasing liquid viscosity increases liquid mixing coefficient. The possible reason provided is that the viscous liquid promotes particle agglomerations, which disturb flow pattern of the liquid phase. Similar findings are found in Chang and Chase's paper (Chang & Chase, 1996). In their study, they used only one type of particles – Streamline SP and measured mixing coefficients under various liquid velocities and viscosities. The settled bed height was kept the same, $H_o = 10.0$ cm, under all conditions. Their results are summarized in the table below.

Table 2.4: Comparison of mixing coefficients in different expanded bed modes (Chang & Chase, 1996)

Mode	% (v/v) glycerol	Viscosity (mPa)	U_1 (cm/h)	H (cm)	D_{ax} (mm ² /s)
A	0	1.09	300	20	6.35
B	25	2.43	121	20	2.58
C	25	2.43	300	40	24.50
D	32	3.48	88.4	20	1.98
E	32	3.48	300	60	31.67

Comparing mode A, C, and E, they operate at the same liquid velocity of 300 cm/h using different glycerol-buffer mixtures as fluidizing liquid. A, C, and E, in the same respective order, have increasing volume percent of glycerol, in turn increasing viscosity. It can be seen that highly viscous solution makes a fluidized bed expand more.

Consequently, mode E has the highest bed height, and the largest voidage while mode A has the lowest bed height, and the smallest voidage. The results show that liquid axial mixing increases with liquid viscosity, expansion degree and bed voidage.

Using the solutions of different viscosities, instead of keeping the same U_1 and getting different bed heights, Chang and Chase varied U_1 to have a constant expanded bed height of 20 cm (mode A, B, and D). This approach eliminates the effects of bed expansion and bed voidage and focuses more on the effect of viscosity. Mode D has the slowest liquid flow but still has the highest mixing rate. This emphasizes the contribution of liquid viscosity in the level of liquid axial mixing.

Liquid distributor certainly plays an important role in causing turbulence within a fluidized bed. Asif et al. (1991) considered 4 designs of distributors. Their design parameters are shown in the table below.

Table 2.5: Liquid distributor design parameters (Asif et al., 1991)

Number of holes	N_{or} (holes/cm ²)	F_{or}	D_{or} (cm)
1	0.022	0.040	1.52
4	0.088	0.040	0.76
20	0.44	0.045	0.36
60	1.32	0.042	0.20

To study the impact of a distributor, Asif et. al. experimented with two cases. The first case was to characterize the distortion caused by distributor. The colour tracer was injected right above the distributor and a Brinkmann colorimeter was positioned 105 cm downstream. The dispersion coefficient was calculated from the residence time distribution (RTD) graph, and termed as D_a . The second case was to measure the true bed dispersion with no distributor effects. It is logical to assume the distributor with most number of holes creates the least distortion for fluidized beds. For the reason, they chose the 60-hole distributor to carry on the second-case experiments. The injection point was 25 cm above distributor and the distance from the injection point to the detection point remained at 105 cm. The dispersion coefficient in this case was termed as D_{ac} . The further away these two values D_a and D_{ac} are, the more distortion the distributor has caused.

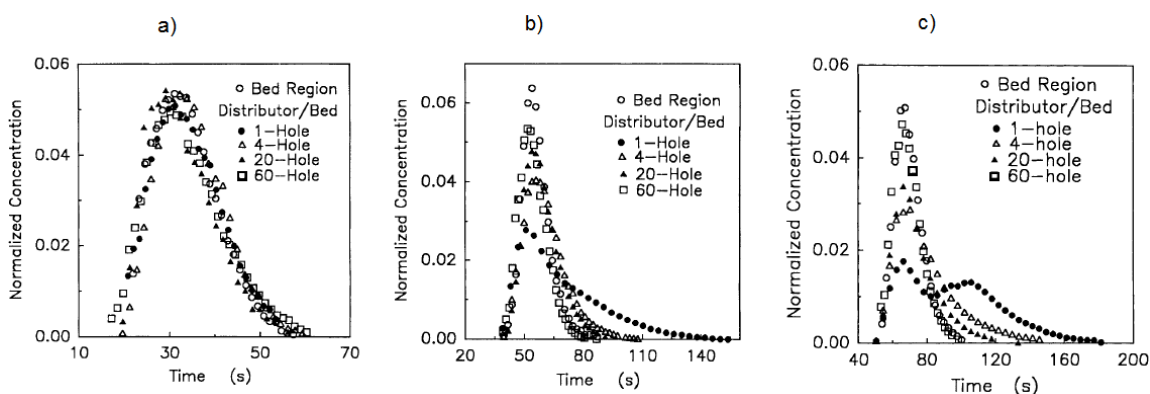


Figure 2.36: Effect of distributors on the response of the liquid fluidized bed at different liquid velocities: a) $U_l = 3.15$ cm/s; b) $U_l = 1.46$ cm/s; c) $U_l = 1.05$ cm/s (Asif et al., 1991)

Figure 2.36a shows that at high liquid velocity, there is no deviation among the RTDs when using different distributors. All of the RTD graphs conducted from case 1 experiments overlap the RTD from case 2. It was concluded that when operating at a high flowrate, distributor design has negligible effect on the flow pattern of liquid phase. As the flowrate reduces, the effect becomes more noticeable. The fewer number of holes a distributor has, the more deviation is observed when comparing its corresponding RTD

with the second case graph. Yet, the 60-hole distributor consistently yields RTDs in the distributor / bed region similar to the ones in the bed region (Figure 2.36b,c).

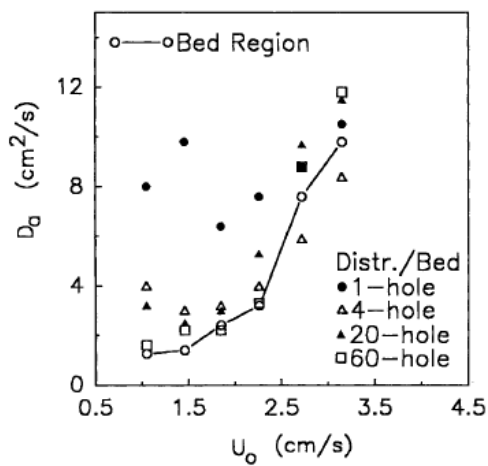


Figure 2.37: Comparison of apparent dispersion coefficients D_a at different liquid superficial velocities (Asif et al., 1991)

Figure 2.37 shows the comparison of D_a for the 4 distributors with the D_{ac} – bed region curve, at different superficial liquid velocities. It confirms the observation made from Figure 2.36 that distributor effect is more pronounced with a reduction of liquid velocity. More specifically, at a low range of U_1 , the data points of D_a are spread out, and higher than D_{ac} . This seems reasonable given the distributor region is always more turbulent than the area above it. Additionally, the scatter observed is more pronounced for the distributors with less number of holes than ones with higher number of holes.

In conclusion, there are many factors affecting liquid mixing in LSFBS including liquid superficial liquid velocity, liquid viscosity, bed expansion, voidage, particle density, particle size, and liquid distributor. To ultimately design and operate expanded beds, to achieve laminar flow with least axial dispersion of liquid, care should be given to all of these parameters.

Solids Mixing

Even though there is no net flow of particles in an expanded bed, the particles are constantly in motion, therefore they also experience dispersion within the bed.

Employing the computer automated radioactive particle tracking (CARPT) technique, solids mixing may be measured. Limtrakul et al. (2005) investigated the effects of bed height, particle density and size, column diameter, distributor type, and liquid velocity on the solids motion in LSFBs. In their study, they used a perforated plate and a bubble cap as liquid distributors, glass beads of 1 and 3 mm diameter, and 2 columns whose diameters were 10 and 14 cm. They stated that solids motion is not a strong function of axial position, and therefore their reported results are one dimensional (radial) and axially averaged at the middle height of the bed. First, presented here is the effect of column size. Figure 2.38 below depicts the radial profiles of local solids velocity, and both axial and radial dispersion coefficients for 3-mm glass beads at $U_1 = 7$ cm/s using a perforated plate. The solids holdups in the two columns are fairly close to each other: $\varepsilon_s = 0.43$ for the 10-cm column and $\varepsilon_s = 0.44$ for the 14-cm column.

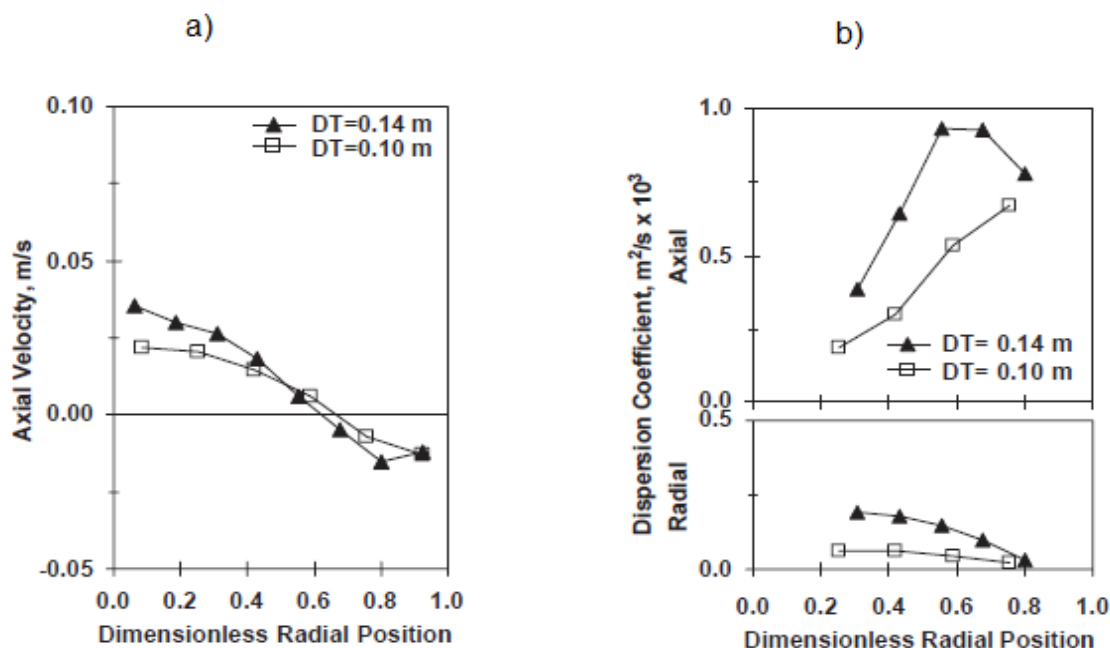


Figure 2.38: Effect of column size on (a) axial mean solids velocity, (b) dispersion coefficients (Limtrakul et al., 2005)

The larger column appears to have more non-uniformity in the axial velocity profile. At the center, solids velocity in the 14-cm column is about 1.6 times higher compared to the one in the 10-cm column. This is due to less wall friction and larger eddies in a larger

column, and this non-uniform velocity profile enhances dispersion. Therefore, the 14-cm column yields higher dispersion coefficients than the 10-cm column. In both columns however, the same trend in local dispersion is observed: more radial dispersion in the core region, more axial dispersion in the annulus region. Due to wall friction, particles are more restricted to move around in the horizontal surface. They can move much easier near center. Consequently, radial dispersion is higher near the center. Oppositely, axial dispersion is more greater the wall than the center because near the wall, some particles travel downward, and some travel upward, which causes circular motions. Another note that should be taken from Figure 2.38b and the following figures (Figure 2.39 - 42) is that the axial dispersion is much more significant than the radial dispersion. Radial dispersion coefficient ranges from 0 - 4 cm^2/s while the axial dispersion may reach as high as 40 cm^2/s .

Following, to examine the effects of distributor type, a bubble cap distributor and a perforated plate distributor were considered. The 14-cm diameter bed was filled with 3-mm glass beads and fluidized at a liquid velocity of 7 cm/s for the purpose of this study.

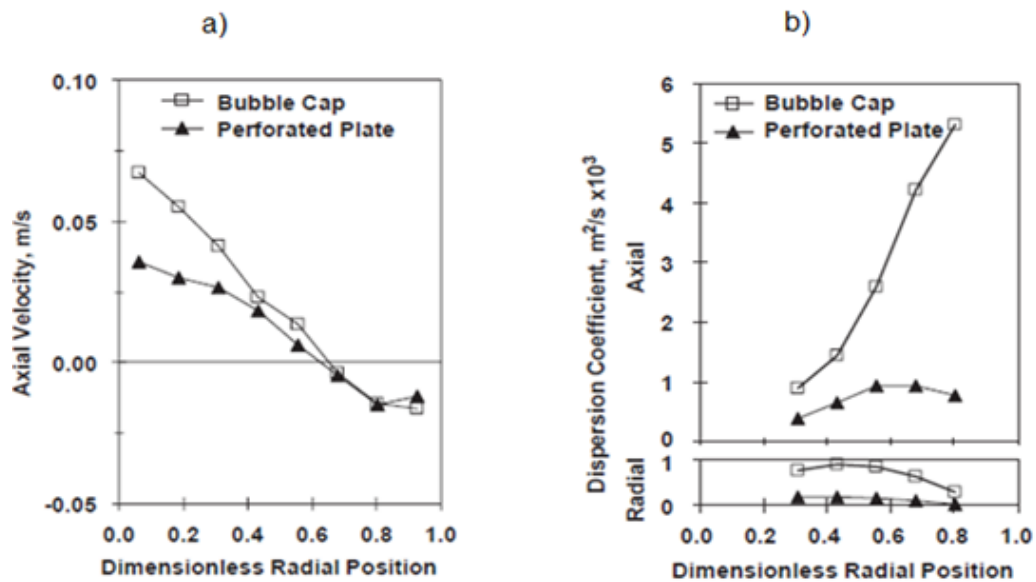


Figure 2.39: Effect of distributor type on (a) axial mean solids velocity, (b) dispersion coefficients (Limtrakul et al., 2005)

The bubble cap distributor used has fewer caps near the wall, leading to higher liquid input at the core region. Fast liquid flow exerts larger drag force onto particles, resulting in higher upward velocity of solids phase. It explains the higher rise of solids axial velocity near the center in the case of bubble cap compared to the perforated plate as seen in Figure 2.39a. In addition to higher non-uniformity of solids velocity, bubble cap distributor generates swirling motion in liquid stream, thus more turbulence. For these reasons, the particles are more dispersed when being fluidized using the bubble cap distributor than the perforated plate.

Fluidizing liquid velocity definitely has influence on the flow pattern of particles. Using same type of particles (3-mm glass beads), operating in the 14-cm column, using perforated plate distributor, the radial profiles of solids velocity and dispersion were obtained under 3 different liquid superficial velocities.

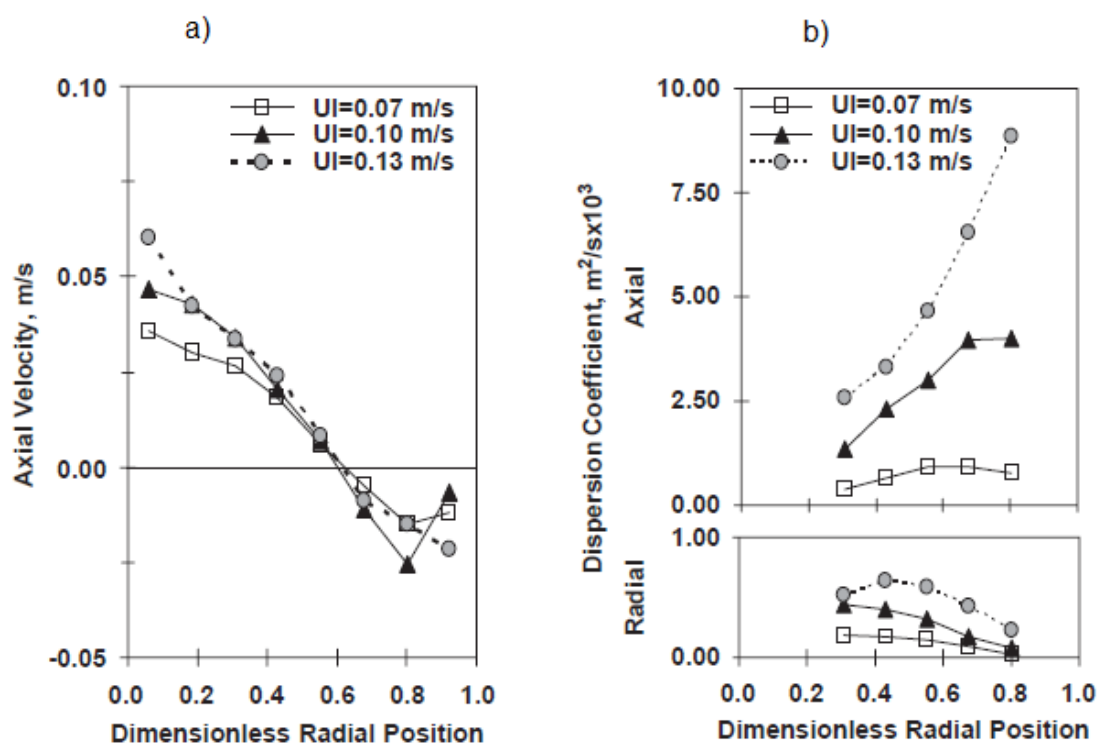


Figure 2.40: Effect of superficial liquid velocity on (a) axial mean solids velocity, (b) dispersion coefficients (Limtrakul et al., 2005)

As liquid velocity increases, liquid phase provides more energy input to the column, which also means more turbulence and more circular motions of solids phase. It supports the fact that the solids velocity non-uniformity and dispersion coefficients increase with increase of liquid velocity, as shown in Figure 2.40.

The effects of particle size and density were also investigated. Limtrakul et al. used 2 glass beads with diameters of 1 mm ($\rho_s = 2900 \text{ kg/m}^3$) and 3 mm ($\rho_s = 2500 \text{ kg/m}^3$) to study size effect since their densities are relatively close. Next, they used acetate beads ($\rho_s = 1300 \text{ kg/m}^3$) and glass beads ($\rho_s = 2500 \text{ kg/m}^3$) whose sizes are 3 mm to examine the density effect. The results are shown in the figures 2.41 and 2.42 below.

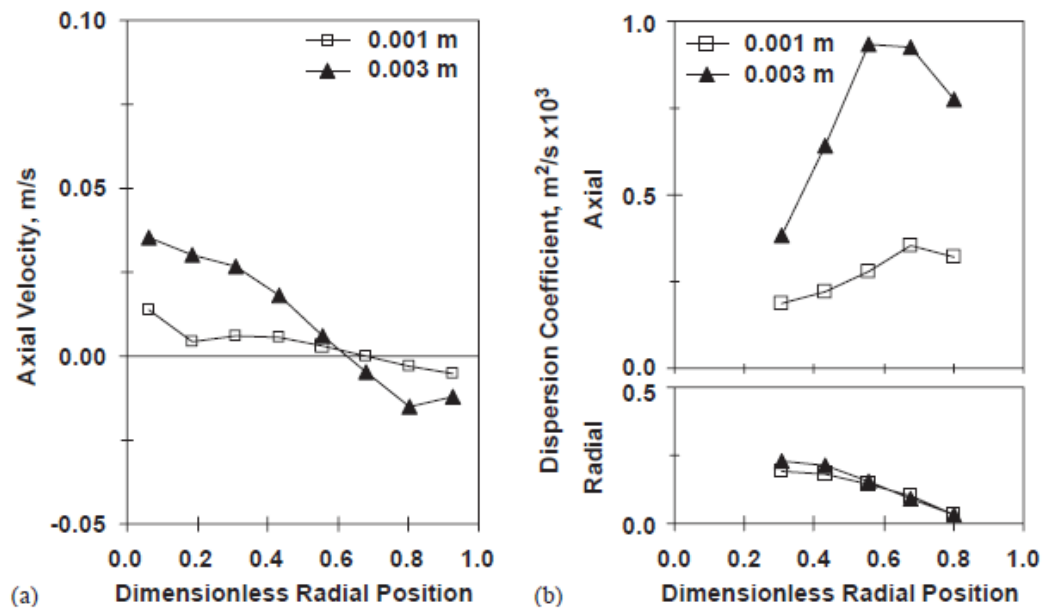


Figure 2.41: Effect of particle size at $U_l/U_{mf} = 1.7$ ($U_l = 7 \text{ cm/s}$ for 0.003 m; $U_l = 2.4 \text{ cm/s}$ for 0.001 m) on (a) axial solids velocity and (b) dispersion coefficients (Limtrakul et al., 2005)

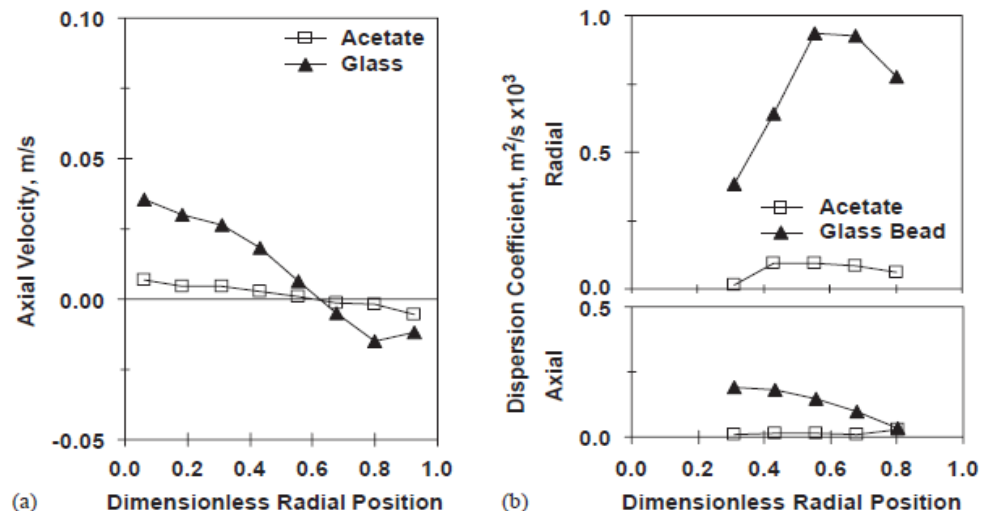


Figure 2.42: Effect of particle density at $U_l/U_{mf} = 1.7$ ($U_l = 7$ cm/s for glass beads; $U_l = 2.4$ cm/s for acetate) on (a) axial solids velocity and (b) dispersion coefficients (Limtrakul et al., 2005)

At a given U_l/U_{mf} , the axial velocity non-uniformity and solids dispersion increase with particle size and density. It may be explained that the liquid velocity is higher in the case of larger and heavier particles, thus it inputs more energy and causes more turbulence within the fluidized bed. It is also noted that the velocity inversion point occurs at different points: 0.62 dimensionless radius for the 0.001 m particle system and 0.72 for 0.003 m particle system. The possible reason is that smaller particles have higher "apparent viscosity" (Song & Fan, 1986), and the inversion point moves closer to the center for higher viscosity emulsion.

To conclude, there are many parameters influencing the mixing of particles in LSFBS, such as particle size and density, column diameter, liquid velocity and distributor type. Relatively, the mixing coefficient of the solids phase, ranging between 1 – 10 cm²/s, is much higher than the one of liquid phase, ranging from 1 – 10 mm²/s in liquid-solids expanded beds. It is understandable because the liquid phase undergoes both convective and diffusive flow and has more tendency to travel forward. Conversely, the solids phase is not driven by convective force, and has no net flow but only circulates inside the bed. The only cause of the particle motions is the diffusivity, therefore the solids dispersion is higher than the liquid dispersion.

Chapter 3

3 Experimental Methods

The following chapter gives details on how the experiments were performed including the materials used, the apparatus setups, procedure, analytical methods and the mathematical treatment. This is a new methodology for solids mixing measurement which is based on the concept of the ion-exchange ability of resins and the residence time distribution method. This chapter describes the steps taken for this study and chapter 6 will discuss the development of this methodology.

3.1 Materials

Two different types of particles were used in this project. They both are strong acid cationic resin, named Lewatit[®] S 1668 (from Lanxess Chemicals Company) and Supergel[™] SGC650 (from Purolite). They both are gel-type resins with very high capacity, chemically stable and physically strong. These are crucial properties that influenced particle selection for a number of reasons:

- Since they are strong acid cationic, they have the ability to exchange ions readily at all pH range, as compared to weak acid cationic resins, which require acidic medium. The steps to prepare the strong cation resins in a proper ionic form are safer and easier.
- Cationic resins have higher density than anionic ones. Cationic resins have density range of 1200 – 1300 kg/m³ while anionic resins' densities are often less than 1100 kg/m³, too close to water density for the purpose. Too light particles are more difficult to settle and maintain in downward flow when being fluidized upward by a liquid stream. This project is devoted to study particle mixing in a downer, therefore it is needed to have a counter-current fluidized bed. Cationic resins are a better choice.
- Both S1668 and SGC650 have permanent negatively charged sulfonic acid groups. They are chemically stable, and do not release and exchange ions in an

ion-free medium such as distilled water, even if the neighbouring resins are in different ionic form.

- Their excellent physical strength is valuable as well. The particles are less likely to break after several uses.

Table 3.1: Properties of the resins

	Size (mm)	Density (kg/m ³)	U _{mf} (mm/s)	U _t (mm/s)	Total capacity for Ca (mg/g _{resin})
Lewatit [®] S 1668	0.61 ± 0.05	1280	0.592	32.5	34.7
Supergel [™] SGC650	0.65 ± 0.05	1300	0.718	34.6	55.7

Beside large quantity of particles (2 liters of S1668 for lab-scale studies, and 17 liters of SGC650 for pilot-scale studies), other materials used were distilled water – the fluidizing liquid in both lab-scale and pilot-scale study, calcium chloride, sodium chloride, EDTA titrant (0.01M), pH 10 buffer, calmagite indicator (0.1 w/v aqueous). All chemicals were bought from Fisher Scientific.

3.2 Apparatus

The experiments were done at two scales. First was the lab scale, a 5-cm I.D. glass cylindrical column, 56.2 cm high (Figure 3.1). The bottom of the column is tapered in order for the particles to settle more easily and be more densely packed. The denser the particles are, the less liquid holdup is, making it somewhat easier to collect solids at the bottom. The opening at the bottom has inner diameter of 0.8 cm attached to tubing. Certainly if the tubing is fully open, all bed content will rush out. Therefore to control the solids exit rate, a clamp was attached to that outlet and only partially open.

Near the top, there were two outlets as well. The lower one was connected to a hopper, which was preloaded with a predetermined amount of particles. This acted as particle feeding system. A small pump was attached to the hopper which constantly pumped liquid into the hopper to create a slurry mixture so that particles could flow down. The upmost outlet was provided for liquid overflow stream. As shown in the sketch, the liquid level was higher than the solids feeding point. Particles were immersed in liquid once they entered the bed to ensure the least disturbance when they landed on the bed

surface. An additional hopper was used to input tracers to the column at the beginning of each run. The hopper had a tubing extension so that the tracer - releasing point would be closer to the bed surface, resulting in gentle settling and minimal mixing for the particles at the injection.

Liquid was distributed using a "plus" distributor (Figure 3.2) which had 3 holes on each arm and faced downward.

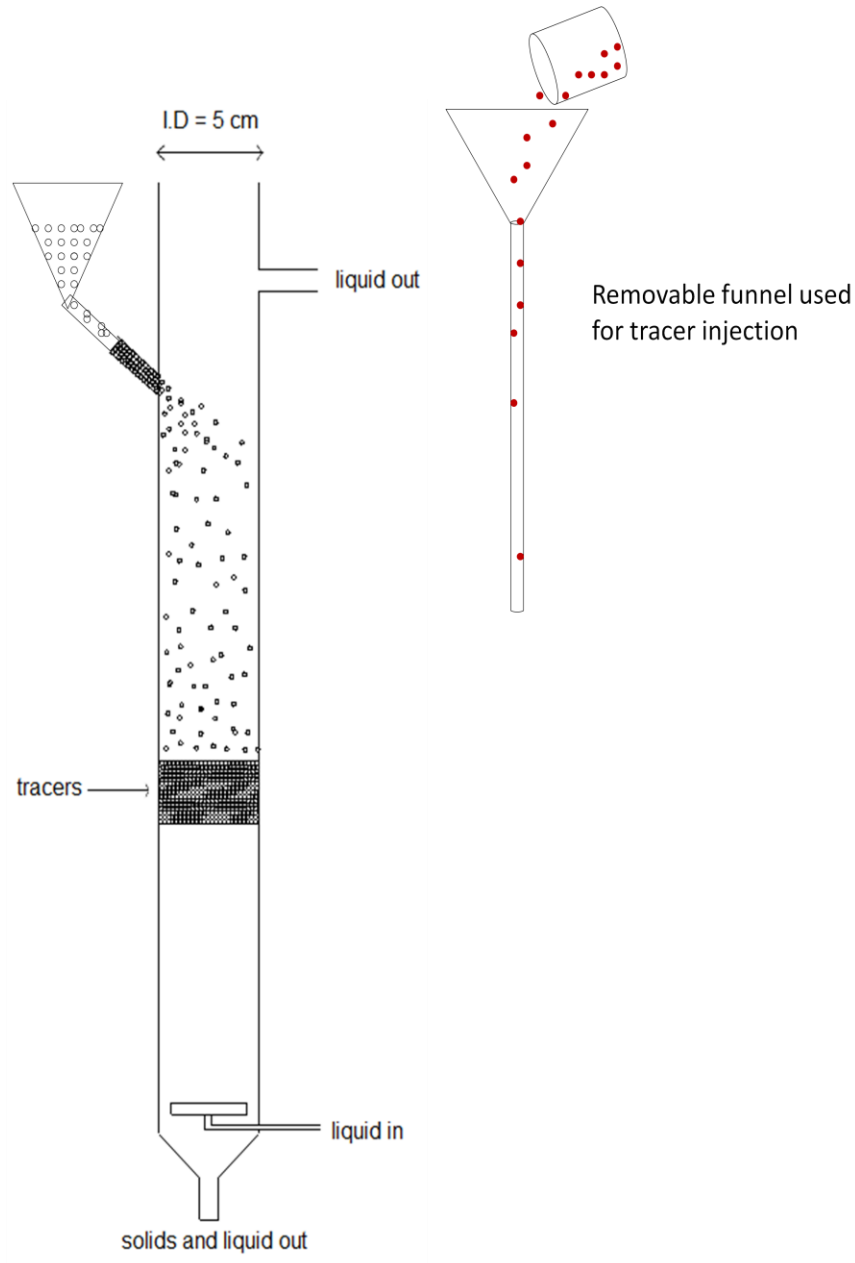


Figure 3.1: 5-cm column apparatus

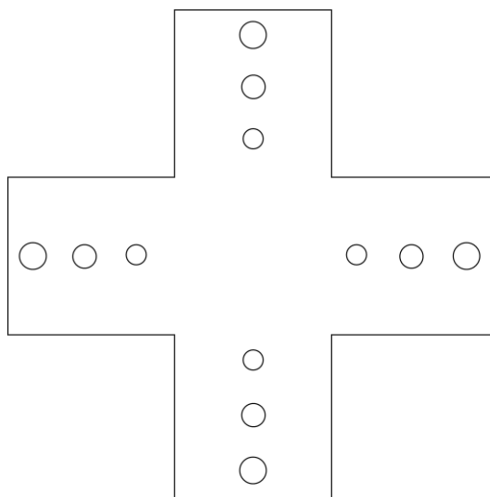


Figure 3.2: Liquid distributor used in lab scale

The larger scale was the pilot scale LSCFB. The full schematic diagram shown in Figure 2.1 is representative of the pilot LSCFB used for this testing with some modifications to the downer. The two main units are a 3.8 cm I.D and 4 m high riser, and a 10.1 cm I.D and 3.5 m high downer. The main distributor in the riser consists of one single stainless steel tube due to the small size of the column. The secondary distributor is a perforated plate. In the downer, there is a ring distributor. The details of the modifications to the downer are depicted in Figure 3.3. In the downer, two tubes are inserted at the elevations of 52 and 144 cm above the ring distributor. The tubes are 0.64 cm I.D. One end of each tube is positioned at the center of the downer column. The other end is extended to outside the wall. This end is connected to a ball valve which is opened periodically to withdraw particle samples.

A large hopper is placed at the top of the downer to pour the tracers in, and connected to an 80 cm long PVC pipe (O.D = 5.08 cm; I.D = 3.81 cm). There is a small funnel at the other end of the pipe which is about 10 cm above the solids circulation rate measuring device. A long nylon rope is tied to the small funnel to make it act like a "gate" to the tracers. When the nylon rope is pulled from the top where the big hopper is, the small funnel being tied to the rope is then pulled up as well and closes the gate. When the tracers are ready to be injected in the downer, the rope is loosened. The gate is then open and the tracers are "released". The extending pipe was used in order to shorten the

distance from the injecting location to the bed surface, thus smoother settling and less mixing at the injection. The small funnel was necessary as well because its conical shape promotes even radial spreading of tracers. All other details are the same as described in the Section 2.1.

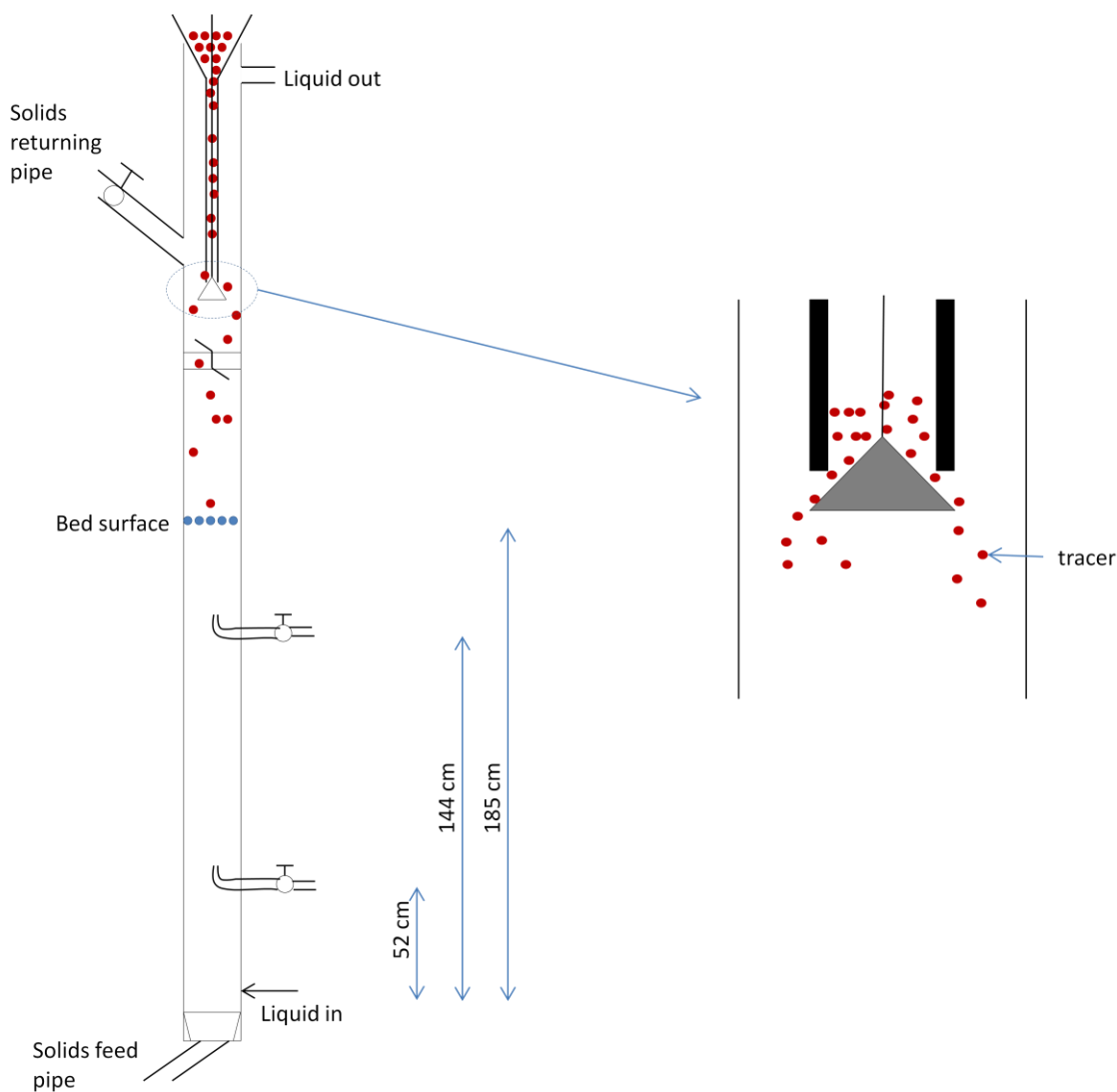


Figure 3.3: Schematic diagram of the downer

3.3 Procedure

3.3.1 Tracers Preparation

Since the resins can change their ionic form readily, the same type of resins were used for both tracers and neutral particles with the only difference being their ionic forms. The

tracers were strong cationic resins in calcium form (Ca^{2+}), sometimes called loaded resin, while the neutral particles were in sodium form (Na^+), also termed as fresh resin. Resins were an excellent candidate as tracers in particle-tracking experiments for a number of reasons:

- They have the same size, shape and density as the neutral particles which constitute the bed because they are the same resins.
- During the desorption process using NaCl solution, the tracers desorb calcium ions to adsorb sodium ions, and as the tracers then become neutral particles, in Na^+ form. This is regeneration step, which is essential to "freshen" the solids bed and avoid tracer accumulation between experiments. The bed is then tracer-free and ready for the next run.

To turn tracers in Ca^{2+} form into neutral particles in Na^+ form, NaCl solution is introduced. Oppositely, to prepare tracers for use, CaCl_2 solution is fed into a resin bed. Since the purpose of this step is to obtain fully-loaded resins, the exhaustion point, the point at which resins are fully loaded with calcium, is the center of attention. Therefore once the concentration of calcium in the outlet is the same as the feed, the resins are fully loaded and can be used as tracers. An example of calcium break through curve, as can be obtained during this resin loading process, is shown below (Appendix 1).

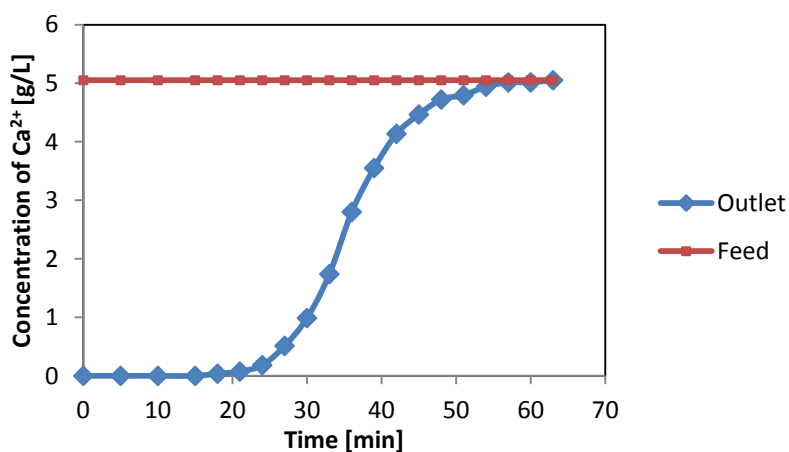


Figure 3.4: Loading Ca^{2+} onto resin

3.3.2 Experiments in Lab Scale

Figure 3.1 shows the setup of lab scale experiments. This lab-scale system was designed to mimic the situation in a downer, having particles exit at the bottom and more particles fed in from the top. It also had two-phase counter-current flow. The basic concept of this procedure was that the tracers were initially a neat layer in a fluidized bed. As the particles flowed downward and eventually exited the column, there was a continuous feeding of solids to maintain the bed level. To see how dispersed the tracers would be after travelling a distance inside the bed, the distribution of the tracers was monitored at the exit.

The S 1668 resins were used for the small scale experiments. The tracers amount was kept at 59 ml, giving a layer of resin 3 cm thick, for all runs. The bed height of fresh resin, H , varied from run to run but was predetermined. The volume of the fresh resin amount, V_{fresh} , was calculated based on the bed height. So the initial total volume of resin inside the bed including fresh resin and tracer was:

$$V_{bed} = V_{fresh} + 59 \quad (\text{Equation 3.1})$$

The volume of fresh solids feed, V_{feed} , was given by:

$$V_{feed} = V_{fresh} + 2 * 59 \quad (\text{Equation 3.2})$$

The feed volume was enough to replace the initial bed plus the additional layer of tracer, in case of high dispersion and to account for some tracers remaining in bed extensively long. The 3 resin volumes were measured, and put in three separate beakers.

Before inserting any particles into the column, the bottom outlet and the connecting tube from the hopper to the column were tightly clamped. The solids feed was put into the funnel. Water was pumped into the column via the distributor. As the column was half full, the fresh resin was poured in. After the particles settled, they were fluidized for about 10 minutes to be stabilized. In addition, water level had reached and passed through the uppermost outlet. The second pump was then turned on to pump some water into the hopper to create slurry so that solids could flow down as the clamp soon would

be opened. The tracers were now injected into the bed via a removable hopper which was temporarily placed at the top of the column. The tracers that had been set aside in a beaker was then poured into this hopper. Once all of the tracers exited the extending tube of the hopper and most of them settled, the hopper was then removed and the top and the bottom clamps were turned partially open. Solids and liquid mixture coming out from the bottom outlet was collected into beakers in intervals of time for a total duration of one minute. Depending on the targeted solids circulation rate, the clamps were turned more or less open such that the bed height was maintained. Once the hopper was empty of particles, the run was then finished and the samples were taken to be analyzed. Lastly, the remaining resins in the column was regenerated using 5% NaCl solution to convert any tracers left behind to the neutral particles.

The solids circulation rate, bed height, and liquid velocity were varied. The time interval between samples was not always the same, depending on the length of the run. Therefore the three mentioned operating conditions (SCR, H, and U_1) will be shown for each run in the results chapter, and the specific time intervals are listed in the raw data appendices.

3.3.3 Experiments in Pilot Scale

At this scale, the experiments were performed by varying only liquid flowrate and keeping the expanded bed height (185 cm from the distributor), and solids circulation rate ($G_s = 0.260 \text{ kg/m}^2\text{s}$) constant (Appendix A-2). The resins used were the SGC 650.

At the beginning, there was only fresh resin inside the riser and downer. Pumps were switched on to feed distilled water into the system. The liquid flowrate in the downer was set to the predetermined value, but the main and secondary liquid flowrates in the riser needed some adjustment in order to obtain the constant volumetric solids circulation rate of 148.2 ml/min.

The secondary flowrate being too high might cause some leakage in the solids feeding pipe, also called the lower seal. The upper seal is the solids returning pipe. Leakage in seals are disruptive in all applications because it transports buffer from one column to the other, leading to mixing of the buffers in the downer and riser. The buffers are

undergoing two opposite processes. Mixing them in any extent not only demotes the system performance, but also contaminates and ruins the product. Even though there was no chemical reaction in this particular system, effort was still made to mimic real-life applications as closely as possible. Ideally, a nicely-packed and slowly-moving-downward bed was desired for this section. In case of leakage, the auxiliary stream was reduced, then the primary stream was increased so that solids circulation rate remained unchanged.

Once the system had relatively stabilized, the downer bed had expanded and the height did not fluctuate very much, some resins deposit or withdrawal might be needed in order to have an expanded bed height of 185 ± 1 cm. Pressure became unbalanced once the solids volume in the downer suddenly changed. More time was given and more flowrate adjusting was done to achieve the overall stabilized system with some preset operating parameters. It was then ready for tracer injection.

The tracers were SGC 650 fully loaded with calcium. 550 ml of tracers were measured and inserted into the downer from the top via the large hopper. The nylon rope was pulled up tightly at first so that the small funnel blocked the other end of the pipe. When all tracers were in the pipe, the rope was held loosely and the small funnel fell down about an inch. The funnel then did not block the pipe anymore and the tracers came out and settled on the surface of the bed. The ball valves at the two sampling probes were then alternately partially opened to obtain solids samples. Since a certain volume - 3 ml approximately - of solid particles constantly remained in the probes after each sampling, it was essential to discard the first 3 ml of solids before taking the next sample. The mixture of solids and liquid was collected via these probes. When each experiment was finished, the samples were then analyzed, and the bed was refreshed using 2% NaCl solution to be ready for the next run.

3.4 Analytical Methods and Calibration Curves

What distinguishes tracers from neutral particles is the calcium content they hold. If the amount of calcium loaded onto the tracers in a particular sample can be measured,

calcium reading can be converted to the tracers mass. Therefore, the analysis method involved two steps: read the calcium and calculate the tracers mass.

First, to determine the calcium content, it was needed to diffuse the calcium from the solids phase to the liquid phase. Resins desorb calcium through the use of a regenerating liquid phase containing cations for them to exchange. NaCl was again selected to desorb the resin and capture the calcium. As the calcium was desorbed into the aqueous NaCl solution, there was possibility that it might be adsorbed back on some other particles because cationic resins have greater affinity for ions with more charge. To overcome this preference, the regenerating solution needed to have high number of moles of sodium. The high mole ratio N_{Na}/N_{Ca} would create a strong driving force to prevent undesirable adsorption of calcium during the desorption process. After vacuuming the excessive water, the resin was desorbed in a proper amount of concentrated NaCl solution using this high mole ratio, and the amount of calcium captured in the liquid was determined by titration method. Pipetting a volumetric amount, for example 1 ml, from the solution into a flask, adding 1 ml of colourless pH 10 buffer, and 0.3 ml of calmagite indicator, gently swirling this mixture, a bright pink solution appeared. Some distilled water could be transferred to the flask if it was easier to swirl. Following, this mixture was titrated using 0.01M EDTA titrant, drop by drop until the light green colour replaced the pink. Knowing the volumes of pipetted solution, $V_{titrated}$, and of titrant used, V_{EDTA} , the total amount of calcium desorbed from a particular solids sample could be found by using the following equation:

$$m_{Ca} = \frac{V_{EDTA} * 0.4}{V_{titrated}} * 200 \quad (\text{Equation 3.3})$$

The standard EDTA solution purchased from Fisher Scientific had molarity of 0.01, so the conversion is $1 \text{ ml EDTA} = 0.4 \text{ mg Ca}$. In some cases, EDTA was diluted, so the conversion factor would change.

Second, to relate the amount of calcium desorbed with the tracers mass collected, calibration curves were prepared. For the S 1668, tracers and fresh resins were weighed and put in 10 numbered labeled flasks. Their masses were recorded. The total masses

were roughly 15 g. Each flask with mixed resins was then desorbed using 200 ml of 9% NaCl, which had been found to be satisfactory as desorbing solution. The resulting mole ratio N_{Na}/N_{Ca} was in the range 30-120 (Appendix A-4). 200 ml of NaCl solution was poured in each flask, then the flask was constantly stirred on a stir plate for 15 minutes to ensure contact between the two phases. Following this batch desorption, calcium concentration was obtained by titration (Appendix A-5). The calculated amount of calcium was graphed against the weighed mass of tracers, which gave the calibration curve as shown below:

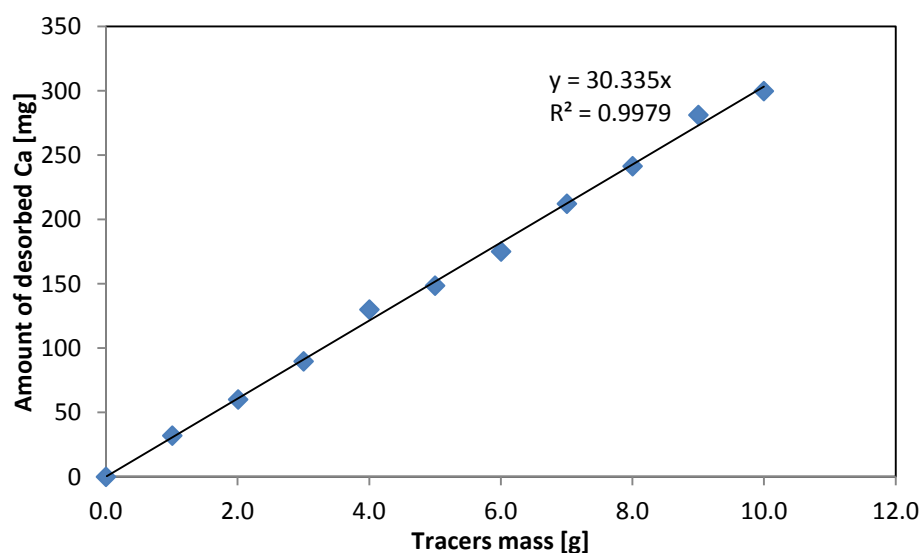


Figure 3.5: Calibration curve for S 1668 resins

Although the fresh resin mass was adjusted so that the total mass of a sample was about 15 g, the calibration equation was verified and thus justified even when the fresh resin mass was random. The calculated value of tracers mass using the equation is within 5% error when compared to the true value (Appendix A-7).

To prepare a calibration curve for the SGC 650, which was used in the pilot-plan experiments, is more difficult than for the S 1668 resin. First, because the samples were withdrawn from the center of the bed via a probe, the collected tracers were only a fraction of the total amount of tracers that had been injected into the column. This was significantly different than the small-scale experiments, in which case the samples were

collected from the column exit, and thus were not just a representative portion, but the entire solid particles. In the pilot, the collected SGC 650 tracers amount was very small compared to the total amount of a sample which included both tracers and fresh resin, so it was more sensitive with respect to the accuracy of the calibration curve formula and titration step. In order to be most accurate as possible, the range of tracer mass was narrowed down to 0 – 3 g, which was an appropriate range because in most cases, the collected tracers amount did not surpass this range. Titrant used was diluted 3 times from 0.01M EDTA to reduce the sensitivity of overshooting. Second, because SGC 650 has higher capacity than S 1668 (55.7 versus 34.7 milligram Ca^{2+} per gram resin), it also has greater affinity for calcium. Regenerating the resins completely 100% was found to be impractical. Therefore, some trace of calcium on fresh SGC 650 resin was accepted and accounted for when producing the calibration curve and when analyzing samples for the runs.

Similarly, tracers and fresh resins were weighed, recorded and put in flasks. The desorption and titration steps were the same. The flask that had only fresh resins revealed quantity of calcium per gram being held on the fresh particles. Using this value, the calcium that was desorbed from tracers was determined, and graphed against the tracers mass. The calibration curve for SGC 650 is presented below:

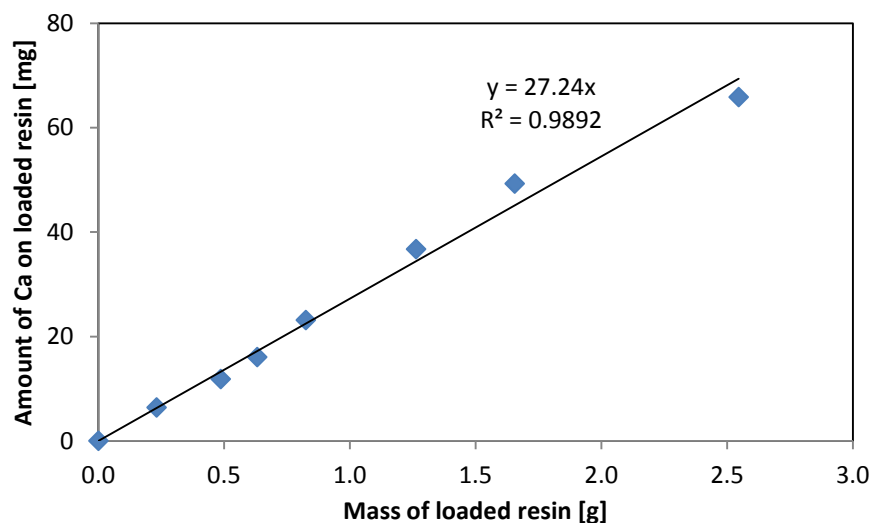


Figure 3.6: Calibration curve 1 for SGC 650 resins

After a number of runs, to check the capacity of the resins, the calibration curve was redone. Satisfyingly, the resins did not experience a significant capacity loss as demonstrated by the fact that the slope of the second curve was close to the one of the first curve with 6.8% deviation. Additionally, this method shows very good correlation despite the variation of calcium on fresh resins from batch to batch, as long as it was recognized and accounted in the calculation steps.

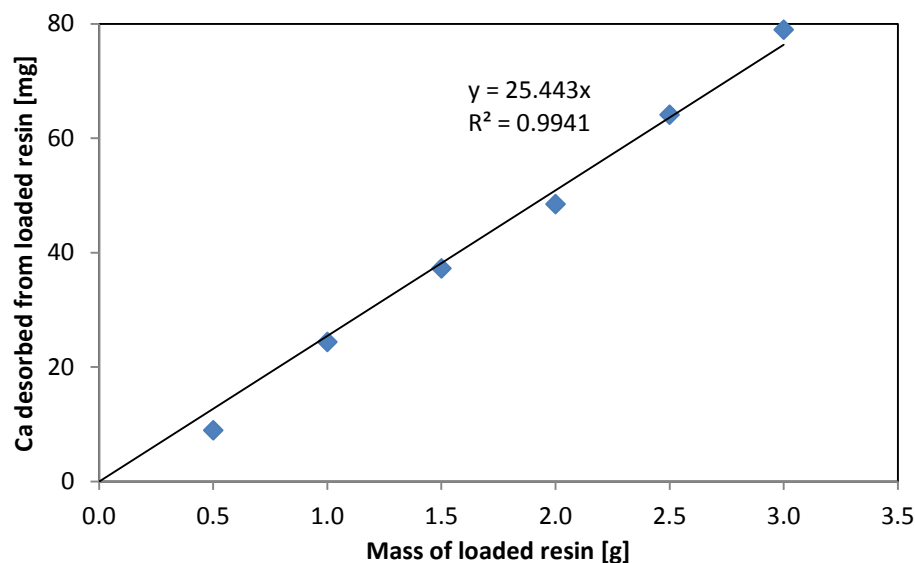


Figure 3.7: Calibration curve 2 for SGC 650 resins

3.5 Mathematical Treatment

Axial phase mixing is quantified by 2 numerical terms: axial dispersion coefficient – D_{ax} , and Peclet number – Pe . The dispersion coefficient D_{ax} (m^2/s) represents the spreading process. Large D_{ax} indicates rapid spreading of the phase once it enters the vessel, as indicated by tracers in this case. Small D_{ax} means slow spreading, $D_{ax} = 0$ means no spreading, hence plug flow. The Peclet number, given by uL/D , is the dimensionless group characterizing the spreading in the whole vessel (Levenspiel, 1999).

The formulae for D_{ax} and Pe are as follows (Levenspiel & Smith, 1957; Levenspiel, 1999):

$$\frac{1}{Pe} = \frac{1}{8} (\sqrt{8\bar{\delta}^2 + 1} - 1) \quad (\text{Equation 3.4})$$

$$D = \frac{uL}{Pe} \quad (\text{Equation 3.5})$$

where $\bar{\delta}^2$ is the dimensionless variance, related to the dimensional variance δ^2 and time average \bar{t} as following:

$$\bar{\delta}^2 = \frac{\delta^2}{\bar{t}^2} \quad (\text{Equation 3.6})$$

The dimensional variance and time average are calculated from a residence time distribution graph for a pulse experiment, using equations below:

$$E(t) = \frac{C(t)}{\int_0^{\infty} C(t) dt} = \frac{C(t)}{\sum C(t)} \quad (\text{Equation 3.7})$$

$$\bar{t} = \int_0^{\infty} E(t) \cdot t dt = \sum E(t) \cdot t \cdot \Delta t \quad (\text{Equation 3.8})$$

$$\delta^2 = \int_0^{\infty} E(t) \cdot (t - \bar{t})^2 dt = \sum E(t) \cdot (t - \bar{t})^2 \cdot \Delta t \quad (\text{Equation 3.9})$$

In literature, when liquid mixing was examined, tracer volume was as little as 5 ml, and injected very sharply. It could be considered as no mixing at the injection point, $D_o = 0$. Thus, only one RTD graph was needed. In the case of examining solids mixing, the ability to inject sharply is impeded, and the tracer concentration was monitored at a distance downstream of the injection point. The dispersion coefficient and Peclet number were then determined from the resultant RTD graph.

In this study, at the pilot scale if the tracers amount was too little, it would be easy to be missed, given that the collected samples were only a representative portion. Therefore the tracers volume was decided to be 550 ml in the pilot-scale experiments. This amount after being inserted and settled on the bed surface would definitely exhibit some mixing with other neutral particles in the bed. Therefore it could not be assume $D_o = 0$. For

these reasons, the solids samples were withdrawn at two axial locations: one closer to the bed surface – location 1, and one further downstream – location 2. For each experimental run, there were 2 resultant RTD graphs. Each of them yielded a time mean, and a variance. Because both time mean and variance are additive (Levenspiel, 1999), the difference between the two time means is the time the tracers take to travel from location 1 to location 2. The difference between the two variances is the additional spreading of the particles group after travelling that distance. Thus, the time mean and variance applied to equation 3.6 are defined by the following:

$$\bar{t} = \bar{t}_2 - \bar{t}_1 \quad (\text{Equation 3.10})$$

$$\delta^2 = \delta^2_2 - \delta^2_1 \quad (\text{Equation 3.11})$$

In the small-scale experiment, the tracers amount was much less, 59 ml. The injection took less than 30 seconds. Therefore it was legitimate to assume $D_0 = 0$, and the solids were collected at the exit only.

Chapter 4

4 Preliminary Results

This chapter presents the results from lab-scale experiments. The three parameters (solids velocity – U_s , liquid velocity – U_l , and expanded bed height – H) were varied to examine their impacts on the axial dispersion. The results showed the significant increase of axial solids dispersion coefficient especially with the increase of liquid velocity even in a 5 cm column. For this reason, the study in the lab-scale unit was discontinued to investigate the solids mixing in a larger column. Even though these data are from 5 experimental runs only, they are still very valuable in terms of method demonstration.

4.1 Impact of Solids Superficial Velocity on Axial Solids Dispersion

In a counter-current liquid-solids fluidized bed, when all operating conditions are kept the same except the solids velocity, including bed height, liquid flowrate, liquid and particle types, the expansion degree and voidage are not changed, and it is expected that the solids flow pattern would change.

For this purpose, two runs were carried out with solids velocities of 0.0874 and 0.123 mm/s. Their operating parameters and calculated values are shown in the table below:

Table 4.1: Impact of solids superficial velocity on solids dispersion

	Run 1	Run 2
H [cm]	14.8	12.2
U_l [cm/min]	4.84	4.84
U_s [cm/min]	0.524	0.739
S/L	0.108	0.153
\bar{t} [min]	25.17	13.0
δ^2 [min ²]	55.8	11.3
$\bar{\delta}^2$	0.0882	0.0672
Pe	26.2	33.3
D_{ax} [cm ² /min]	0.297	0.270

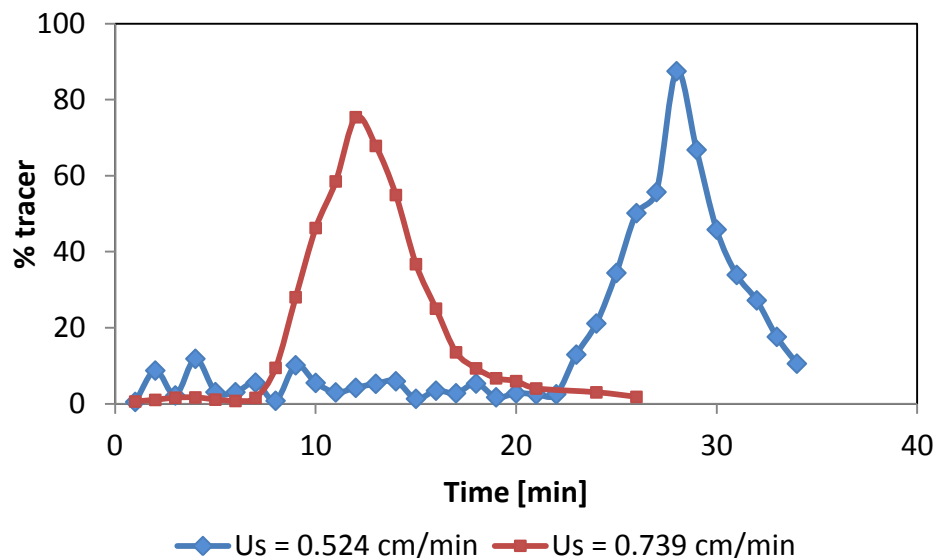


Figure 4.1: Comparing RTD at different solids velocities

The two experiments have very slightly different bed heights so they are considered as the same. The only variation is the solids circulation rate, or the solids velocity. Since the solids flow faster in run 2 than run 1, it is understandable that the time mean is shorter. The variance is much less in run 2, possibly because the residence time of the particles inside the fluidized bed is shorter when solids circulation is faster. The Peclet number is much higher in run 2 than run 1 as a result of lower variance. The dispersion coefficient is calculated to be 0.297 and 0.270 cm^2/min for run 1 and run 2 respectively. It can be seen that when solids velocity increases, it helps hinder the mixing of solids. This is thought to be reasonable because when the solid phase has a higher velocity, the time spent inside the bed is lower, so the particles would not get "rearranged" as much. However, given there are only two data points, this statement needs to be taken with caution. Also noted from this testing was the fact that the determined values of dispersion coefficients are very small compared to the reported ones in an expanded bed, up to 40 cm^2/s , and in a riser, D_{ax} of 245 cm^2/s or higher. There are a number of possible reasons including small column, liquid below U_{mf} , light particles and non-viscous liquid. The bed was in very close to an ideal case.

4.2 Impact of Bed Height on Axial Solids Dispersion

An experimental trial – run 3, was operated under very similar conditions as run 2 with only a difference of bed height, 12.2 and 34.7 cm respectively. Because the solids feeding and solids exiting were controlled manually by adjusting the clamps, it was difficult to obtain exactly same solids circulation rate, or solids velocity, however, their values were maintained closely for the two runs. Therefore these two trials are put in comparison to examine if the bed height has impact on the dispersion rate.

Table 4.2: Impact on solids dispersion when bed height changes

	Run 2	Run 3
H [cm]	12.2	34.7
U_1 [cm/min]	4.84	4.84
U_s [cm/min]	0.739	0.815
S/L	0.153	0.168
\bar{t} [min]	13.0	39.5
δ^2 [min ²]	11.3	98.7
$\bar{\delta}^2$	0.0672	0.0632
Pe	33.3	35.3
D_{ax} [cm²/min]	0.270	0.802

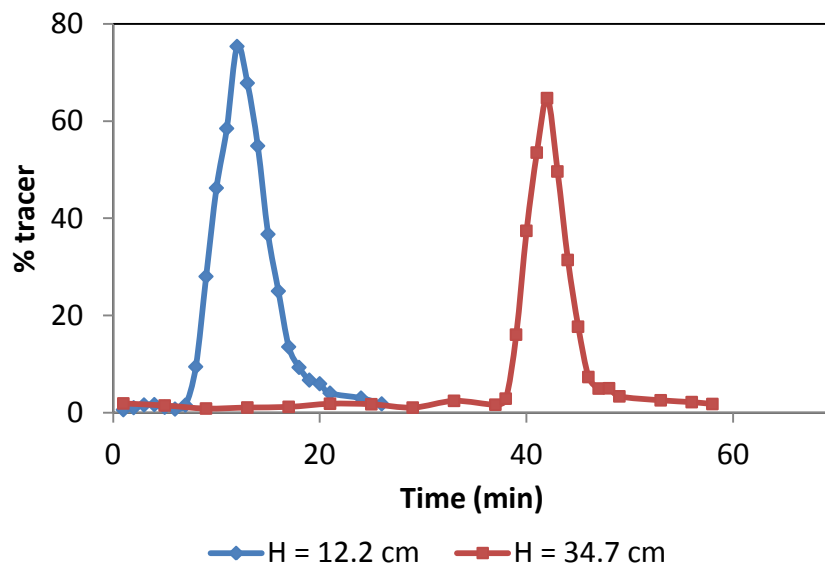


Figure 4.2: Comparing RTD when bed height changes

As the bed height increased 3 fold while the solids velocity remained almost the same, the time mean increased about the same factor as expected. However, the variance

increased significantly, 9 fold, indicating high dispersion of particles. The resultant Peclet numbers are about the same, providing the mixing coefficient in the run 3 is three times higher than run 2 since D_{ax} is proportional with the bed height ($D_{ax} = U_s H / Pe$). The substantial increase of D_{ax} was unexpected because dispersion coefficient defines the rate of tracers spreading per unit time. If tracers are injected at the same location in a fluidization unit, as long as the liquid and solids flows are unchanged, tracers spreading after a minute should not be influenced by the bed height. Under the same liquid flowrate, the solids concentrations would be the same for both cases, thus bed denseness cannot be a reason for this observation. The only factor that might be accountable for this is the distribution of liquid flow. The distributor used likely provided insufficient phase contact, leading to some dead zone near the base of the column. This section was not exerted any drag force on it, and therefore moved as a plug flow. The section above the dead zone experienced an upward force, therefore mixed more. Whereas the dead zone is the same, the section that had exertion of drag force would be longer in a higher bed. This is could be the reason why run 3 had higher dispersion coefficient than run 2.

4.3 Impact of Liquid Superficial Velocity on Axial Solids Dispersion

Three different trials were carried out at different liquid velocities. All other conditions were kept the same. The summary of operating parameters and the dispersion results are shown in the table 4.3.

Table 4.3: Impact on solids dispersion when liquid velocity changes

	Run 3	Run 4	Run 5
H [cm]	34.7	34.2	34.2
U_l [cm/min]	4.84	7.13	10.2
U_s [cm/min]	0.815	0.842	0.841
S/L	0.168	0.118	0.0824
\bar{t} [min]	39.5	39.1	26.3
δ^2 [min ²]	98.7	49.4	270
$\bar{\delta}^2$	0.0632	0.0322	0.392
Pe	35.3	65.8	7.74
D_{ax} [cm²/min]	0.802	0.437	3.71

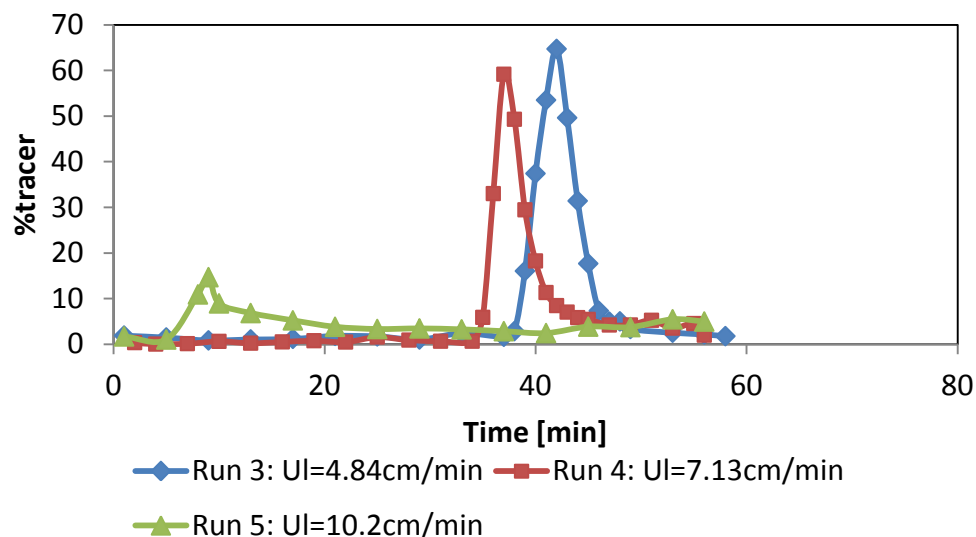


Figure 4.3: Comparing RTD when liquid velocity changes

During run 3, the unit was operated at liquid velocity lower than U_{mf} . During run 4, the liquid velocity just passed the minimum fluidization velocity, thus the solids started to become loosened up and the solids hold up decreased very slightly. The solids volumes therefore were about the same in these two trials, consequently the time means are quite close. They both appeared to have very sharp peak, indicating the tracers particles had about the same retention time, and posed minimum back-mixing inside the bed. It was different in run 5. Perhaps there was a large group of tracer passed through the bed and exited earlier, leading to the early occurrence of the peak. Lots of tracer particles got mixed with the fresh resin, and left the bed much later, leading to the long tail of the RTD graph. The dispersion coefficient increased significantly as well, the result of the well-spread tracers.

The increase of dispersion as liquid velocity increases was the motive for the solids mixing study in the pilot-scale LSCFB. As the column size is bigger, the solids phase undergoes greater extent of back-mixing (Limtrakul et al., 2005). Other than measuring the solids mixing degree in the aforementioned LSCFB apparatus, some internals designs were considered and examined their effects on flow pattern of solids phase.

Chapter 5

5 Internals Design

Internal baffles were added to the pilot scale assembly in order to evaluate their impact on solids mixing. Three different designs of baffles are described in this chapter, including their dimensions and assembly inside the downer bed.

5.1 Louver

Louver baffles are widely used in industrial gas-solid fluidization units due to its effectiveness of breaking bubbles (Zhang et al., 2009). They found that axial solids dispersion in baffle-free gas-solids fluidized beds ranges from 0.01 to 0.13 m²/s. When multi-layers of louver were installed, the resultant mixing coefficient was significantly reduced. It demonstrated that louver had strong suppression on solids back-mixing.

In the current testing unit which is a liquid solids fluidized bed, the ability of the louver to break bubbles becomes unnecessary. However, the way a louver is designed with inclined plates is still promising for the purpose of hindering the random motion of particles. If louver baffles are inserted into a counter-current LSF_B, while the particles flow downward, some of them are dispersed axially and move upward. The inclined plates would have the tendency to prevent the backward path of the solids, and therefore suppress the axial solids mixing.

To design a louver, the three critical dimensions are the height of the plates, the angle of inclination, and the spacing. The downer diameter is 10 cm. To make a louver, a PVC pipe whose O.D. is 9.9 cm and I.D. is 8.9 cm is selected to be the outer ring. The plates are made of acrylic with a thickness of 1.6 mm. With the space inside the ring, the dimensions of the louver was selected as shown in Figure 5.1.

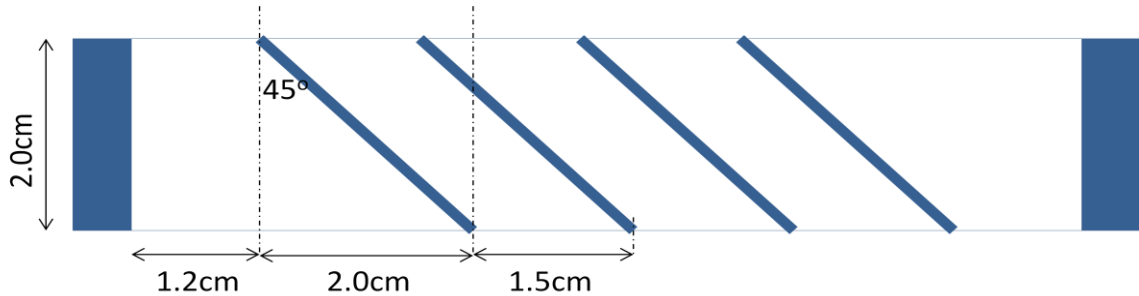


Figure 5.1: Louver baffles

The ring is 2 cm thick. There are 4 inclined plates inside, 1.5 cm apart. If the number of plates were more, the spacing between two plates would be too small, making the opening path too narrow. It may result in clogging and too much restriction on particles flow. This is definitely undesirable for a solids circulation system. If there were fewer plates, then the effect of a louver on solids dispersion might not be noticeable. The angle was decided to be 45° so that the horizontal projection of the plates is 2.0 cm, which is longer than the spacing. This ensures there is no opening from the top view of the louver. As the particles are moving upward, this backward movement is interrupted by the louver because there is almost no straight path, except the path near the edge. The down flow of the solids should not be constricted due to the gravitational force and pressure difference.

There is some negative in this design to be considered as well. As the particles flow downward, they are constrained to move in one direction. As a result, one side of the bed could have high concentration of solids while the other side could become more dilute. It may create a swirl of solids underneath the louver to balance out the solids holdup. The small circulation of solids is another cause of solids dispersion. Therefore, the louver may reduce but also promote solids mixing. It is important to know which effect is more dominant and under what conditions.

Four layers of louvers are inserted inside the downer bed, 47 cm apart. They are arranged so that the direction of the plates are alternative. The bottom layer is at 20 cm and the top layer is at 169 cm above the ring distributor. The top sampling probe (Probe 1) is between the top two layers while the other probe is between the bottom two layers of louver (Figure 5.4a)

5.2 Mesh

The next design of baffles is a mesh. It came from a completely different approach than the louver. While the louver has a thickness, so creates a "hallway" path which constrains the solids flow patterns. That constraint has both positive and negative effects. For this mesh design, there is no inclination angle or narrow pathways. The particles passing through the mesh would not get pushed to one direction, thus are unlikely to circulate in the area below the baffle.

In order not to cause much restriction to the fluidized bed, the mesh was designed not too dense, half inch apart. The rod itself is 1 mm diameter. The percent opening area at these dimensions is 84.6%. There are also 4 layers of mesh inside the bed at the same locations as the louver (Figure 5.4b).

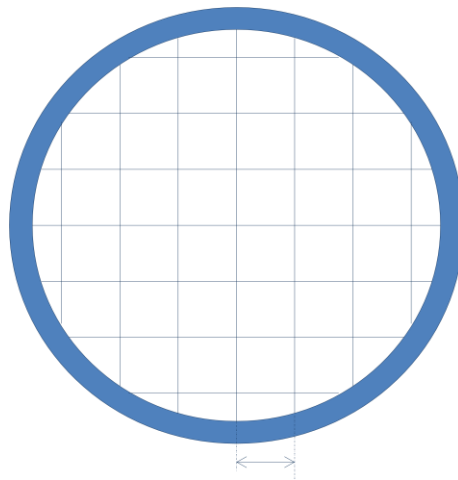


Figure 5.2: Mesh baffle

5.3 Vertical Plane

In addition to experimenting with two horizontal baffles, this project included the opportunity to investigate a vertical baffle. A vertical plane made of acrylic, 1.6 mm thick is put inside the downer bed. The purpose of this approach is to add extra wall friction to the unit. Observed in a conventional LSFb, the solids axial dispersion is worse near the wall region. It is because most particles flow upward in the core region, so not so much back-mixing there. Yet, in the annulus, some flow upward, some flow downward, leading to more severe mixing. In the riser, although there is no information

on local dispersion, it still can be expected to have the same trend as in an expanded bed – more severe mixing near the wall. The particle-wall collision extracts energy from the fluid. The energy becomes less sufficient to support the particles, thus the particles fall down. The wall effect does not work in favour of the riser and expanded bed, but works in favour of the downer because convective motion of particles is also downward.



Figure 5.3: Vertical plane

As vertical baffle is inserted into the column, it divides the bed into two halves. It has 8 evenly spaced windows. The windows are to reconnect the two sides of the bed so that the solids concentration can balance itself out if it happens to have one side denser than the other. These openings should be arranged so that the length of the plane sections, 9 cm in this case, should be less than the diameter of the column. The plane is placed at 40 cm above the distributor and extends 113 cm long. The tip of probe 1 is at the center of

the bed and at the very top window while the tip of probe 2 is at the very bottom window (Figure 5.4c).

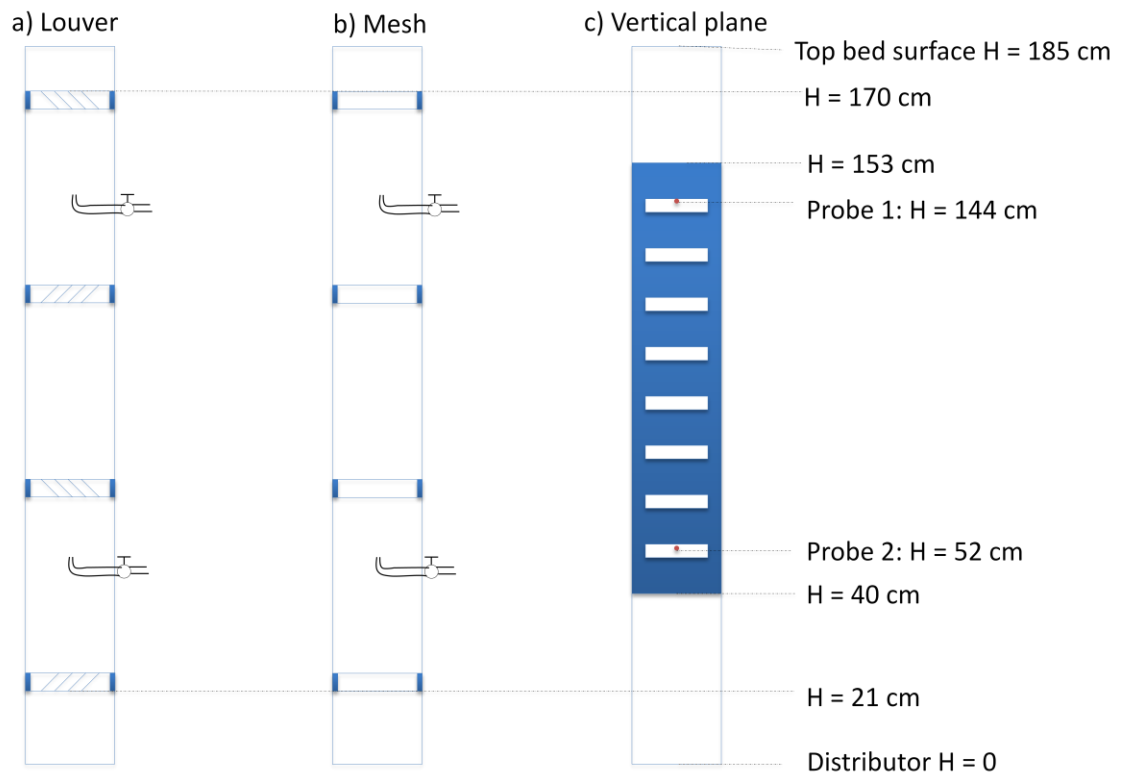


Figure 5.4: Positions of the baffles in the downer

Chapter 6

6 Formal Results

The development of the methodology used and the results of the pilot-scale testing are discussed in this chapter. The experiments were carried out at three different operating liquid velocities using all 4 setups: baffle-free, 4 layers of louver, 4 layers of mesh, and 1 vertical plane, such there are 13 sets of data in total including one repeated run to check the reproducibility of the method. The residence time distribution graphs were collected at two probes and used to calculate D_{ax} and Peclet number. The results were then compared among the setups.

6.1 Development of Methodology

Measuring phase mixing is used to gain insight into how the particular phase behaves within the bed. Regardless of what methods are used, a type of tracer(s) has to be introduced. For example, when liquid mixing is the object of study, aqueous tracer is injected into the bed. A commonly used aqueous tracer is concentrated NaCl or KCl. The tracer concentration (C) is measured at a distance away from its injection point downstream. The dimensionless concentration (C/C_0) is graphed against time, resulting in a residence time distribution graph.

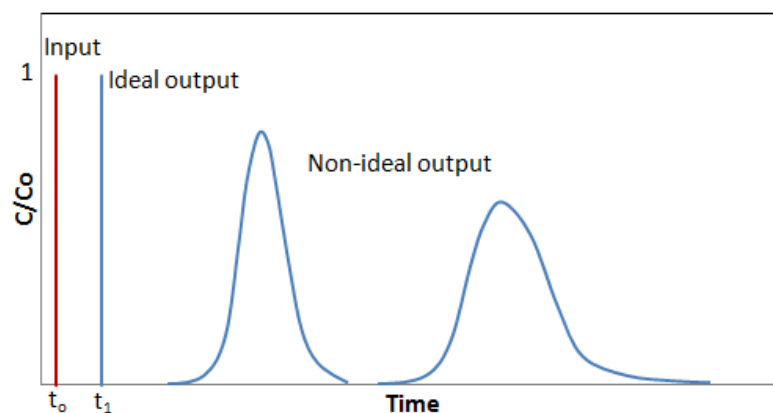


Figure 6.1: Residence time distribution graph

To have a sharp input as shown in Figure 6.1, the volume of tracer has to be small and must not disrupt the flow of liquid. In an ideal case, the output response curve would look exactly the same as the input curve. In reality, there is always mixing between the tracer and the other elements present in the bed. The narrower curve shows an example of an excellent phase flow in a fluidized bed with little mixing. A broader curve indicates mixing increase, therefore less favourable.

Particle tracking is more difficult than liquid phase tracking. It requires solid tracers that have the same physical properties such as size, density and shape, as the fluidized particles, while also being detectable, e.g. distinguishable from normal particles. At the same time, they have to be reversible, e.g. such that they can become indistinguishable from normal particles when necessary, to avoid tracer accumulation within the bed.

The second requirement for mixing study experiments is a tracer-tracking method. There are several methods that have been used to measure solids mixing in a riser, and an expanded bed, yet none of them can be used in a downer.

One of the tracking methods is called phosphorescent tracer particle technique. The method employs the use of phosphorescent material which becomes fluorescent after being illuminated by a pulse of strong light. The fluorescent light intensity is measured at some points downstream, and then analogically converted to the amount of the phosphorescent tracers. A calibration curve is conducted in readiness for this analog conversion. The limitation of the technique is that the tracers stay fluorescent for a very short period of time, about 60 seconds. The retention time of particles in a downer is relatively long, depending on bed volume and the solids circulation rate, but substantially longer than 60 seconds. Therefore this technique cannot be used in a downer.

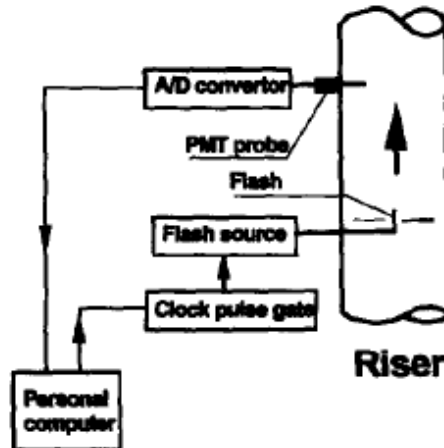


Figure 6.2: Illustration of the phosphorescent tracer method (Wei & Zhu, 1996)

The second method is optical fiber probe. Using this method, the particle velocity can be obtained at different locations of a cross-sectional area. Having a radial distribution of particle velocity also yields solids dispersion coefficient. Optical fiber probes use one or more fibers to project light on the flow, then two or more fibers that detect the reflected light. Figure 6.3 shows the 2-fiber probe detector. These probes are used to study particles in the riser, where the particles travel quite fast and therefore keep the same arrangement, a frozen pattern map, as they pass from the lower fiber to the higher fiber, resulting in two similar signals with the only difference being a time shift. Knowing the distance and the time shift, the particle velocity is determined at a particular location (Figure 6.3). Although this works well in the riser, this instrument cannot be used in downer because particles travel very slowly, thus becoming rearranged within the distance between the two fibers. The signals received at the lower and the higher fiber then look dissimilar, leading the computer to be unable to recognize it is the same group or particles passing by. It therefore cannot measure the velocity of the particles.

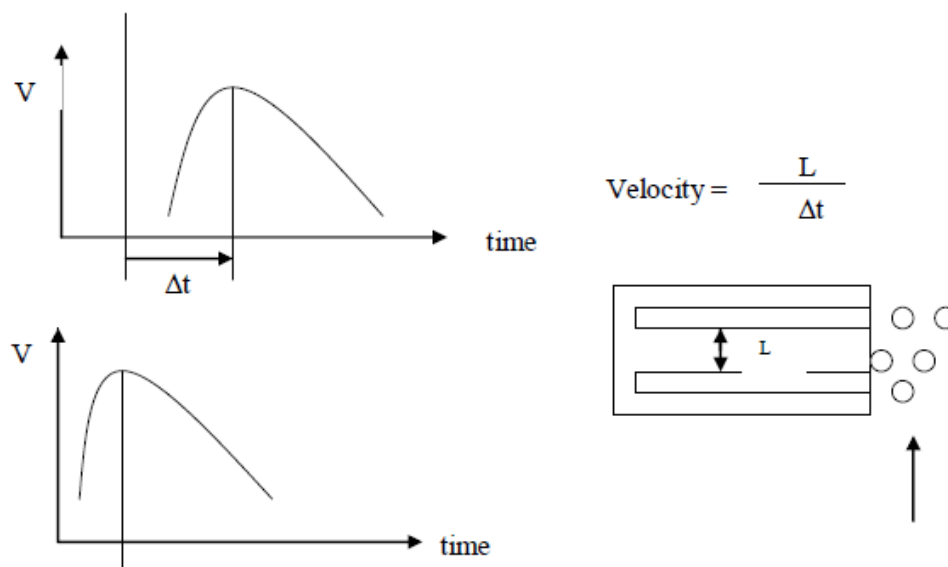


Figure 6.3: Particle velocity measurement by using two-fiber sensor (Nieuwland et al., 1996)

Other available sensor techniques, including capacitive (Green, 1981; Sun et al., 2008), electrostatic (Gajewski, 1999a; Gajewski, 1999b; Xu et al., 2009), ultrasonic (Sheen & Raptis, 1985), and radiometric (Linn & Sample, 1982) sensors, all of which require a frozen pattern map, similar to the optical fiber probe method described above. Therefore they cannot be utilized in the downer study.

A popular method that has been used to track particles is the computer-automated radioactive particle tracking (CARPT) technique. The concept of its functionality was described in Section 2.3.3 and most commonly, it is used in the riser. There is one study in which the authors used CARPT to successfully measure solids mixing in a dense bed (Limtrakul et al., 2005), where solids holdup was as high as 0.51. This method possibly can be used in a downer. However, the access to this instrumentation was unavailable.

Due to the limits of available instrumentations that can detect the motion of particles non-invasively in a dense and slow-moving fluidized bed, a new method was developed which was still based on the residence time distribution concept.

6.1.1 Ion-exchange Resin

It is challenging to find an appropriate type of tracer. As mentioned, the tracer is required to have the same physical properties (size, density and shape) as the neutral particles which constitute the bed. In addition, the tracer has to be detectable but not permanently. Ion-exchange resin is a great option because of the ability to change the ionic form.

Resin is categorized into 4 groups: strong acid cationic (SAC) resin, weak acid cationic (WAC) resin, strong base anionic (SBA) resin, and weak base anionic (WBA) resin.

- SAC resin has functional group of sulfonic acid groups and can exchange cations at any pH. It also has the highest density range $1200 - 1300 \text{ kg/m}^3$. This type of resin however requires a large amount of solution for regeneration, 2 to 3 times of the solution amount required for WAC resin. SAC resin has high affinity towards ions with high electron charge and high molecular weight and vice versa.
- WAC resin derives their functionality from carboxylic groups. WAC is regenerated much more efficiently compared to SAC. Almost complete regeneration can be achieved with a stoichiometric amount of acid. This type of resin has limited capacity below a pH of 6.
- SBA resin has quaternary ammonium exchange sites. This ion-exchanger can operate at all, or almost all, range of pH. Some SBA resin has pH range of 0 – 12, for example Lewatit S 6368. Anionic resin commonly has low density range of $1010 - 1100 \text{ kg/m}^3$.
- WBA resin contains polyamine functional groups. Since it adsorbs only strong acids, it has limited capacity above pH of 6. This weakly ionized resin is also easy to be regenerated as WAC resin.

Any type of resin can be employed. Tracer and neutral particles are same kind of resin but in different ionic forms. SAC resin was used in this study for the ease of tracer preparation and regeneration without restriction of pH range. Also SAC has the highest density, therefore it is easier to settle and works in favour of a down flow for particle bed.

Two ionic forms – Na^+ for neutral particles and Ca^{2+} for tracer – were selected among many other ionic forms such as H^+ and Ba^{2+} for a number of reasons. Firstly, to regenerate the entire bed of particles after each run to obtain tracer-free bed, in other words, to convert any remaining tracer to neutral particles, Na^+ solution was fed into the column. NaCl was used since it was not as costly as many other chemicals. Secondly, NaCl was also used to desorb particle samples during the analytical steps. Using a chemical that is inexpensive, benign and still serves the purpose makes the most economical sense. Lastly, calcium chloride was used to prepare tracer. Calcium concentration can be determined easily and accurately using titration method. Certainly a different ionic form may be employed if a convenient method to measure the concentration of that particular ion is available.

The calcium content is what makes the tracer detectable. As the tracer is in a bed of neutral particles, it is important that the tracer do not exchange calcium for sodium with the neutral particles. To determine if this situation occurs, random amounts of tracer and neutral particles were put into a beaker filled with distilled water – the fluidizing liquid in the experiments. After 48 hours, the concentrations of calcium and sodium in the liquid phase were zero. Consequently, resin does not exchange ions in a ion-free medium. This again proves resin is an excellent choice of particles when studying solids mixing.

6.1.2 Procedure

The procedure of this method includes 5 main steps. (More details can be found in chapter 3)

1. Tracer preparation: resin is loaded with calcium and becomes tracer
2. Operation and sample collection: the particle bed is fluidized stably, the tracer is injected into the column and the concentration of the tracer is measured downstream by collecting particles samples.
3. Analysis: determine amount of tracer in each sample collected. A calibration curve, which relates desorbed amount of calcium with the mass of tracer, is prepared in advance.

4. Mathematical treatment: conduct residence time distribution graph and calculate the dispersion coefficient and Peclet number.
5. Bed regeneration: load resin with sodium to obtain a bed of neutral particles for the next experiment.

6.1.3 Limitations

The methodology has some limitations that make it more suitable for lab-scale experiments. In a large column, such as the pilot-scale unit used in this study, the volume of the neutral particle bed is very high. Therefore, the required amount of tracer is very high as well. Injecting this amount into a stably fluidized bed may cause disturbance. Moreover, the sample collection is more difficult and more challenging in a large column than in a small column. Samples withdrawn from a lab-scale unit can be all particles that pass by the measuring point at a certain time. To replace the particle loss and maintain the bed height, new particles can be fed in by a separate and simple solid feeding system. It is infeasible to perform sample collection in the same manner in a pilot-scale unit because withdrawing the entire layer that passes by the measuring point for each sample will quickly reduce the bed height, thus affect the pressure balance of the system. For this reason, particle samples can only be withdrawn locally. The tracer is more difficult to be detected in that case.

This methodology was used to measure solid mixing in a pilot-scale LSCFB system. The experimental procedure and mathematical treatment were kept consistently in order to compare the solid mixing in baffle-free and baffled models.

6.2 Operating at $U_l = 1.45U_{mf}$

Since the solids samples were taken at two different axial locations, there are two resultant RTD graphs under each condition. In this section, 4 setups of the downer were run at the same fluidizing liquid velocity of 1.04 mm/s. The resultant RTD graphs for each model are shown below.

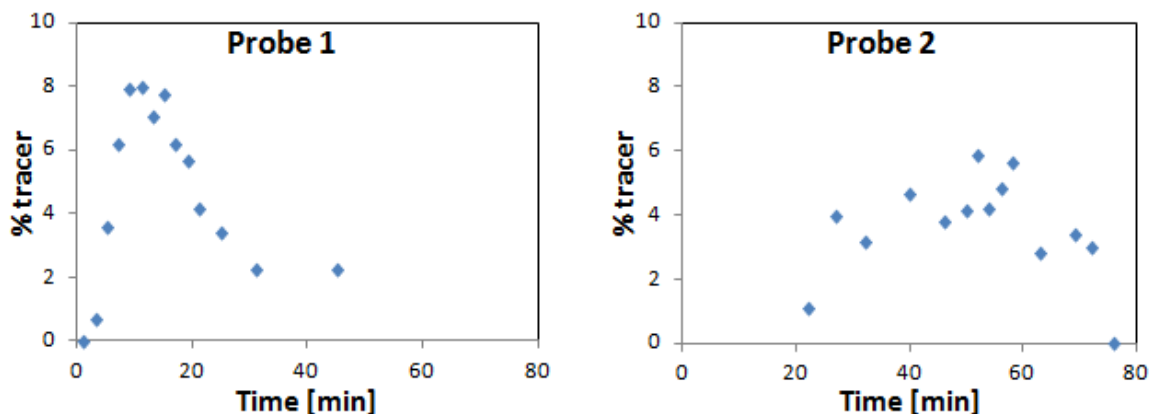


Figure 6.4: RTD graphs in baffle-free setup at $U_1 = 1.45U_{mf}$

It is seen that the RTD graphs at this scale do not show sharp peaks as in the lab-scale unit due to a number of reasons. The first is the amount of tracers input compared to the neutral particles present in the bed. In the small-scale unit, the resin bed volume is small (180 – 622 ml), so the tracers load is about 9.5% to 32.7% of the fresh resins inside the bed. In the large scale, the volume of fresh resin in the beds is almost 15 L, so the 550 ml tracer represents only 3.7% of the fresh resin bed. Increasing the tracer amount would have made the detection task easier, however too large a volume of particles settling on bed surface could cause too much disturbance to the bed. Combined with the increased time and cost of chemicals that would be required to prepare the tracers and regenerate the bed after each run, it was decided to keep the tracer amount at 550 ml. The second reason for the broad peak of the RTD graphs is the local sampling method. In the lab-scale setup, the sampling was done at the column exit and collected all exiting particles. In this pilot-scale setup, the sampling was within the bed and collected some particles at the center to represent the particle layer at that cross-section, therefore requiring extrapolation to total tracer volume. The third reason is the distances from the injection point to the measuring points. Probe 1 and probe 2 are 41 cm and 133 cm from the injection point respectively, such that the RTD graphs would look broader. For all of these reasons, the RTD graphs conducted at this pilot scale do not have clear peaks as seen in the preliminary results section.

Following are the resultant RTD graphs after one of the baffle designs is installed.

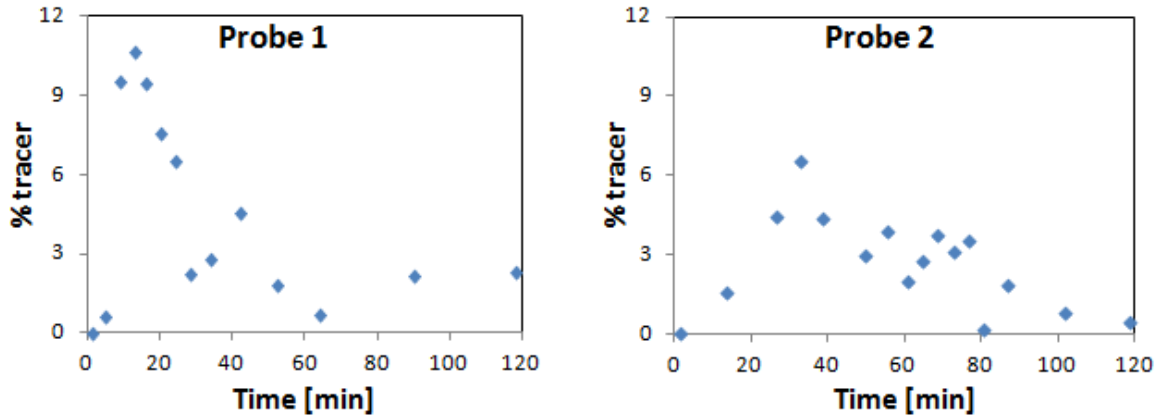


Figure 6.5: RTD graphs in lower baffle setup at $U_1 = 1.45U_{mf}$

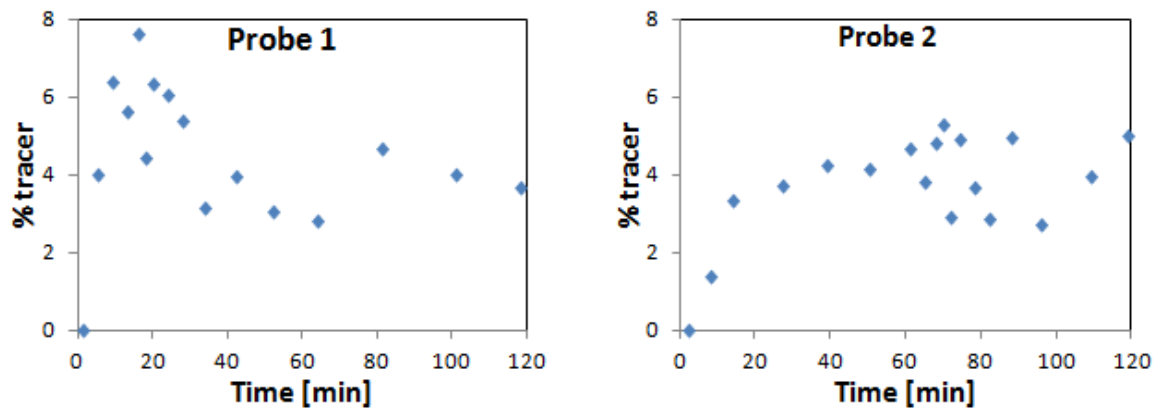


Figure 6.6: RTD graphs in mesh baffle setup at $U_1 = 1.45U_{mf}$

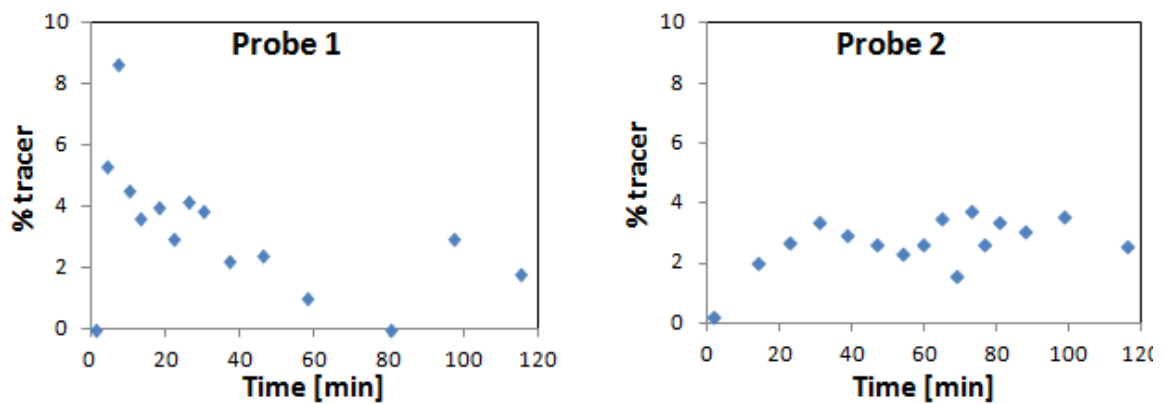


Figure 6.7: RTD graphs in vertical baffle setup at $U_1 = 1.45U_{mf}$

It is consistent that the RTD at the lower location, a greater distance from the tracer injection point, is broader than the one at the higher location. Also the shape of the probe 1 RTD can predict how the probe 2 RTD shape will appear. More specifically, among the three baffled models, in the louver case, the probe 1 RTD looks narrowest, which leads to the neater shape of the graph at the probe 2. In the mesh case, the graphs look most dispersed.

The injection was done similarly for all cases but because it is still a manual method, it is possible to have deviation between runs. Thus, the probe 2 graph is compared with probe 1 graph to determine the additional time mean and variance. These two values are used to calculate the Peclet number and the mixing coefficient. They reveal how much axial dispersion the particles undergo as they travel from probe 1 to probe 2, a distance of 92 cm.

The table below summarizes the numerical results:

Table 6.1: Result summary ($U_1 = 1.45U_{mf}$)

	Baffle-free		Louver		Mesh		Vertical plane	
	Probe 1	Probe 2	Probe 1	Probe 2	Probe 1	Probe 2	Probe 1	Probe 2
$\bar{t}_{1,2}$ [min]	19.4	48.4	21.4	44.7	22.3	48.0	19.9	46.3
$\delta^2_{1,2}$ [min ²]	123	205	119	256	128	282	145	290
\bar{t} [min]	29.0		23.4		25.7		26.4	
δ^2 [min ²]	81.3		137		155		145	
$\bar{\delta}^2$	0.0969		0.250		0.234		0.208	
Pe	24.1		10.9		11.5		12.6	
D_{ax} [cm ² /min]	7.07		15.6		14.8		13.5	
[mm ² /s]	11.8		26.0		24.6		22.4	
Effect	100%		220%		208%		199%	

The result shows at a low velocity of fluidizing liquid, the baffle-free model produces the least axial dispersion of solid phase while other three models increase the solids dispersion by 99% to 120%. Among these three, the louver has the most negative effect, possibly due to the swirl of particles in the area below the baffles.

At this low flowrate, the bed expands about 7%. With this little expansion, the bed is still very close to the packed bed state and therefore experiences very minor solid back-

mixing. In this case, when internals are inserted within the bed, they only act as disruption to the smooth flow of particles. In conclusion, at very low liquid flowrate the use of baffles would have a negative impact on axial dispersion, and are therefore to be avoided.

6.3 Operating at $U_l = 2.66U_{mf}$

The liquid velocity was increased to 1.90 mm/s, which is 2.66 times the minimum fluidization velocity. At this velocity, the downer bed expanded about 17%. The liquid flows faster, making the solids mix randomly to a greater degree. Consequently, detecting the tracers becomes somewhat more difficult. Nevertheless, if every experiment is done the same, the final results should still be comparable. Below are the residence time distribution graphs for 4 setup models at liquid velocity of 1.90 mm/s.

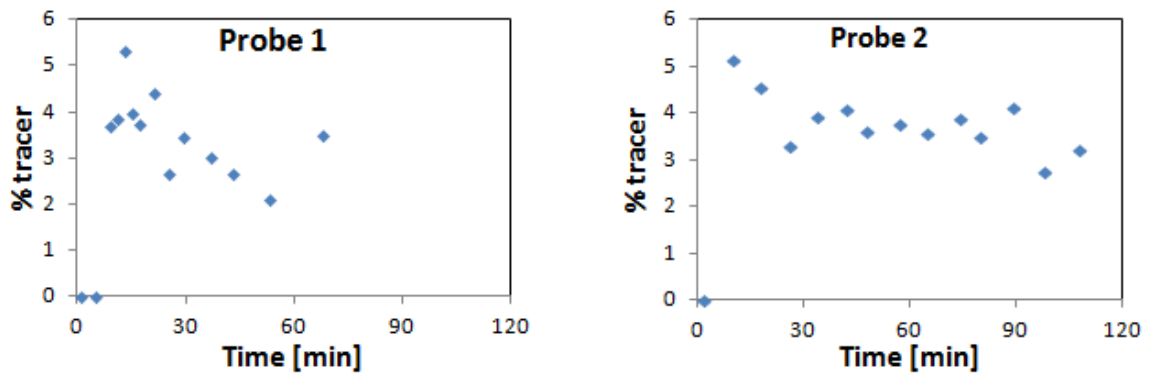


Figure 6.8: RTD graphs in baffle-free setup at $U_l = 2.66U_{mf}$

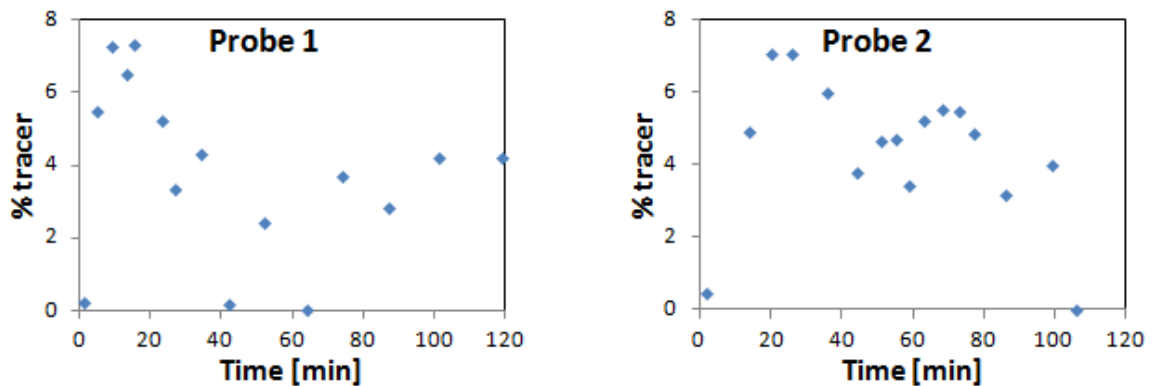


Figure 6.9: RTD graphs in lower baffle setup at $U_l = 2.66U_{mf}$

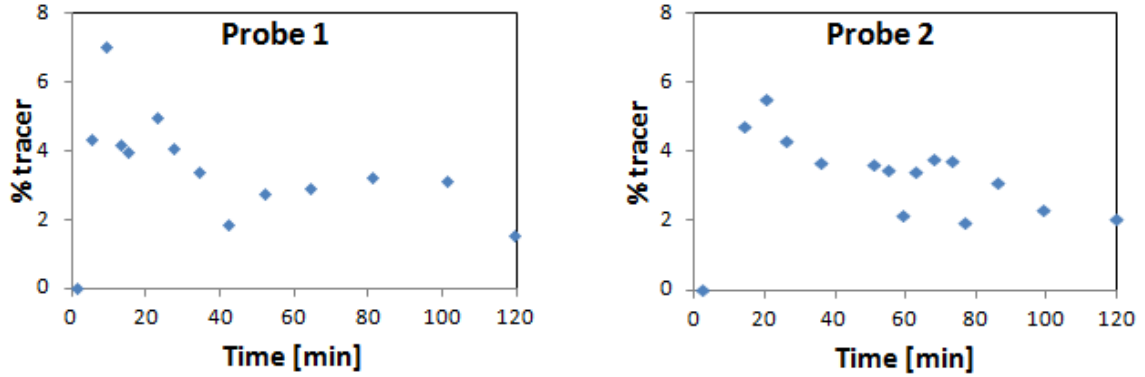


Figure 6.10: RTD graphs in mesh baffle setup at $U_1 = 2.66U_{mf}$

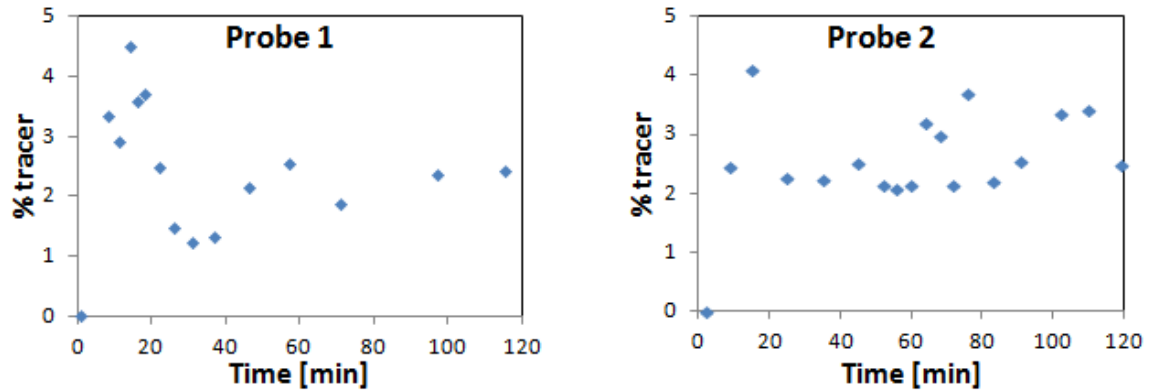


Figure 6.11: RTD graphs in vertical plane baffle setup at $U_1 = 2.66U_{mf}$

From the shape of the RTD graphs, one can tell that the solids are more dispersed at this velocity of liquid. Among these models, the baffle-free bed has the most severe solids mixing as the peak in the probe 2 graph is least discernible. The graphs of the louver and mesh models appear to be most promising. The Peclet number and the dispersion coefficient were calculated for each case.

Table 6.2: Result summary ($U_1 = 2.66U_{mf}$)

	Baffle-free		Louver		Mesh		Vertical plane	
	Probe 1	Probe 2	Probe 1	Probe 2	Probe 1	Probe 2	Probe 1	Probe 2
$\bar{t}_{1,2}[\text{min}]$	35.0	54.0	22.7	50.8	30.6	51.2	33.4	54.7
$\delta^2_{1,2} [\text{min}^2]$	351	881	204	724	363	784	377	898
$\bar{t} [\text{min}]$	19.0		28.1		20.6		21.3	
$\delta^2 [\text{min}^2]$	530		520		420		522	
$\overline{\delta^2}$	1.47		0.657		0.988		1.15	

Pe	3.11	5.33	4.03	3.66
D_{ax} [cm ² /min]	54.8	32.0	42.2	46.6
[mm ² /s]	91.3	53.3	70.4	77.6
Effect	100%	58%	77%	85%

When the liquid velocity is higher, bed expansion increases no longer acting close to plug flow, and the solids motion in the bed is no longer smooth. At this point, the presence of the baffles begins to hinder the random solids arrangement. It is confirmed that the downer with the layers of louver baffles has the lowest dispersion coefficient and the highest Peclet number. Although the inclined plates cause some local solids circulation, they disrupt the upward path of particles. At this operating condition, the positive effect outweighs the negative effect of local solids circulation, and consequently the overall outcome of louver is desirable as it helps reduce the back-mixing of particles in the downer by 42%. The mesh baffle and the vertical plane also suppress the solids dispersion by 23% and 15% respectively. It is supposed that these baffles not only add some internal friction to the bed, but also calm the motion randomness of the solids phase. However, their designs are probably too simple in that many particles bypass the mesh via the openings, or do not feel the friction caused by the plane. As a result, the mesh baffle and vertical plane help constrain the longitudinal dispersion of solids but not as effectively as the louver.

6.4 Operating at $U_l = 3.86U_{mf}$

With further increase of liquid velocity, the effectiveness of the baffles were again observed. The liquid velocity was 2.77 mm/s and bed expansion was about 27%. All other parameters were kept the same, including expanded bed height, solids circulation rate. At this liquid velocity, some circulation of solids inside the bed became more visibly obvious despite the bed was dense with dark resin particles, indicating the intensive mixing of particles. The conducted RTD graphs are below:

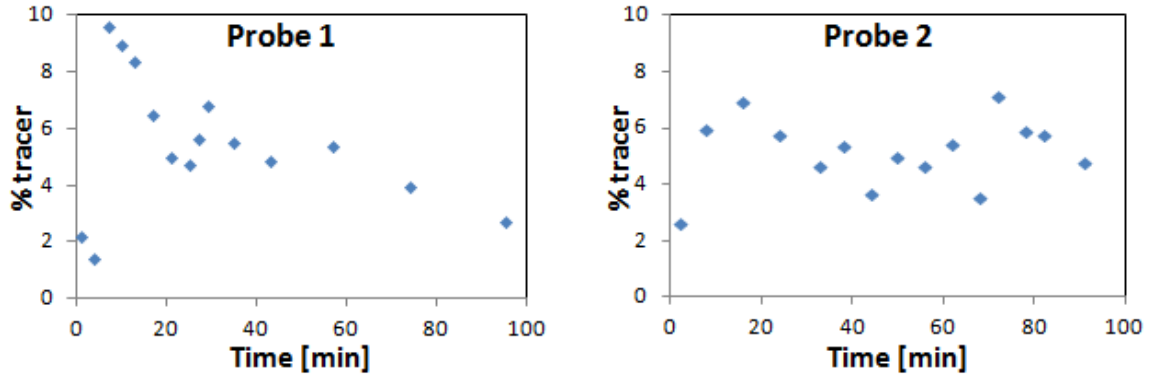


Figure 6.12: RTD graphs in baffle-free setup at $U_1 = 3.86U_{mf}$

At the starting point – probe 1, the solids were not dispersed much as a clear peak is observed. At the lower sampling point, the graph shows double peaks. It means there was a large group of particle that passed through the bed quickly while the other group delayed. It can be predicted that the Peclet number will be low and the mixing coefficient will be quite high at this condition.

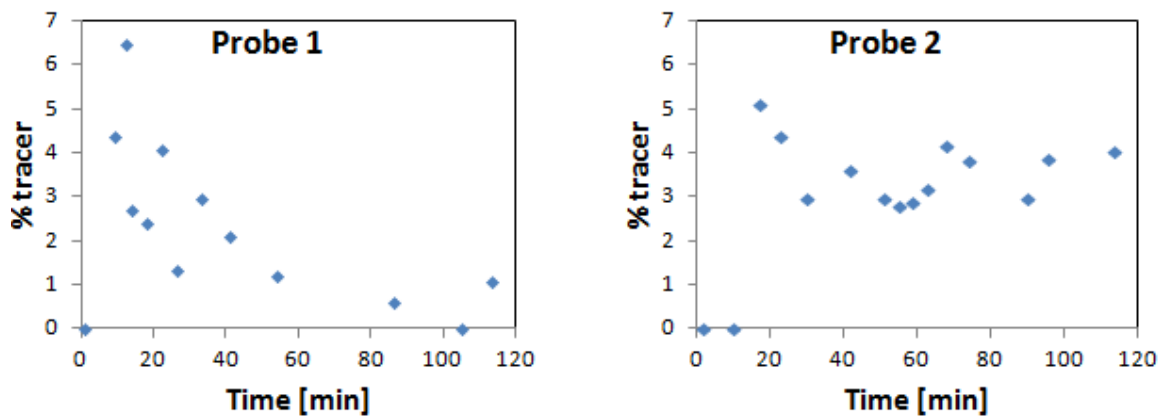


Figure 6.13: RTD graphs in lower-baffled setup at $U_1 = 3.86U_{mf}$

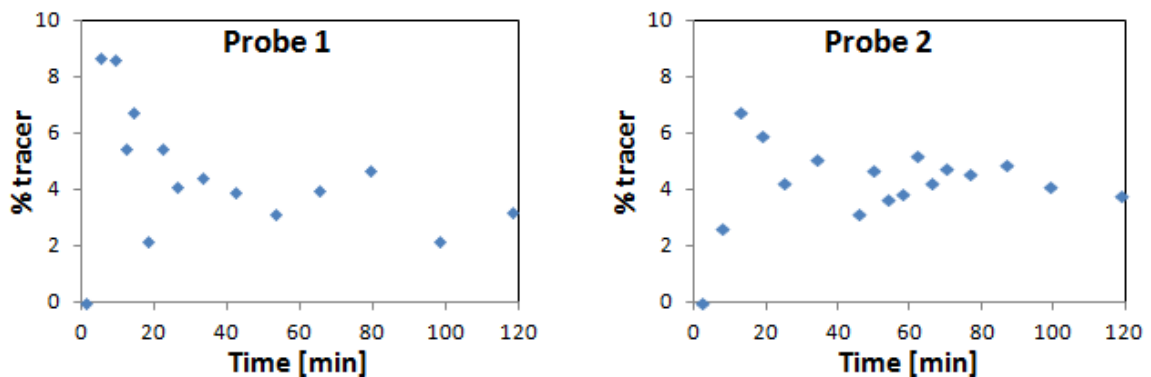


Figure 6.14: RTD graphs in mesh-baffled setup at $U_1 = 3.86U_{mf}$

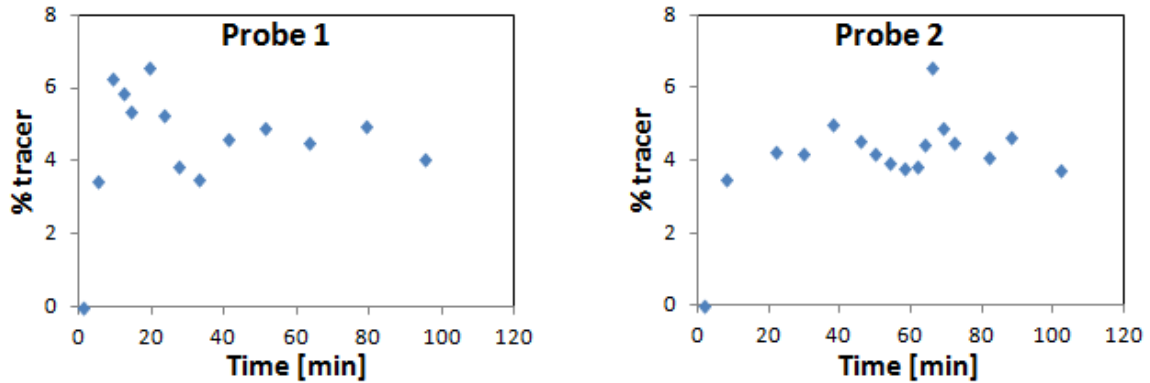


Figure 6.15: RTD graphs in vertical plane setup at $U_1 = 3.86U_{mf}$

No double peaks are observed in the RTD graphs for the baffled trials. It is the first sign of the dispersion reduction due to existence of the internals. Among the three baffles, the vertical plane has the broadest shape. It does not appear to offer as strong mixing suppression as the mesh and the louver baffle. For each setup, the solids dispersion is quantified. Time mean and variance are calculated for each graph. With the information of bed height and solids velocity, Pe and D_{ax} are determined. The summarized values are shown below.

Table 6.3: Result summary ($U_1 = 3.86U_{mf}$)

	Baffle-free		Louver		Mesh		Vertical plane	
	Probe 1	Probe 2	Probe 1	Probe 2	Probe 1	Probe 2	Probe 1	Probe 2
$\bar{t}_{1,2}$ [min]	35.0	45.8	29.2	50.4	33.7	47.7	37.4	49.2
$\delta^2_{1,2}$ [min ²]	433	702	280	539	464	635	418	591
\bar{t} [min]	10.8		21.2		13.9		11.8	
δ^2 [min ²]	269		258.5		171		173	
$\bar{\delta}^2$	2.31		0.574		0.884		1.24	
Pe	2.34		5.86		4.35		3.47	
D_{ax} [cm ² /min]	72.6		29.0		39.2		49.1	
[mm ² /s]	121		48.4		65.3		81.8	
Effect	100%		40%		54%		68%	

The baffles show even more positive results in solids dispersion hindering at a higher liquid velocity. It is noted that the baffles keep the same rank in terms of effectiveness as seen at the condition $U_1 = 2.66U_{mf}$ with the louver consistently having the most appreciable effect and the plane having the least.

At a very low liquid velocity, having baffles only worsened axial solids mixing, the louver has the most negative effect while the plane has the least negative effect. This makes sense based on the way the baffles were designed.

In the case of the plane, it is installed parallel to the major solids path, in a narrow column diameter of only 10 cm. Therefore, little effect of vertical plane is not surprising compared to other two designs. Yet, reducing the dispersion by 32% is still considered as a successful result.

The layers of mesh baffles are perpendicular to the major solids path, which means they intervene in the movement of the particles to some extent, more than the vertical plane, but still allow some particles to move freely through the openings. It limits the dispersion to 54% compared to the ordinary unit.

The louver has the most profound impact. The way the plates are designed disrupt the upward flow of particles, there is almost no straight path for the solids to travel if they are about to return to upward flow pattern. At high velocities this impact is substantial in comparison to the smaller local solids circulation that might occur under the baffle due to the inclined plates of the baffle. The louver reduces the solids back-mixing by 60% at this condition.

In conclusion, the effect of the baffles is enhanced with the increase of liquid velocity. Unless operating at a liquid velocity less than or close to U_{mf} , it is recommended to install the baffles inside the downer. Among the considered designs, the louver is the most impactful.

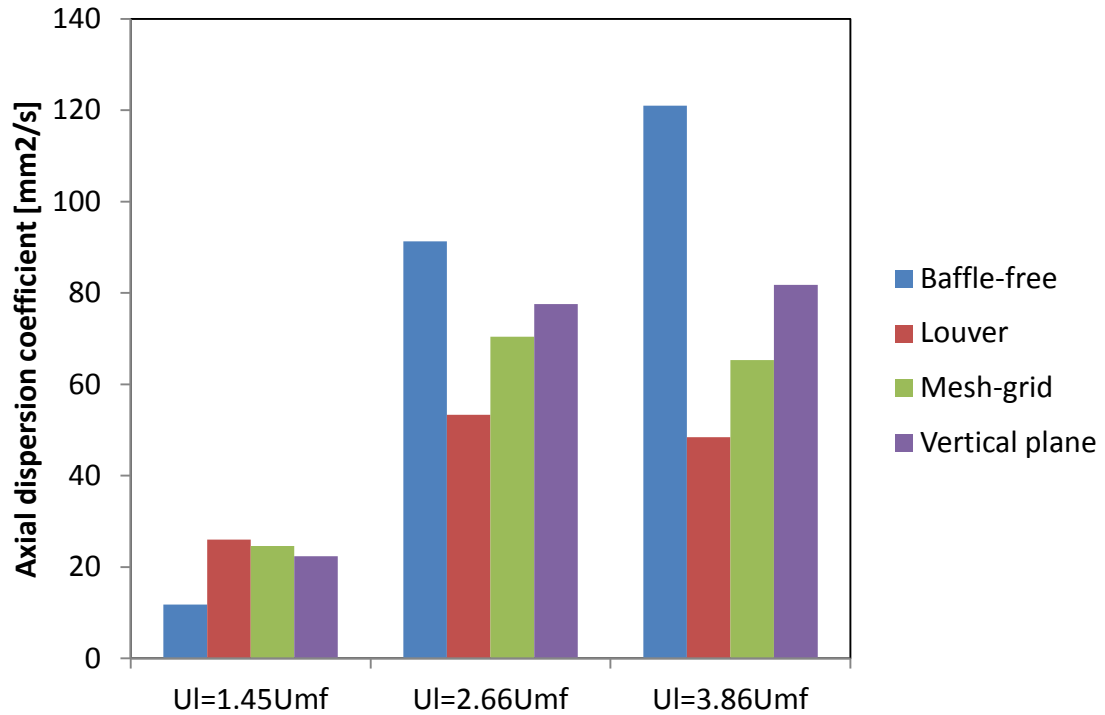


Figure 6.16: Summary of experimental axial dispersion coefficients

6.5 Repeatability of the Method

Because of high chemical cost and time requirement for each experiment, reduplication of all the trials was out of the scope of this study. For this reason, only one run was repeated to check the reliability of this resin sampling method. The repeated run is the baffle-free model at $U_l = 2.66U_{mf}$. The graphs have very similar shapes, except that the injection was not done as smoothly in trial 1 as in trial 2. Thus, the probe 1 graph in trial 1 is somewhat more random, leading to more dispersion seen in probe 2 graph.

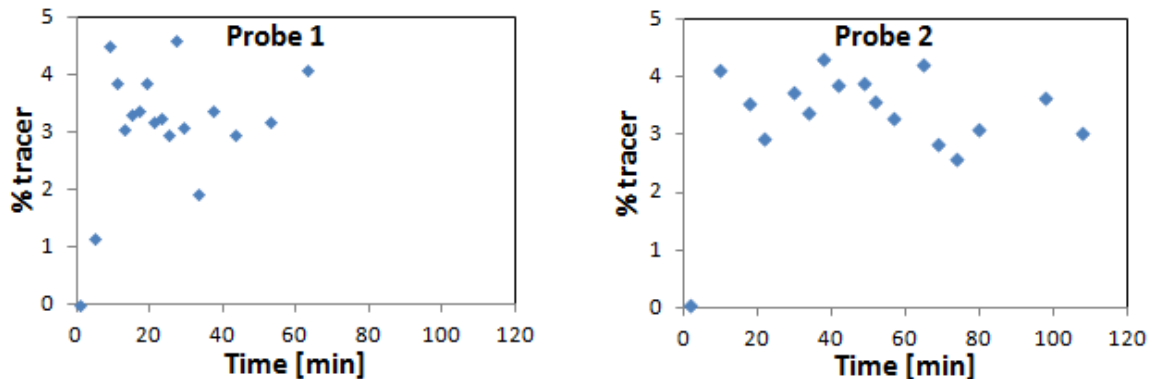


Figure 6.17: RTD graphs Trial 1

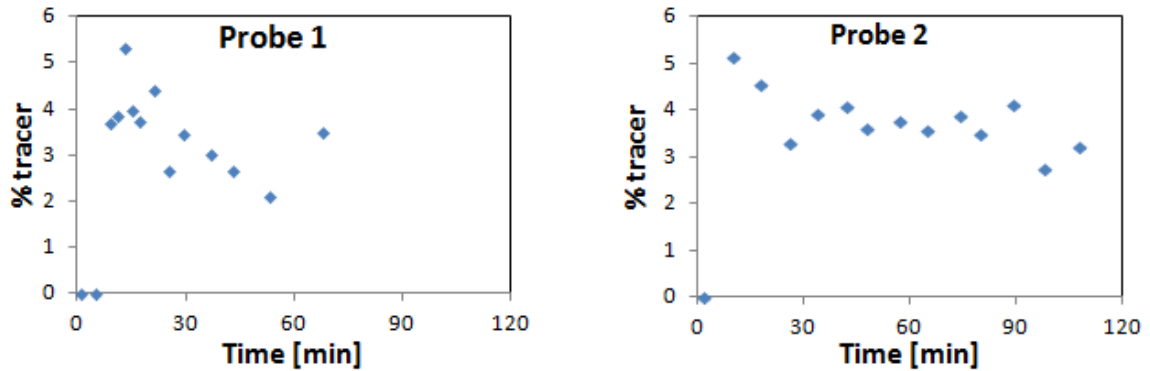


Figure 6.18: RTD graphs Trial 2

Table 6.4: Result summary for the repeated runs

	Trial 1		Trial 2	
	Probe 1	Probe 2	Probe 1	Probe 2
$\bar{t}_{1,2}$ [min]	36.8	55.6	35.0	54.0
$\delta^2_{1,2}$ [min ²]	353	882	351	881
\bar{t} [min]	18.8		19.0	
δ^2 [min ²]	529		530	
$\bar{\delta}^2$	1.50		1.47	
Pe	3.07		3.11	
D_{ax} [cm ² /min] [mm ² /s]	55.4 92.3		54.8 91.3	

The values of Pe and D_{ax} are calculated for the two runs. In spite of the difference in injection as noted, the Peclet and mixing coefficient values are very coinciding. It demonstrates the reproducibility and reliability of this method.

Chapter 7

7 Conclusions and Recommendations

7.1 Conclusions

- In this LSCFB system, when the liquid velocity is about or slightly higher than the minimum fluidization velocity, the fluidized bed exhibits minimal solids back-mixing. In this case, there is no need for internals to reduce axial solids mixing.
- As the liquid velocity increases, from about 2.5 times the minimum fluidization velocity, installing baffles inside the bed helps calm the dispersive motion of solids and therefore the dispersion coefficient is reduced.
- Among the three baffles considered (louver, mesh and plane), the louver consistently had the most appreciable suppression on solids back-mixing.
- The effects of the baffles is enhanced with the increase of liquid velocity.
- The RTD graphs obtained from the pilot-scale study were dispersed. They did not have a typical shape of a distribution graph, but the graphs in the lab-scale study did. Therefore, this newly developed methodology works delicately in small-scale units, however has limitations in large-scale units.
- Due to the limited amount of tests conducted, there are not enough data to confirm the results with enough statistical sensitivity. However, they still are qualitatively correct and give the right trend.

7.2 Recommendations

- More operating conditions could be examined, such as increasing liquid velocity, or changing the solids velocity.
- Study the effectiveness of baffles if different particles are used.

- The dimensions of the baffles may be changed and tested to obtain the optimal design of a particular baffle, especially of the louver.
- More experiments should be repeated to increase the statistical sensitivity to the results.

Nomenclature

Symbol	Unit	Definition
d_p	m	Particle diameter
D	m	Dispersion coefficient
g	m/s^2	Gravitational acceleration
G_s	kg/m^2s	Mass solids circulation rate
H	cm	Bed height
N		Equivalent number of tanks in series
P	Pa	Pressure head
Pe		Peclet number
r	m	Radial location
R	m	Column radius
SCR	ml/min	Volumetric solids circulation rate
\bar{t}	min	Time mean
S/L		Velocity ratio of solids to liquid
U	m/s	Velocity
U_{cf}	m/s	Onset velocity
U_{cr}	m/s	Critical transition velocity from the conventional to the circulation regime
U_{lc}	m/s	Critical transition velocity from the initial circulating to the fully developed circulating regime
U_{mf}	m/s	Minimum fluidization velocity
U_t	m/s	Terminal velocity of particle
V_{feed}	ml	Volume of fresh resins added to the bed later to maintain bed height
V_{fresh}	ml	Volume of fresh resins initially in the bed
V_{tracer}	ml	Volume of tracers (loaded resins) used
ϵ		Voidage
ϵ_{packed}		Voidage of a packed bed
ρ_o	kg/m^3	Density of two-phase bed
δ^2	min^2	Variance
$\overline{\delta^2}$		Dimensionless variance
μ_f	Pa•s	Fluid viscosity

Subscripts:

Symbol	Definition
ax	Axial
l	Liquid
r	Radial
s	Solids

References

- Al-Dibouni, M., & Garside, J. (1979). Particle Mixing and Classification in Liquid Fluidised Beds. *Transactions of the Institution of Chemical Engineers* v57 n2 , 94-103.
- Anon. (1962). *Special Report: Fluid Catalytic Cracking*. Exxon Research and Engineering Co.
- Asif, M., Kalogerakis, N., & Behie, L. A. (1991). Distributor Effects in Liquid Fluidized Beds of Low-Density Particles. *AIChE Journal Vol 37 No 12* , 1825-1832.
- Atta, A., Razzak, S., Nigam, K., & Zhu, J.-X. (2009, issue 48). (Gas)-Liquid-Solid Circulating Fluidized Bed Reactors: Characteristics and Applications. *Ind. Eng. Chem.* , 7876-7892.
- Chang, Y., & Chase, H. (1996). Development of Operating Conditions for Protein Purification Using Expanded Bed Techniques: The Effect of the Degree of Bed Expansion on Adsorption Performance. *Biotechnology and Bioengineering* , 512-526.
- Chase, G. G. *Solids Notes 5 Fluidization*. The University of Akron.
- Chhabra, R. P. (2007). *Bubbles, Drops, and Particles In Non-Newtonian Fluids, Second Edition*. Boca Raton: Taylor & Francis Group.
- Couderc, J.-P. (1985). Chapter 1. Incipient Fluidization and Particulate Systems. In J. F. Davidson, R. Clift, & D. Harrison, *Fluidization, 2nd edition* (pp. 1-44). Orlando: Academic Press Inc. .
- Gajewski, J. (1999). Electrostatic flow probe and measuring system calibration for solids mass flow rate measurement. *J. Electrostat* 45 , 255-264.
- Gajewski, J. (1999). Static characteristics of an electrostatic flow probe. *J. Electrostat* 48 , 49-64.
- Green, R. (1981). *Capacitance flow transducers for multiphase systems*. University of Bradford: PhD thesis.

Karpagavallie. (2009, 02 06). *Fluidization*. Retrieved 12 03, 2012, from Classle:
<https://www.classle.net/book/fluidization>

Levenspiel, O. (1999). *Chemical Reaction Engineering 3rd ed.* New York: John Wiley & Sons.

Levenspiel, O., & Smith, W. (1957). Notes on the diffusion-type model for the longitudinal mixing of fluids in flow. *Chem. Eng. Sci.* 6 , 227-233.

Liang, W., Zhang, S., Zhu, J.-X., Jin, Y., Yu, Z., & Wang, Z. (1997). Flow Characteristics of the Liquid - Solid Circulating Fluidized Bed. *Powder Technology* , 95-102.

Limtrakul, S., Chen, J., Ramachandran, P. A., & Dudukovic, M. (2005). Solids motion and holdup profiles in liquid fluidized beds. *Chemical Engineering Science (60)* , 1889-1900.

Linn, J., & Sample, D. (1982). Mass flow measurement of solids/gas stream using radiometric technique . *Proc. Symp. Instrumentation and Control of Fossil Energy Processes* , 12-20.

Menkhaus, T. J., & Glatz, C. E. (2005). Antibody Capture from Corn Endosperm Extracts by Packed Bed and Expanded Bed Adsorption. *Biotechnol. Prog.* 21 , 473-485.

Natarajan, P.; Velraj, R.; Seeniraj, R.V. (2007). Regime transition, Operating range and System stability in a Liquid-solid circulating fluidized bed. *Chem. Eng. and Tech.*

Nieuwland, J., Meijer, R., Kuipers, J., & Swaaij, W. v. (1996). Measurement of solids concentration and axial solids velocity in gas-solid two-phase flows. *Powder Technology v87 n2* , 127-139.

Nikitina, N., Baryshnikova, L., Kasandopulo, G., Razumov, I., & Terrekhov, N. (1981). Selection of Diameter of Model Vessel for Studies of Liquid Fluidization. *Process Vessels and Equipment* , 504-506.

Palani, N., & Ramalingam, V. (2008). Effect of Various Parameters on the Solids Holdup in a Liquid-Solid Circulating Fluidized Bed. *International Journal of Chemical Reactor Engineering* , Volume 6, Article A44.

Razzak, S., Zhu, J.-X., & Barghi, S. (2009). Particle Shape, Density, and Size Effects on the Distribution of Phase Holdups in a LSCFB Riser. *Chemical Engineering Technology* , 1236-1244.

Roy, S., & Dudukovic, M. (2001). Flow Mapping and Modeling of Liquid-Solid Risers. *Ind. Eng. Chem. Res.* 40 , 5440-5454.

Roy, S.; J. Chen; S.B. Kumar; M.H. Al-Dahhan; M.P. Dudukovic. (1997). Tomographic and particle tracking studies in a liquid-solid riser. *Ind. Eng. Chem. Res* 36 , 466-469.

S.A. Razzak; S. Barghi; J-X. Zhu; Y. Mi. (2009). Phase holdup measurement in a gas-liquid-solid circulating fluidized bed (GLSCFB) riser using electrical resistance tomography and optical fibre probe. *Chemical Engineering Journal* 147 , 210-218.

Shantanu Roy; Abdenour Kemoun; M.H. Al-Dahhan; M.P. Dudukovic . (2005). Experimental Investigation of the Hydrodynamics in a Liquid-Solid Riser. *AIChE Journal Vol. 51, No. 3* , 802-835.

Sheen, S., & Raptis, A. (1985). Active ultrasonic cross-correlation flowmeters for mixed-phase pipe flows . *ISA Trans.* 24 , 53-58.

Song, G., & Fan, L. (1986). Rheological behavior of a gas-liquid-solid fluidized bed. *World Congress III of Chemical Engineering 3* , 540-607.

Subramanian, R. S. *Flow through Packed Beds and Fluidized Beds.*

Sun, M., Liu, S., Lei, J., & Li, Z. (2008). Mass flow measurement of pneumatically conveyed solids using electrical capacitance. *Meas. Sci. Technol.* 19 , 450-503.

Umang J. Trivedi; Amarjeet S. Bassi; Jesse Zhu. (2005). Liquid-solid circulating fluidized beds: An immobilized bioreactor system from a product inhibition perspective.

AIChE Annual Meeting and Fall Showcase (pp. 9036-9040). American Institute of Chemical Engineers.

Wei Chen; Weiguo Yang; Jinfu Wang; Yong Jin; Atsushi Tsutsumi. (2001). Characterization of Axial and Radial Liquid Mixing in a Liquid-Solid Circulating Fluidized Bed. *Ind. Eng. Chem. Res.* 40 , 5431-5435.

Wei, F., & Zhu, J.-X. (1996). Effect of flow direction on axial solid dispersion in gas-solids cocurrent upflow and downflow systems. *The Chemical Engineering Journal* 64 , 345-352.

Xiao-Dong Tong, Y. S. (2001). Nd-Fe-B alloy-densified agarose gel for expanded bed adsorption of proteins. *Journal of Chromatography A* 943 , 63-75.

Xu, C., Tang, G., Zhou, B., & Wang, S. (2009). The spatial filtering method for solid particle velocity measurement based on an electrostatic sensor. *Measurement Science and Technology* , 1-8.

Yang, W.-C. (2003). *Handbook of Fluidization and Fluid-Particle Systems*. CRC Press.

Zhang, Y., Lu, C., & Shi, M. (2009). Evaluating solids dispersion in fluidized beds of fine particles by gas backmixing experiments. *Chemical Engineering Research and Design* 87 , 1400-1408.

Zheng, Y. (2001). Axial Liquid Dispersion in a Liquid-Solid Circulating Fluidized Bed. *The Canadian Journal of Chemical Engineering* 79 , 564-569.

Zheng, Y., & Zhu, J. (2003). Radial Distribution of Liquid Velocity in a Liquid - Solids Circulating Fluidized Bed. *International Journal of Chemical Reactor Engineering* , 1-7.

Zheng, Y., & Zhu, J.-X. (. (2001). The onset velocity of a Liquid - Solid Circulating Fluidized Bed. *Powder Technology* , 244-251.

Zheng, Y., Zhu, J.-X. (., Wen, J., Martin, S. A., Bassi, A. S., & Margaritis, A. (1999). The Axial Hydrodynamic Behavior in a Liquid - Solid Circulating Fluidized Bed. *The Canadian Journal of Chemical Engineering Volume 77* , 1-7.

Zheng, Y., Zhu, J.-X., Marwaha, N. S., & Bassi, A. S. (2002). Radial Solids Flow Structure in a Liquid - Solids Circulating Fluidized Bed. *Chemical Engineering Journal* , 141-150.

Zhu, J.-X., Zheng, Y., Karamanev, D. G., & Bassi, A. B. (2000). (Gas-) Liquid - Solid Circulating Fluidized Beds and Their Potential Applications to Bioreactor Engineering. *The Canadian Journal of Chemical Engineering* , 82-94.

A. Appendices

Appendix A-1: Maximum capacity of SGC 650 resins for calcium

To determine maximum capacity of resin for calcium, a predetermined amount of fresh resin – resin in a different form other than calcium form – is put in a small column. A calcium chloride solution is fed into the column from the bottom. The column is in conventional fluidization. Calcium concentration in the raffinate is periodically measured and recorded. Once this concentration reaches the feed concentration, then the resin is fully loaded with Ca^{2+} .

There is more than one way to determine the maximum capacity of resin using the data collected. For SGC 650 resin, the capacity was calculated using the volume and concentration of the total raffinate at the end of the loading process. The data are represented below.

Resin mass: 10.003 g

Feed concentration: 5.0508 g/L Ca

Feed flowrate: 3 ml/min

Titrate solution using EDTA titrant: 1 ml titrant = 0.366 mg Ca

Time [min]	Titrated Volume [ml]	EDTA used [ml]	C [g/L]	$m_{\text{Ca, titrated}}$ [mg]
0	1	0	0	0.00
5	1	0	0	0.00
10	1	0	0	0.00
15	1	0	0	0.00
18	1	0.1	0.037	0.04
21	1	0.2	0.073	0.07
24	1	0.5	0.183	0.18
27	1	1.4	0.512	0.51
30	1	2.7	0.988	0.99
33	1	4.75	1.739	1.74
36	1	7.65	2.800	2.80
39	1	9.7	3.550	3.55
42	0.5	5.65	4.136	2.07

45	0.5	6.1	4.465	2.23
48	0.5	6.45	4.721	2.36
51	0.5	6.55	4.795	2.40
54	0.5	6.75	4.941	2.47
57	0.5	6.85	5.014	2.51
60	0.5	6.85	5.014	2.51
63	0.5	6.9	5.051	2.53

$$m_{Ca,titrated} = C * V_{titrated}$$

Measure raffinate: $V = 186$ ml; $C = 2.3058$ g/L

Including the total titrated volume, feed volume used was 201 ml

$$\text{Total mass in: } m_{in} = 201 * 5.0508 = 1015.2 \text{ mg}$$

$$\text{Total mass out: } m_{out} = 186 * 2.3058 + \sum m_{Ca,titrated} = 457.8 \text{ mg}$$

$$m_{adsorbed} = m_{in} - m_{out} = 557.4 \text{ mg}$$

$$\text{Capacity} = \frac{557.4 \text{ mgCa}}{10.003 \text{ gresin}} = 55.7 \text{ mgCa/gresin}$$

Appendix A-2: Maximum capacity of S 1668 resins for calcium

S 1668 resin was loaded with calcium in a conventional fluidized bed. The concentration of calcium in the raffinate was measured and recorded. This appendix shows a different way to calculate the maximum capacity of resin. The method does not require total volume of the raffinate or its calcium concentration but uses integrations of concentration over time. The details are shown as follows.

Resin mass: 47.36 g

Feed concentration: 1800 mg/L Ca

Feed flowrate: 20 ml/min

Titrate solution using EDTA titrant: 1 ml titrant = 0.4 mg Ca

Time [min]	V _{titrated} [ml]	V _{EDTA} [ml]	C [mg/L]	m _{out} [mg]
5	10	0	0	0
10	10	0	0	0
15	10	0	0	0
20	10	0	0	0
25	10	0.3	12	1
30	10	0.8	32	3
35	10	2.8	112	11
40	10	8.3	332	32
45	5	7.6	608	58
50	2	5.2	1040	99
55	1	3.8	1520	144
60	1	4.5	1800	171

$$\text{Mass in} = 60\text{min} * 20 \frac{\text{ml}}{\text{min}} * 1800 \frac{\text{mg}}{\text{L}} * \frac{1\text{L}}{1000\text{ml}} = 2160 \text{ mg}$$

$$\text{Mass out} = \sum m_{out} = 518 \text{ mg}$$

$$\text{Mass adsorbed} = \text{mass in} - \text{mass out} = 1642 \text{ mg}$$

$$\text{Capacity} = \frac{1642 \text{ mgCa}}{47.36 \text{ gresin}} = 34.7 \text{ mgCa/gresin}$$

Appendix A-3: Calculate mass rate of solids circulation

Cross sectional area of the downer:

$$A = \frac{\pi}{4} * d^2 = \frac{\pi}{4} * 10.1^2 = 80.1 \text{ cm}^2$$

Volumetric rate of solids circulation is measured via measuring device in the downer, just below the solids returning pipe. Solids are collected and accumulated in one side, so the base area of this section is half of the downer cross-sectional area. The liquid flowrates in the riser are adjusted to provide the same solids circulation rate always. The height of the solids accumulation in the measuring device is 3.7 cm after 1 minute collecting.

$$SCR = 3.7 * \frac{80.1}{2} = 148.2 \text{ cm}^3/\text{min}$$

A small test is done to check true density of hydrated and swelled SGC 650 resins, and to determine the voidage of packed bed. A small amount of resins is vacuumed, and weighed – 10.074 g. A 25 ml gradual cylinder is filled with water up to 10-ml mark. The resin is added to the cylinder. Water level rises to 17.6 ml, so the voidage-free volume of resins is 7.6 ml, giving the density of resins is:

$$\rho_s = \frac{10.074}{7.6} = 1.33 \frac{\text{g}}{\text{ml}}$$

The top of the resin level reads 12.0 ml. This is the volume of resins and voidage. So the solids holdup in a packed bed is:

$$\varepsilon_s = \frac{7.60}{12.0} = 0.633$$

Mass rate of solids circulation is:

$$G_s = \frac{SCR * \varepsilon_s * \rho_s}{A} = 148.2 \frac{\text{ml}}{\text{min}} * 0.633 * \frac{1\text{min}}{60\text{s}} * 1.33 \frac{\text{g}}{\text{ml}} * \frac{1\text{kg}}{1000\text{g}} \div 80.1\text{cm}^2$$

$$G_s = 2.60 * 10^{-5} \frac{\text{kg}}{\text{cm}^2\text{s}} = 0.260 \frac{\text{kg}}{\text{m}^2\text{s}}$$

Appendix A-4: Mole ratio between sodium and calcium in a sample desorption

Lower range of mole ratio

In small lab scale experiments, more tracers were collected in each sample than in the larger scale experiments. One of the samples with highest amount of desorbed calcium was in S1668 – Run #1, the amount of Ca was 393.33 mg.

$$N_{Ca} = \frac{393.33 \text{ mg}}{40 \text{ g/mol}} = 9.83 \text{ mmol} = 9.83 * 10^{-3} \text{ mol}$$

Amount of sodium available in 200 ml of 9% NaCl solution is:

$$m_{Na} = 0.2L * 90 \frac{\text{gNaCl}}{L} * \frac{23\text{gNa}}{58.5\text{gNaCl}} = 7.07\text{gNa}$$

$$N_{Na} = \frac{7.07\text{g}}{23\text{g/mol}} = 0.308 \text{ mol}$$

Mole ratio:

$$\frac{N_{Na}}{N_{Ca}} = \frac{0.308}{9.83 * 10^{-3}} = 31$$

Higher range of mole ratio

In pilot-scale experiments, most samples had about 100 mg of calcium.

$$N_{Ca} = \frac{100 \text{ mg}}{40 \text{ g/mol}} = 2.5 \text{ mmol} = 2.5 * 10^{-3} \text{ mol}$$

Mole ratio:

$$\frac{N_{Na}}{N_{Ca}} = \frac{0.308}{2.5 * 10^{-3}} = 123$$

Appendix A-5: Calibration curve for S 1668 resins

Masses of tracer resin and fresh resin were weighed and transferred to numbered labeled flasks. They were desorbed using 200 ml of 9% NaCl solution in batch for 15 minutes. A small volume of the solution was then pipetted and titrated to determine the amount of calcium desorbed from the tracers. The calcium amount was graphed against the weighed tracer mass, forming the calibration curve.

EDTA used is diluted 3 times from 0.01M, so the conversion factor is:

$$1ml\ EDTA = \frac{0.4}{3} mg\ Ca$$

$$m_{Ca} = \frac{V_{EDTA} * 0.4/3}{V_{titrated}} * 200$$

Tracer mass [g]	Fresh resin mass [g]	V _{titrated} [ml]	V _{EDTA} [ml]	m _{Ca} [mg]
1.008	13.998	4	4.8	32.0
2.009	12.997	4	9.2	60.1
3.003	11.994	2	6.8	89.8
4.003	10.992	1	4.9	130.0
5.001	9.995	1	5.6	148.6
6.004	8.995	1	6.6	175.1
7.004	7.991	1	8	212.3
8.002	6.992	1	9.1	241.5
9.996	5.990	1	10.6	281.3

Appendix A-6: Calibration curve for SGC 650 resins

EDTA used is diluted 3 times from 0.01M, so the conversion factor is:

$$1 \text{ ml EDTA} = \frac{0.4}{3} \text{ mg Ca}$$

$$m_{Ca} = \frac{V_{EDTA} * 0.4/3}{V_{titrated}} * 200$$

Calibration curve 1

$$V_{titrated} = 2 \text{ ml}$$

From the first sample: $m_{\text{fresh}} = 22.467 \text{ g}$ and $m_{Ca} = 103.0 \text{ mg}$

$$\therefore \frac{103.0}{22.467} = 4.585 \frac{\text{mg Ca}}{\text{g freshresin}}$$

$$m_{Ca\text{-on tracers}} = m_{Ca\text{-total}} - 4.585 * m_{\text{fresh}}$$

Fresh resin [g]	Tracers [g]	V_{EDTA} [ml]	Total m_{Ca} [mg]	m_{Ca} on fresh resin [mg]	m_{Ca} on tracers [mg]
22.467	0.000	7.70	102.7	103.0	0.0
22.131	0.487	8.50	113.3	101.5	11.8
21.267	0.825	9.05	120.7	97.5	23.1
20.485	1.263	9.80	130.7	93.9	36.7
20.075	1.656	10.60	141.3	92.1	49.3
21.283	0.231	7.80	104.0	97.6	6.4
22.376	0.632	8.90	118.7	102.6	16.0
23.729	2.546	13.10	174.7	108.8	65.8

Calibration curve 2

$$V_{titrated} = 1 \text{ ml}$$

From the first sample: $m_{\text{fresh}} = 23.5 \text{ g}$ and $m_{Ca} = 112.0 \text{ mg}$

$$\therefore \frac{112.0}{23.5} = 4.77 \frac{\text{mg Ca}}{\text{g freshresin}}$$

$$m_{Ca\text{-on tracers}} = m_{Ca\text{-total}} - 4.77 * m_{\text{fresh}}$$

Fresh resin [g]	Tracers [g]	V _{EDTA} [ml]	Total m _{Ca} [mg]	m _{Ca} on fresh resin [mg]	m _{Ca} on tracers [mg]
23.5	0.0	4.2	112.0	112.0	0.00
23.3	0.5	4.5	120.0	111.0	8.95
22.3	1.0	4.9	130.7	106.3	24.38
22.4	1.5	5.4	144.0	106.8	37.24
22	2.0	5.75	153.3	104.9	48.48
21.8	2.5	6.3	168.0	103.9	64.10
21.2	3.0	6.75	180.0	101.0	78.96

Appendix A-7: Verification of calibration curve

$$y = 30.335x$$

where y is the amount of calcium desorbed (mg); x is the tracers mass (g).

There were 6 samples. Mass of tracers in each sample were known. Mass of fresh resins were known in 3 samples only.

$$1 \text{ ml EDTA} = \frac{0.4}{3} \text{ mgCa}$$

Weighed tracers [g]	Weighed fresh resin [g]	V _{titrated} [ml]	V _{EDTA} [ml]	m _{Ca} [mg] (y)	Calculated tracers [g] (x)	% error
3.004	11.99	2	7.20	96.0	3.158	5.1
5.002	9.989	1	5.75	153	5.036	0.7
7.000	7.995	1	8.00	213	7.002	0.04
3.014	Unknown	2	7.00	93.3	3.069	1.8
5.017	Unknown	1	6.00	160	5.256	4.8
7.025	Unknown	1	8.25	220	7.222	2.8

B. Appendices: Lab Scale Testing Data

Appendix B-1: Data for lab-scale run 1

Cross-sectional area of 5 cm column is:

$$A = \frac{\pi}{4} * 5^2 = 19.63 \text{ cm}^2$$

Liquid flowrate: 95 ml/min

$$\therefore U_l = \frac{95}{19.63} = 4.84 \text{ cm/min}$$

Bed height: $H = H_{fresh} + H_{tracer} = 11.8 + 3 = 14.8 \text{ cm}$

$V_{feed} = 350 \text{ ml}$; time run = 34 min

$$\therefore SCR = \frac{350}{34} = 10.3 \text{ ml/min}$$

$$\therefore U_s = \frac{10.3}{19.63} = 0.524 \text{ cm/min}$$

EDTA used was diluted: 1 ml EDTA = 0.4/3 mg Ca

Time [min]	m_{total} [g]	$V_{titrated}$ [ml]	V_{EDTA} [ml]	m_{Ca} [mg]	$m_{tracers}$ [g]	% tracers
1	10.0	3	0.20	1.78	0.05	0.5
2	1.9	3	0.60	5.33	0.17	8.7
3	10.3	3	0.80	7.11	0.22	2.2
4	1.9	3	0.80	7.11	0.22	11.8
5	8.3	3	0.90	8.00	0.25	3.1
6	10.3	3	1.10	9.78	0.31	3.0
7	5.1	3	1.00	8.89	0.28	5.6
8	10.0	3	0.30	2.67	0.08	0.8
9	2.8	3	1.00	8.89	0.28	10.1
10	6.5	3	1.25	11.11	0.36	5.5
11	9.0	3	0.95	8.44	0.27	3.0
12	7.8	3	1.15	10.22	0.33	4.2
13	4.0	3	0.75	6.67	0.21	5.3
14	3.8	3	0.80	7.11	0.22	5.9
15	10.0	5	0.80	4.27	0.13	1.3

16	4.4	3	0.55	4.89	0.15	3.4
17	6.0	3	0.60	5.33	0.17	2.8
18	4.5	3	0.85	7.56	0.24	5.3
19	25.3	1	0.50	13.33	0.43	1.7
20	7.1	3	0.70	6.22	0.20	2.8
21	9.0	3	0.80	7.11	0.22	2.5
22	9.0	3	0.80	7.11	0.22	2.5
23	3.1	3	1.40	12.44	0.40	12.9
24	4.4	3	3.20	28.44	0.93	21.1
25	8.5	3	10.00	88.89	2.92	34.4
26	6.3	2	7.20	96.00	3.16	50.1
27	23.3	1	14.75	393.33	12.97	55.7
28	1.8	3	5.40	48.00	1.57	87.5
29	12.2	3	27.80	247.11	8.15	66.8
30	14.2	1	7.40	197.33	6.50	45.8
31	11.4	1	4.40	117.33	3.86	33.9
32	10.0	1	3.10	82.67	2.72	27.2
33	16.2	1	3.25	86.67	2.85	17.6
34	16.6	1	2.00	53.33	1.75	10.5

In the table above: m_{total} is the weighed mass of a solids sample which includes both neutral particles – fresh resins, and tracers – loaded resins.

$$m_{Ca} = \frac{0.4/3 * V_{EDTA}}{V_{titrated}} * 200$$

$$m_{tracers} = \frac{m_{Ca}}{30.335}$$

$$\%tracers = \frac{m_{tracers}}{m_{total}} * 100\%$$

Next, %tracers from the table above is considered as concentration in liquid study, both essentially mean the same – how much tracers in the medium at that location at that time. So time and %tracer – C are used to calculate time mean, variance, then Peclet number and dispersion coefficient.

t	C(t)	Δt	$C * \Delta t$	E(t)	$E(t) * t * \Delta t$	$(t-25.17)^2 * E * \Delta t$
1	0.5	1.5	0.75	0.001	0.00	0.80
2	8.7	1	8.70	0.016	0.03	8.48
3	2.2	1	2.20	0.004	0.01	1.96
4	11.8	1	11.80	0.021	0.09	9.61
5	3.1	1	3.10	0.006	0.03	2.29

6	3.0	1	3.00	0.005	0.03	2.00
7	5.6	1	5.60	0.010	0.07	3.36
8	0.8	1	0.80	0.001	0.01	0.43
9	10.1	1	10.10	0.018	0.17	4.80
10	5.5	1	5.50	0.010	0.10	2.30
11	3.0	1	3.00	0.005	0.06	1.09
12	4.2	1	4.20	0.008	0.09	1.32
13	5.3	1	5.30	0.010	0.13	1.43
14	5.9	1	5.90	0.011	0.15	1.34
15	1.3	1	1.30	0.002	0.04	0.24
16	3.4	1	3.40	0.006	0.10	0.52
17	2.8	1	2.80	0.005	0.09	0.34
18	5.3	1	5.30	0.010	0.17	0.49
19	1.7	1	1.70	0.003	0.06	0.12
20	2.8	1	2.80	0.005	0.10	0.14
21	2.5	1	2.50	0.005	0.10	0.08
22	2.5	1	2.50	0.005	0.10	0.05
23	12.9	1	12.90	0.023	0.54	0.11
24	21.1	1	21.10	0.038	0.92	0.05
25	34.4	1	34.40	0.062	1.56	0.00
26	50.1	1	50.10	0.091	2.37	0.06
27	55.7	1	55.70	0.101	2.73	0.34
28	87.5	1	87.50	0.159	4.45	1.27
29	66.8	1	66.80	0.121	3.52	1.78
30	45.8	1	45.80	0.083	2.50	1.94
31	33.9	1	33.90	0.062	1.91	2.09
32	27.2	1	27.20	0.049	1.58	2.30
33	17.6	1	17.60	0.032	1.06	1.96
34	10.5	0.5	5.25	0.019	0.32	0.74

$$\sum C(t) \cdot \Delta t = 550.5 \rightarrow E(t) = \frac{C(t)}{550.5}$$

$$\bar{t} = \sum E(t) \cdot t \cdot \Delta t = 25.17 \text{ min}$$

$$\delta^2 = \sum (t - 25.17)^2 \cdot E(t) \cdot \Delta t = 55.85 \text{ min}^2$$

$$\bar{\delta}^2 = \frac{55.85}{25.17^2} = 0.0882$$

$$\frac{1}{Pe} = \frac{1}{8} * (\sqrt{8 * 0.0882 + 1} - 1) = 0.0382 \rightarrow Pe = \frac{1}{0.0382} = 26.2$$

$$D_{ax} = \frac{U_s H}{Pe} = \frac{0.524 \text{ cm/min} * 14.8 \text{ cm}}{26.2} = 0.297 \text{ cm}^2/\text{min}$$

Appendix B-2: Data for lab scale run 2

$$U_l = \frac{95 \text{ ml/min}}{19.63 \text{ cm}^2} = 4.84 \text{ cm/min}$$

$$H = 9.2 + 3 = 12.2 \text{ cm}$$

$$SCR = \frac{376 \text{ ml}}{26 \text{ min}} = 14.5 \text{ ml/min}$$

$$U_s = \frac{14.5 \text{ ml/min}}{19.63 \text{ cm}^2} = 0.739 \text{ cm/min}$$

$$1 \text{ ml EDTA} = \frac{0.4}{3} \text{ mgCa}$$

Time [min]	m _{total} [g]	V _{titrated} [ml]	V _{EDTA} [ml]	m _{Ca} [mg]	m _{tracers} [g]	% tracers
1	23.5	3	0.50	4.4	0.1	0.6
2	19.3	3	0.70	6.2	0.2	1.0
3	12.4	3	0.70	6.2	0.2	1.6
4	12.7	3	0.75	6.7	0.2	1.7
5	20.8	3	0.80	7.1	0.2	1.1
6	28.9	3	0.75	6.7	0.2	0.7
7	12.7	3	0.70	6.2	0.2	1.5
8	10.0	3	3.25	28.9	0.9	9.4
9	10.7	3	10.25	91.1	3.0	28.0
10	7.5	1	3.95	105.3	3.5	46.2
11	12.1	1	8.05	214.7	7.1	58.5
12	11.9	3	30.60	272.0	9.0	75.4
13	15.3	1	11.80	314.7	10.4	67.8
14	8.0	1	5.00	133.3	4.4	54.9
15	15.5	2	12.95	172.7	5.7	36.7
16	7.0	1	2.00	53.3	1.8	25.0
17	16.2	2	5.00	66.7	2.2	13.5
18	10.3	1	1.10	29.3	1.0	9.3
19	14.1	3	3.25	28.9	0.9	6.7
20	6.5	3	1.35	12.0	0.4	5.9
21	16.2	3	2.25	20.0	0.7	4.0
24	7.5	3	0.80	7.1	0.2	3.0
26	8.4	3	0.55	4.9	0.2	1.8

Next, the time mean, variance, dimensionless variance, Peclet number and dispersion coefficient are calculated.

t	C(t)	Δt	C * Δt	E(t)	E(t) * t * Δt	$(t-12.98)^2 * E * \Delta t$
1	0.6	1.5	0.9	0.001	0.002	0.279
2	1.0	1	1	0.002	0.004	0.260
3	1.6	1	1.6	0.003	0.010	0.344
4	1.7	1	1.7	0.004	0.015	0.296
5	1.1	1	1.1	0.002	0.012	0.151
6	0.7	1	0.7	0.002	0.009	0.074
7	1.5	1	1.5	0.003	0.023	0.116
8	9.4	1	9.4	0.020	0.162	0.503
9	28.0	1	28	0.060	0.544	0.956
10	46.2	1	46.2	0.100	0.998	0.884
11	58.5	1	58.5	0.126	1.390	0.494
12	75.4	1	75.4	0.163	1.954	0.155
13	67.8	1	67.8	0.146	1.903	0.000
14	54.9	1	54.9	0.119	1.660	0.124
15	36.7	1	36.7	0.079	1.189	0.324
16	25.0	1	25	0.054	0.864	0.493
17	13.5	1	13.5	0.029	0.496	0.472
18	9.3	1	9.3	0.020	0.361	0.507
19	6.7	1	6.7	0.014	0.275	0.525
20	5.9	1	5.9	0.013	0.255	0.628
21	4.0	2	8	0.009	0.363	1.112
24	3.0	2.5	7.5	0.006	0.389	1.968
26	1.8	1	1.8	0.004	0.101	0.659

$$\sum C(t) \cdot \Delta t = 463.1 \rightarrow E(t) = \frac{C(t)}{463.1}$$

$$\bar{t} = \sum E(t) \cdot t \cdot \Delta t = 12.98 \text{ min}$$

$$\delta^2 = \sum (t - 12.98)^2 \cdot E(t) \cdot \Delta t = 11.32 \text{ min}^2$$

$$\bar{\delta}^2 = \frac{11.32}{12.98^2} = 0.06724$$

$$\frac{1}{Pe} = \frac{1}{8} * (\sqrt{8 * 0.06724 + 1} - 1) = 0.0300 \rightarrow Pe = \frac{1}{0.0300} = 33.3$$

$$D_{ax} = \frac{U_s H}{Pe} = \frac{0.739 \text{ cm/min} * 12.2 \text{ cm}}{33.3} = 0.270 \text{ cm}^2/\text{min}$$

Appendix B-3: Data for lab scale run 3

$$U_l = \frac{95 \text{ ml/min}}{19.63 \text{ cm}^2} = 4.84 \text{ cm/min}$$

$$H = 31.7 + 3 = 34.7 \text{ cm}$$

$$SCR = \frac{926 \text{ ml}}{58 \text{ min}} = 16.0 \text{ ml/min}$$

$$U_s = \frac{16.0 \text{ ml/min}}{19.63 \text{ cm}^2} = 0.815 \text{ cm/min}$$

$$1 \text{ ml EDTA} = \frac{0.4}{3} \text{ mgCa}$$

Time [min]	m _{total} [g]	V _{titrated} [ml]	V _{EDTA} [ml]	m _{Ca} [mg]	m _{tracers} [g]	% tracers
1	4.9	3	0.35	3.11	0.1	1.9
5	8.3	3	0.45	4.00	0.1	1.5
9	21.5	3	0.65	5.78	0.2	0.8
13	15.8	3	0.60	5.33	0.2	1.1
17	15.3	3	0.65	5.78	0.2	1.2
21	13.9	3	0.90	8.00	0.3	1.8
25	13.9	3	0.85	7.56	0.2	1.7
29	23.1	3	0.85	7.56	0.2	1.0
33	12.9	3	1.10	9.78	0.3	2.4
37	18.3	3	1.05	9.33	0.3	1.6
38	15.5	3	1.55	13.78	0.4	2.9
39	15.3	2	5.60	74.67	2.5	16.0
40	13.5	1	5.75	153.33	5.1	37.4
41	12.4	3	22.65	201.33	6.6	53.5
42	14.4	1	10.60	282.67	9.3	64.7
43	20.2	1	11.40	304.00	10.0	49.6
44	13.7	1	4.90	130.67	4.3	31.4
45	18.7	3	11.30	100.44	3.3	17.7
46	23.3	3	5.85	52.00	1.7	7.3
47	15.8	3	2.70	24.00	0.8	5.0
48	16.8	3	2.90	25.78	0.8	5.0
49	16.8	3	1.95	17.33	0.6	3.3
53	14.1	3	1.25	11.11	0.4	2.5
56	14.5	3	1.10	9.78	0.3	2.2
58	15.2	3	0.95	8.44	0.3	1.8

Next, the time mean, variance, dimensionless variance, Peclet number and dispersion coefficient are calculated.

t	C(t)	Δt	C * Δt	E(t)	E(t) * t * Δt	(t-39.54) ² *E* Δt
1	1.9	3.0	5.70	0.005	0.015	22.848
5	1.5	4.0	6.00	0.004	0.081	19.317
9	0.8	4.0	3.20	0.002	0.078	8.054
13	1.1	4.0	4.40	0.003	0.154	8.363
17	1.2	4.0	4.80	0.003	0.220	6.580
21	1.8	4.0	7.20	0.005	0.408	6.678
25	1.7	4.0	6.80	0.005	0.459	3.879
29	1.0	4.0	4.00	0.003	0.313	1.199
33	2.4	4.0	9.60	0.006	0.855	1.107
37	1.6	2.5	4.00	0.004	0.399	0.069
38	2.9	1.0	2.90	0.008	0.297	0.018
39	16.0	1.0	16.00	0.043	1.684	0.012
40	37.4	1.0	37.40	0.101	4.038	0.022
41	53.5	1.0	53.50	0.144	5.920	0.309
42	64.7	1.0	64.70	0.175	7.334	1.059
43	49.6	1.0	49.60	0.134	5.757	1.605
44	31.4	1.0	31.40	0.085	3.729	1.688
45	17.7	1.0	17.70	0.048	2.150	1.426
46	7.3	1.0	7.30	0.020	0.906	0.823
47	5.0	1.0	5.00	0.013	0.634	0.752
48	5.0	1.0	5.00	0.013	0.648	0.967
49	3.3	2.5	8.25	0.009	1.091	1.994
53	2.5	3.5	8.75	0.007	1.252	4.281
56	2.2	2.5	5.50	0.006	0.831	4.023
58	1.8	1.0	1.80	0.005	0.282	1.656

$$\sum C(t) \cdot \Delta t = 370.5 \rightarrow E(t) = \frac{C(t)}{370.5}$$

$$\bar{t} = \sum E(t) \cdot t \cdot \Delta t = 39.54 \text{ min}$$

$$\delta^2 = \sum (t - 39.53)^2 \cdot E(t) \cdot \Delta t = 98.73 \text{ min}^2$$

$$\bar{\delta}^2 = \frac{98.73}{39.54^2} = 0.0632$$

$$\frac{1}{Pe} = \frac{1}{8} * (\sqrt{8 * 0.0632 + 1} - 1) = 0.0284 \rightarrow Pe = \frac{1}{0.0284} = 35.3$$

$$D_{ax} = \frac{U_s H}{Pe} = \frac{0.815 \text{ cm/min} * 34.7 \text{ cm}}{35.3} = 0.802 \text{ cm}^2/\text{min}$$

Appendix B-4: Data for lab scale run 4

$$U_l = \frac{140 \text{ ml/min}}{19.63 \text{ cm}^2} = 7.13 \text{ cm/min}$$

$$H = 31.2 + 3 = 34.2 \text{ cm}$$

$$SCR = \frac{926 \text{ ml}}{56 \text{ min}} = 16.5 \text{ ml/min}$$

$$U_s = \frac{16.5 \text{ ml/min}}{19.63 \text{ cm}^2} = 0.842 \text{ cm/min}$$

$$1 \text{ ml EDTA} = \frac{0.4}{3} \text{ mgCa}$$

Time [min]	m _{total} [g]	V _{titrated} [ml]	V _{EDTA} [ml]	m _{Ca} [mg]	m _{tracers} [g]	% tracers
2	13.9	3	0.20	1.8	0.0	0.3
4	16.1	3	0.05	0.4	0.0	0.0
7	15.4	3	0.10	0.9	0.0	0.1
10	7.7	3	0.20	1.8	0.0	0.6
13	21.1	3	0.20	1.8	0.0	0.2
16	15.3	3	0.30	2.7	0.1	0.5
19	14.0	3	0.40	3.6	0.1	0.8
22	16.3	3	0.30	2.7	0.1	0.5
25	12.4	3	0.70	6.2	0.2	1.6
28	13.4	3	0.45	4.0	0.1	0.9
31	22.9	3	0.55	4.9	0.2	0.7
34	18.5	2	0.30	4.0	0.1	0.7
35	20.0	2	2.70	36.0	1.2	5.9
36	13.3	1	5.00	133.3	4.4	33.0
37	21.7	1	14.60	389.3	12.8	59.2
38	31.4	1	17.60	469.3	15.5	49.3
39	16.1	1	5.40	144.0	4.7	29.5
40	12.0	1	2.50	66.7	2.2	18.3
41	12.6	3	4.90	43.6	1.4	11.3
42	12.7	3	3.70	32.9	1.1	8.5
43	8.4	3	2.05	18.2	0.6	7.0
44	10.9	3	2.20	19.6	0.6	5.8
45	10.6	3	2.00	17.8	0.6	5.4
47	12.3	3	1.80	16.0	0.5	4.2
49	13.3	3	1.95	17.3	0.6	4.2
51	6.8	3	1.25	11.1	0.4	5.2
53	12.6	3	1.55	13.8	0.4	3.5
55	5.6	3	0.90	8.0	0.3	4.5
56	18.7	3	1.30	11.6	0.4	2.0

Next, the time mean, variance, dimensionless variance, Peclet number and dispersion coefficient are calculated.

t	C(t)	Δt	C * Δt	E(t)	E(t) * t * Δt	(t-39.13) ² *E* Δt
2	0.3	3.0	0.90	0.001	0.006	4.166
4	0.0	2.5	0.00	0.000	0.000	0.000
7	0.1	3.0	0.30	0.000	0.007	1.040
10	0.6	3.0	1.80	0.002	0.060	5.128
13	0.2	3.0	0.60	0.001	0.026	1.375
16	0.5	3.0	1.50	0.002	0.081	2.694
19	0.8	3.0	2.40	0.003	0.153	3.265
22	0.5	3.0	1.50	0.002	0.111	1.478
25	1.6	3.0	4.80	0.005	0.403	3.218
28	0.9	3.0	2.70	0.003	0.254	1.123
31	0.7	3.0	2.10	0.002	0.219	0.466
34	0.7	2.0	1.40	0.002	0.160	0.124
35	5.9	1.0	5.90	0.020	0.693	0.338
36	33.0	1.0	33.00	0.111	3.988	1.087
37	59.2	1.0	59.20	0.199	7.353	0.903
38	49.3	1.0	49.30	0.165	6.289	0.212
39	29.5	1.0	29.50	0.099	3.862	0.002
40	18.3	1.0	18.30	0.061	2.457	0.046
41	11.3	1.0	11.30	0.038	1.555	0.132
42	8.5	1.0	8.50	0.029	1.198	0.235
43	7.0	1.0	7.00	0.023	1.010	0.352
44	5.8	1.0	5.80	0.019	0.857	0.461
45	5.4	1.5	8.10	0.018	1.224	0.936
47	4.2	2.0	8.40	0.014	1.325	1.746
49	4.2	2.0	8.40	0.014	1.382	2.746
51	5.2	2.0	10.40	0.017	1.780	4.917
53	3.5	2.0	7.00	0.012	1.245	4.519
55	4.5	1.5	6.75	0.015	1.246	5.705
56	2.0	0.5	1.00	0.007	0.188	0.955

$$\sum C(t) \cdot \Delta t = 263.7 \rightarrow E(t) = \frac{C(t)}{263.7}$$

$$\bar{t} = \sum E(t) \cdot t \cdot \Delta t = 39.13 \text{ min}$$

$$\delta^2 = \sum (t - 39.13)^2 \cdot E(t) \cdot \Delta t = 49.37 \text{ min}^2$$

$$\bar{\delta}^2 = \frac{49.37}{39.13^2} = 0.0322$$

$$\frac{1}{Pe} = \frac{1}{8} * (\sqrt{8 * 0.0322 + 1} - 1) = 0.0152 \rightarrow Pe = \frac{1}{0.0152} = 65.8$$

$$D_{ax} = \frac{U_s H}{Pe} = \frac{0.842 \text{ cm/min} * 34.2 \text{ cm}}{65.8} = 0.437 \text{ cm}^2/\text{min}$$

Appendix B-5: Data for lab scale run 5

$$U_l = \frac{200 \text{ ml/min}}{19.63 \text{ cm}^2} = 10.2 \text{ cm/min}$$

$$H = 31.2 + 3 = 34.2 \text{ cm}$$

$$SCR = \frac{924 \text{ ml}}{56 \text{ min}} = 16.5 \text{ ml/min}$$

$$U_s = \frac{16.5 \text{ ml/min}}{19.63 \text{ cm}^2} = 0.841 \text{ cm/min}$$

$$1 \text{ ml EDTA} = \frac{0.4}{3} \text{ mgCa}$$

Time [min]	m _{total} [g]	V _{titrated} [ml]	V _{EDTA} [ml]	m _{Ca} [mg]	m _{tracers} [g]	% tracers
1	9.7	3	0.60	5.33	0.2	1.7
5	11.8	3	0.45	4.00	0.1	1.0
8	16.3	3	6.10	54.22	1.8	10.9
9	17.9	3	9.00	80.00	2.6	14.7
10	15.3	3	4.70	41.78	1.4	8.9
13	16.6	2	2.60	34.67	1.1	6.8
17	15.8	2	1.90	25.33	0.8	5.2
21	15.3	2	1.35	18.00	0.6	3.8
25	17.3	3	2.00	17.78	0.6	3.3
29	17.5	3	2.10	18.67	0.6	3.5
33	14.1	3	1.60	14.22	0.5	3.3
37	12.5	3	1.25	11.11	0.4	2.9
41	13.4	3	1.15	10.22	0.3	2.4
45	13.8	3	1.85	16.44	0.5	3.9
49	13.8	3	1.80	16.00	0.5	3.8
53	11.1	3	2.10	18.67	0.6	5.5
56	11.3	3	1.95	17.33	0.6	5.0

Next, the time mean, variance, dimensionless variance, Peclet number and dispersion coefficient are calculated.

t	C(t)	Δt	C * Δt	E(t)	E(t) * t * Δt	(t-26.25) ² * E * Δt
1	1.7	3.0	5.13	0.007	0.021	13.544
5	1.0	3.5	3.62	0.004	0.075	6.761
8	10.9	2.0	21.84	0.045	0.723	30.100
9	14.7	1.0	14.70	0.061	0.547	18.098
10	8.9	2.0	17.90	0.037	0.740	19.557

13	6.8	3.5	23.92	0.028	1.286	17.378
17	5.2	4.0	20.92	0.022	1.471	7.409
21	3.8	4.0	15.27	0.016	1.327	1.743
25	3.3	4.0	13.34	0.014	1.379	0.087
29	3.5	4.0	13.86	0.014	1.662	0.432
33	3.3	4.0	13.03	0.013	1.779	2.454
37	2.9	4.0	11.42	0.012	1.747	5.454
41	2.4	4.0	9.77	0.010	1.657	8.792
45	3.9	4.0	15.44	0.016	2.875	22.451
49	3.8	4.0	15.02	0.016	3.044	32.144
53	5.5	3.5	19.11	0.023	4.190	56.561
56	5.0	1.5	7.46	0.021	1.729	27.314

$$\sum C(t) \cdot \Delta t = 241.7 \rightarrow E(t) = \frac{C(t)}{241.7}$$

$$\bar{t} = \sum E(t) \cdot t \cdot \Delta t = 26.25 \text{ min}$$

$$\delta^2 = \sum (t - 26.25)^2 \cdot E(t) \cdot \Delta t = 270.3 \text{ min}^2$$

$$\bar{\delta}^2 = \frac{270.3}{26.25^2} = 0.392$$

$$\frac{1}{Pe} = \frac{1}{8} * (\sqrt{8 * 0.392 + 1} - 1) = 0.129 \rightarrow Pe = \frac{1}{0.129} = 7.74$$

$$D_{ax} = \frac{U_s H}{Pe} = \frac{0.841 \text{ cm/min} * 34.2 \text{ cm}}{7.74} = 3.71 \text{ cm}^2/\text{min}$$

C. Appendices: Pilot Scale Testing Data

Appendix C-1: Data for the baffle-free trial at $U_1 = 1.45U_{mf}$

Cross-sectional area of 10.1 cm column is:

$$A = \frac{\pi}{4} * 10.1^2 = 80.12 \text{ cm}^2$$

Liquid flowrate: 30 L/h = 500 ml/min

$$\therefore U_l = \frac{500}{80.12} = 6.2 \text{ cm/min}$$

0.01M EDTA was used: 1 ml EDTA = 0.4 mg Ca

Fresh resin was holding 1.425 milligram calcium per gram resin.

Probe 1

Time [min]	m_{total} [g]	V_{EDTA} [ml]	m_{Ca} [mg]	$m_{tracers}$ [g]	% tracers
1	20.9	0.37	29.3	0.0	0.0
3	23.3	0.47	37.3	0.2	0.7
5	23.9	0.70	56.0	0.9	3.6
7	29.7	1.12	89.3	1.8	6.2
9	27.1	1.17	93.3	2.1	7.9
11	25.8	1.12	89.3	2.1	8.0
13	27.3	1.10	88.0	1.9	7.0
15	22.7	0.97	77.3	1.8	7.8
17	24.4	0.92	73.3	1.5	6.2
19	20.4	0.73	58.7	1.2	5.7
21	27.4	0.85	68.0	1.1	4.1
25	21.5	0.62	49.3	0.7	3.4
31	26.7	0.67	53.3	0.6	2.2
45	27.4	0.68	54.7	0.6	2.2

In the table above: m_{total} is the weighed mass of a solids sample which includes both neutral particles – fresh resins, and tracers – loaded resins.

$$m_{Ca} = 0.4 * V_{EDTA} * 200$$

Assuming the calcium amount adsorbed back to the resin during the batch desorption was negligible due to a high molar ratio N_{Na}/N_{Ca} , the calcium amount was desorbed from neutral resin and tracer resin, therefore:

$$m_{Ca} = 1.425 * m_{fresh} + 27.24 * m_{tracer}$$

$$\text{where } m_{fresh} = m_{total} - m_{tracer};$$

and 27.24 is the slope of the calibration curve 1

Rearranging the equation above gives:

$$m_{tracer} = \frac{m_{Ca} - 1.425 * m_{total}}{27.24 - 1.425}$$

Next, %tracers from the table above is considered as concentration in liquid study, both essentially mean the same – how much tracers in the medium at that location at that time.

So time and %tracer – C are used to calculate time mean, variance.

t	C(t)	Δt	C * Δt	E(t)	E(t) * t * Δt	$(t-19.42)^2 * E * \Delta t$
1	0.0	2	0.0	0.000	0.00	0.00
3	0.7	2	1.4	0.004	0.02	2.16
5	3.6	2	7.2	0.021	0.21	8.62
7	6.2	2	12.4	0.036	0.50	11.02
9	7.9	2	15.8	0.046	0.82	9.90
11	8.0	2	15.9	0.046	1.01	6.52
13	7.0	2	14.1	0.041	1.05	3.35
15	7.8	2	15.5	0.045	1.34	1.75
17	6.2	2	12.4	0.036	1.21	0.42
19	5.7	2	11.4	0.033	1.24	0.01
21	4.1	3	12.4	0.024	1.50	0.18
25	3.4	5	17.0	0.020	2.45	3.05
31	2.2	10	22.4	0.013	4.00	17.31
45	2.2	7	15.6	0.013	4.05	58.90

$$\sum \Delta t = 45 \text{ min}$$

$$\sum C(t) \cdot \Delta t = 173.5 \rightarrow E(t) = \frac{C(t)}{173.5}$$

$$\bar{t}_1 = \sum E(t) \cdot t \cdot \Delta t = 19.42 \text{ min}$$

$$\delta^2_1 = \sum (t - 19.42)^2 \cdot E(t) \cdot \Delta t = 123.2 \text{ min}^2$$

Probe 2

Time [min]	m _{total} [g]	V _{EDTA} [ml]	m _{Ca} [mg]	m _{tracers} [g]	% tracers
22	24.3	0.52	41.3	0.3	1.1
27	21.4	0.65	52.0	0.8	3.9
32	19.7	0.55	44.0	0.6	3.2
40	19.9	0.65	52.0	0.9	4.6
46	18.4	0.55	44.0	0.7	3.8
50	27.4	0.85	68.0	1.1	4.1
52	17.3	0.63	50.7	1.0	5.9
54	26.7	0.83	66.7	1.1	4.2
56	23.1	0.77	61.3	1.1	4.8
58	20.0	0.72	57.3	1.1	5.6
63	31.7	0.85	68.0	0.9	2.8
69	28.0	0.80	64.0	0.9	3.4
72	38.3	1.05	84.0	1.2	3.0
76	22.3	0.30	24.0	0.0	0.0

These data were then used to calculate the time mean and the variance as follow:

t	C(t)	Δt	C * Δt	E(t)	E(t) * t * Δt	(t-48.39) ² * E * Δt
22	1.1	7.5	8.1	0.005	0.89	27.55
27	3.9	5.0	19.7	0.020	2.65	43.72
32	3.2	6.5	20.6	0.016	3.29	26.62
40	4.6	7.0	32.5	0.023	6.50	10.66
46	3.8	5.0	18.9	0.019	4.34	0.42
50	4.1	3.0	12.4	0.021	3.10	0.22
52	5.9	2.0	11.8	0.029	3.06	0.90
54	4.2	2.0	8.4	0.021	2.26	1.46
56	4.8	2.0	9.6	0.024	2.69	3.00
58	5.6	3.5	19.7	0.028	5.72	9.67
63	2.8	5.5	15.5	0.014	4.88	17.19
69	3.4	4.5	15.2	0.017	5.22	33.08
72	3.0	3.5	10.5	0.015	3.78	30.03
76	0.0	2.0	0.0	0.000	0.00	0.00

$$\sum \Delta t = 59 \text{ min}$$

$$\sum C(t) \cdot \Delta t = 202.9 \rightarrow E(t) = \frac{C(t)}{202.9}$$

$$\bar{t}_2 = \sum E(t) \cdot t \cdot \Delta t = 48.39 \text{ min}$$

$$\delta^2_2 = \sum(t - 48.39)^2 \cdot E(t) \cdot \Delta t = 204.5 \text{ min}^2$$

Using the time means and the variances from probe 1 and probe 2 data, the Peclet number and the mixing coefficient were calculated.

$$\bar{t} = \bar{t}_2 - \bar{t}_1 = 48.4 - 19.4 = 29.0 \text{ min}$$

$$\delta^2 = \delta^2_2 - \delta^2_1 = 204.5 - 123.2 = 81.3 \text{ min}^2$$

$$\bar{\delta}^2 = \frac{81.3}{29.0^2} = 0.0969$$

$$\frac{1}{Pe} = \frac{1}{8} * (\sqrt{8 * 0.0969 + 1} - 1) = 0.0416 \rightarrow Pe = \frac{1}{0.0416} = 24.1$$

$$D_{ax} = \frac{U_s H}{Pe} = \frac{1.85 \text{ cm/min} * 92.0 \text{ cm}}{24.1} = 7.07 \text{ cm}^2/\text{min}$$

Appendix C-2: Data for the louver trial at $U_1 = 1.45U_{mf}$

Diluted EDTA was used: $1 \text{ ml EDTA} = 0.4/3 \text{ mg Ca}$

Fresh resin was holding 5.240 milligram calcium per gram resin.

Probe 1

Time [min]	m_{total} [g]	V_{EDTA} [ml]	m_{Ca} [mg]	$m_{tracers}$ [g]	% tracers
1	28.4	4.90	130.7	0.0	0.0
5	24.3	4.90	130.7	0.2	0.6
9	23.3	6.40	170.7	2.2	9.5
13	25.0	7.10	189.3	2.7	10.7
16	24.8	6.80	181.3	2.4	9.5
20	22.6	5.85	156.0	1.7	7.6
24	22.2	5.55	148.0	1.4	6.5
28	26.1	5.60	149.3	0.6	2.2
34	25.5	5.60	149.3	0.7	2.8
42	20.1	4.70	125.3	0.9	4.6
52	23.9	5.05	134.7	0.4	1.8
64	24.5	4.95	132.0	0.2	0.7
90	25.2	5.40	144.0	0.5	2.2
118	24.6	5.30	141.3	0.6	2.3

Calculation was done similarly as in the baffle-free trial (Appendix C-1), except the neutral resin was holding more calcium on them, thus:

$$m_{tracer} = \frac{m_{Ca} - 5.240 * m_{total}}{27.24 - 5.240}$$

Time and %tracer – C are used to calculate time mean, variance.

t	C(t)	Δt	$C * \Delta t$	E(t)	$E(t) * t * \Delta t$	$(t-21.4)^2 * E * \Delta t$
1	0.0	3.0	0.0	0.000	0.00	0.00
5	0.6	4.0	2.5	0.003	0.05	2.93
9	9.5	4.0	38.2	0.041	1.49	25.40
13	10.7	3.5	37.4	0.046	2.11	11.40
16	9.5	3.5	33.2	0.041	2.30	4.17
20	7.6	4.0	30.4	0.033	2.64	0.25
24	6.5	4.0	26.1	0.028	2.72	0.78
28	2.2	5.0	11.0	0.010	1.34	2.09
34	2.8	7.0	19.7	0.012	2.91	13.64
42	4.6	7.0	31.9	0.020	5.81	58.82

$$\sum \Delta t = 45 \text{ min}$$

$$\sum C(t) \cdot \Delta t = 230.4 \rightarrow E(t) = \frac{C(t)}{230.4}$$

$$\bar{t}_1 = \sum E(t) \cdot t \cdot \Delta t = 21.4 \text{ min}$$

$$\delta^2_1 = \sum (t - 21.4)^2 \cdot E(t) \cdot \Delta t = 119.5 \text{ min}^2$$

It should be noted that the solids were sampled for 118 minutes, yet to calculate time mean and the variance, the time range was limited from 1 to 45 minutes, which was the same as in the baffle-free trial (Appendix C-1).

Probe 2

Time [min]	m _{total} [g]	V _{EDTA} [ml]	m _{Ca} [mg]	m _{tracers} [g]	% tracers
2	28.7	4.90	130.7	0.0	0.0
14	20.8	4.35	116.0	0.3	1.5
27	24.3	5.65	150.7	1.1	4.4
33	17.6	4.40	117.3	1.1	6.5
39	22.8	5.30	141.3	1.0	4.4
50	24.7	5.45	145.3	0.7	2.9
56	23.0	5.25	140.0	0.9	3.9
61	20.7	4.40	117.3	0.4	2.0
65	21.0	4.60	122.7	0.6	2.8
69	19.8	4.50	120.0	0.7	3.8
73	21.2	4.70	125.3	0.7	3.1
77	20.4	4.60	122.7	0.7	3.5
81	27.3	5.40	144.0	0.0	0.2
87	20.8	4.40	117.3	0.4	1.8
102	23.2	4.70	125.3	0.2	0.7
119	25.5	5.10	136.0	0.1	0.4

These data were then used to calculate the time mean and the variance as follow:

t	C(t)	Δt	C * Δt	E(t)	E(t) * t * Δt	(t-44.7) ² *E*Δt
17	1.5	3.5	5.4	0.007	0.42	18.82
27	4.4	9.5	41.7	0.020	5.11	59.54
33	6.5	6	39.2	0.030	5.86	24.47
39	4.4	8.5	37.3	0.020	6.59	5.57
50	2.9	8.5	25.0	0.013	5.68	3.14
56	3.9	5.5	21.3	0.018	5.41	12.25
61	2.0	4.5	8.8	0.009	2.44	10.57

65	2.8	4	11.0	0.012	3.24	20.47
69	3.8	4	15.0	0.017	4.70	40.06
73	3.1	4	12.3	0.014	4.07	44.52
77	3.5	1	3.5	0.016	1.23	16.68

$\sum \Delta t = 59 \text{ min}$ (Time range is from 17 to 76 minutes)

$$\sum C(t) \cdot \Delta t = 220.6 \rightarrow E(t) = \frac{C(t)}{220.6}$$

$$\bar{t}_2 = \sum E(t) \cdot t \cdot \Delta t = 44.7 \text{ min}$$

$$\delta^2_2 = \sum (t - 44.7)^2 \cdot E(t) \cdot \Delta t = 256.1 \text{ min}^2$$

Using the time means and the variances from probe 1 and probe 2 data, the Peclet number and the mixing coefficient were calculated.

$$\bar{t} = \bar{t}_2 - \bar{t}_1 = 44.7 - 21.4 = 23.4 \text{ min}$$

$$\delta^2 = \delta^2_2 - \delta^2_1 = 256.1 - 119.5 = 136.6 \text{ min}^2$$

$$\bar{\delta}^2 = \frac{136.6}{23.4^2} = 0.250$$

$$\frac{1}{Pe} = \frac{1}{8} * (\sqrt{8 * 0.250 + 1} - 1) = 0.092 \rightarrow Pe = \frac{1}{0.092} = 10.9$$

$$D_{ax} = \frac{U_s H}{Pe} = \frac{1.85 \text{ cm/min} * 92.0 \text{ cm}}{10.9} = 15.6 \text{ cm}^2/\text{min}$$

Appendix C-3: Data for the mesh trial at $U_1 = 1.45U_{mf}$

Diluted EDTA was used: $1 \text{ ml EDTA} = 0.4/3 \text{ mg Ca}$

Probe 1

Time [min]	m_{total} [g]	V_{EDTA} [ml]	m_{Ca} [mg]	$m_{tracers}$ [g]	% tracers
1	29.9	4.95	132.0	0.0	0.0
5	21.8	4.80	128.0	0.9	4.0
9	22.1	5.30	141.3	1.4	6.4
13	21.4	5.00	133.3	1.2	5.6
16	20.0	5.00	133.3	1.5	7.6
18	24.8	5.55	148.0	1.1	4.4
20	21.7	5.20	138.7	1.4	6.4
24	21.5	5.10	136.0	1.3	6.1
28	23.3	5.40	144.0	1.3	5.4
34	27.2	5.80	154.7	0.9	3.2
42	23.0	5.05	134.7	0.9	3.9
52	23.8	5.05	134.7	0.7	3.0
64	25.2	5.30	141.3	0.7	2.8
81	21.7	4.90	130.7	1.0	4.7
101	21.8	4.80	128.0	0.9	4.0
118	22.1	4.80	128.0	0.8	3.6

Calculation was done similarly as in the baffle-free trial (Appendix C-1), except the neutral resin was holding 4.986 mg calcium per gram resin, thus:

$$m_{tracer} = \frac{m_{Ca} - 4.986 * m_{total}}{27.24 - 4.986}$$

Time and %tracer – C are used to calculate time mean, variance.

t	C(t)	Δt	$C * \Delta t$	E(t)	$E(t) * t * \Delta t$	$(t-22.3)^2 * E * \Delta t$
1	0.0	3.0	0.0	0.000	0.00	0.00
5	4.0	4.0	16.0	0.019	0.38	22.88
9	6.4	4.0	25.5	0.030	1.10	21.50
13	5.6	3.5	19.7	0.027	1.22	8.11
16	7.6	2.5	19.0	0.036	1.45	3.58
18	4.4	2.0	8.9	0.021	0.76	0.78
20	6.4	3.0	19.1	0.030	1.82	0.47
24	6.1	4.0	24.2	0.029	2.78	0.34
28	5.4	5.0	27.0	0.026	3.62	4.23
34	3.2	7.0	22.2	0.015	3.61	14.57
42	3.9	7.0	27.5	0.019	5.53	51.19

$\sum \Delta t = 45 \text{ min}$ (Time range was from 1 to 45 minutes)

$$\sum C(t) \cdot \Delta t = 209.1 \rightarrow E(t) = \frac{C(t)}{209.1}$$

$$\bar{t}_1 = \sum E(t) \cdot t \cdot \Delta t = 22.3 \text{ min}$$

$$\delta^2_1 = \sum (t - 22.3)^2 \cdot E(t) \cdot \Delta t = 127.6 \text{ min}^2$$

Probe 2

Time [min]	m _{total} [g]	V _{EDTA} [ml]	m _{Ca} [mg]	m _{tracers} [g]	% tracers
2	28.6	4.90	130.7	0.0	0.0
8	23.2	4.60	122.7	0.3	1.4
14	19.8	4.25	113.3	0.7	3.3
27	21.6	4.70	125.3	0.8	3.7
39	20.7	4.60	122.7	0.9	4.3
50	20.8	4.60	122.7	0.9	4.1
61	19.5	4.40	117.3	0.9	4.7
65	22.4	4.90	130.7	0.9	3.8
68	19.4	4.40	117.3	0.9	4.8
70	19.5	4.50	120.0	1.0	5.3
72	21.3	4.50	120.0	0.6	2.9
74	20.2	4.60	122.7	1.0	4.9
78	22.3	4.85	129.3	0.8	3.7
82	23.0	4.85	129.3	0.7	2.9
88	20.4	4.65	124.0	1.0	4.9
96	24.6	5.15	137.3	0.7	2.7
109	21.4	4.70	125.3	0.8	3.9
119	21.0	4.80	128.0	1.1	5.0

These data were then used to calculate the time mean and the variance as follow:

t	C(t)	Δt	C * Δt	E(t)	E(t) * t * Δt	(t-48.0) ² *E* Δt
17	3.3	3.5	11.7	0.014	0.82	46.06
27	3.7	12.5	46.2	0.015	5.12	83.50
39	4.3	11.5	48.9	0.017	7.83	16.23
50	4.1	11	45.3	0.017	9.31	0.75
61	4.7	7.5	35.0	0.019	8.76	24.28
65	3.8	3.5	13.4	0.016	3.58	15.92
68	4.8	2.5	12.0	0.020	3.35	19.73
70	5.3	2	10.6	0.022	3.04	21.00
72	2.9	2	5.9	0.012	1.73	13.86
74	4.9	3	14.7	0.020	4.48	40.93

$\sum \Delta t = 59 \text{ min}$ (Time range is from 17 to 76 minutes)

$$\sum C(t) \cdot \Delta t = 243.7 \rightarrow E(t) = \frac{C(t)}{243.7}$$

$$\bar{t}_2 = \sum E(t) \cdot t \cdot \Delta t = \mathbf{48.0 \text{ min}}$$

$$\delta^2_2 = \sum (t - 48.0)^2 \cdot E(t) \cdot \Delta t = 282.3 \text{ min}^2$$

Using the time means and the variances from probe 1 and probe 2 data, the Peclet number and the mixing coefficient were calculated.

$$\bar{t} = \bar{t}_2 - \bar{t}_1 = 25.7 \text{ min}$$

$$\delta^2 = \delta^2_2 - \delta^2_1 = 154.6 \text{ min}^2$$

$$\bar{\delta}^2 = \frac{154.6}{25.7^2} = 0.234$$

$$\frac{1}{Pe} = \frac{1}{8} * (\sqrt{8 * 0.234 + 1} - 1) = 0.087 \rightarrow Pe = \frac{1}{0.087} = 11.5$$

$$D_{ax} = \frac{U_s H}{Pe} = \frac{1.85 \text{ cm/min} * 92.0 \text{ cm}}{11.5} = 14.8 \text{ cm}^2/\text{min}$$

Appendix C-4: Data for the vertical plane trial at $U_1 = 1.45U_{mf}$

Probe 1

Time [min]	m_{total} [g]	V_{EDTA} [ml]	m_{Ca} [mg]	$m_{tracers}$ [g]	% tracers
1	34.3	5.60	149.3	0.0	0.0
4	20.9	5.00	133.3	1.1	5.3
7	22.0	5.85	156.0	1.9	8.7
10	21.9	5.10	136.0	1.0	4.5
13	21.5	4.85	129.3	0.8	3.6
18	22.5	5.15	137.3	0.9	4.0
22	24.7	5.45	145.3	0.7	3.0
26	22.8	5.25	140.0	1.0	4.2
30	21.5	4.90	130.7	0.8	3.9
37	24.7	5.30	141.3	0.5	2.2
46	22.2	4.80	128.0	0.5	2.4
58	26.6	5.45	145.3	0.3	1.0
80	25.3	4.65	124.0	0.0	0.0
97	22.9	5.05	134.7	0.7	3.0
115	25.1	5.30	141.3	0.4	1.8

Calculation was done similarly as in the baffle-free trial (Appendix C-1), except the neutral resin was holding 5.240 mg calcium per gram resin, thus:

$$m_{tracer} = \frac{m_{Ca} - 5.240 * m_{total}}{25.4430 - 5.240}$$

Time and %tracer – C are used to calculate time mean, variance.

t	C(t)	Δt	C * Δt	E(t)	E(t) * t * Δt	$(t-19.9)^2 * E * \Delta t$
1	0.0	2.5	0.0	0.000	0.00	0.00
4	5.3	3	15.9	0.032	0.39	24.60
7	8.7	3	26.0	0.053	1.11	26.41
10	4.5	3	13.5	0.027	0.82	8.12
13	3.6	4	14.4	0.022	1.14	4.20
18	4.0	4.5	18.0	0.024	1.98	0.41
22	3.0	4	11.9	0.018	1.60	0.31
26	4.2	4	16.7	0.025	2.65	3.77
30	3.9	5.5	21.4	0.024	3.91	13.24
37	2.2	8	17.7	0.014	4.00	31.51
45	2.4	3.5	8.5	0.015	2.32	32.49

$\sum \Delta t = 45 \text{ min}$ (Time range was from 1 to 45 minutes)

$$\sum C(t) \cdot \Delta t = 164.0 \rightarrow E(t) = \frac{C(t)}{164.0}$$

$$\bar{t}_1 = \sum E(t) \cdot t \cdot \Delta t = \mathbf{19.9 \text{ min}}$$

$$\delta^2_1 = \sum (t - 19.9)^2 \cdot E(t) \cdot \Delta t = 145.1 \text{ min}^2$$

Probe 2

Time [min]	m _{total} [g]	V _{EDTA} [ml]	m _{Ca} [mg]	m _{tracers} [g]	% tracers
2	20.4	4.05	108.0	0.0	0.2
14	22.8	4.85	129.3	0.5	2.0
23	21.3	4.65	124.0	0.6	2.7
31	21.9	4.90	130.7	0.7	3.4
39	23.6	5.20	138.7	0.7	2.9
47	23.2	5.05	134.7	0.6	2.6
54	23.0	4.95	132.0	0.5	2.3
60	21.8	4.75	126.7	0.6	2.6
65	20.7	4.65	124.0	0.7	3.5
69	23.9	5.00	133.3	0.4	1.5
73	21.6	4.90	130.7	0.8	3.8
77	21.1	4.60	122.7	0.6	2.6
81	21.9	4.90	130.7	0.7	3.4
88	20.8	4.60	122.7	0.6	3.0
99	21.3	4.80	128.0	0.8	3.6
116	21.6	4.70	125.3	0.6	2.6

These data were then used to calculate the time mean and the variance as follow:

t	C(t)	Δt	C * Δt	E(t)	E(t) * t * Δt	(t-46.3) ² *E*Δt
17	2.0	1.5	3.0	0.0120	0.31	15.46
23	2.7	8.5	22.8	0.0162	3.17	75.04
31	3.4	8.0	26.9	0.0203	5.04	38.27
39	2.9	8.0	23.5	0.0177	5.53	7.66
47	2.6	7.5	19.5	0.0157	5.54	0.05
54	2.3	6.5	14.9	0.0139	4.86	5.27
60	2.6	5.5	14.5	0.0159	5.24	16.27
65	3.5	4.5	15.6	0.0210	6.14	32.85
69	1.5	4.0	6.2	0.0093	2.57	19.09
73	3.8	5.0	18.8	0.0227	8.27	80.47

$\sum \Delta t = 59 \text{ min}$ (Time range is from 17 to 76 minutes)

$$\sum C(t) \cdot \Delta t = 165.7 \rightarrow E(t) = \frac{C(t)}{165.7}$$

$$\bar{t}_2 = \sum E(t) \cdot t \cdot \Delta t = 46.3 \text{ min}$$

$$\delta^2_2 = \sum (t - 48.0)^2 \cdot E(t) \cdot \Delta t = 290. \text{ min}^2$$

Using the time means and the variances from probe 1 and probe 2 data, the Peclet number and the mixing coefficient were calculated.

$$\bar{t} = \bar{t}_2 - \bar{t}_1 = 26.4 \text{ min}$$

$$\delta^2 = \delta^2_2 - \delta^2_1 = 145.4 \text{ min}^2$$

$$\bar{\delta}^2 = \frac{145.4}{26.4^2} = 0.208$$

$$\frac{1}{Pe} = \frac{1}{8} * (\sqrt{8 * 0.208 + 1} - 1) = 0.079 \rightarrow Pe = \frac{1}{0.079} = 12.6$$

$$D_{ax} = \frac{U_s H}{Pe} = \frac{1.85 \text{ cm/min} * 92.0 \text{ cm}}{12.6} = 13.5 \text{ cm}^2/\text{min}$$

Appendix C-5: Data for the baffle-free trial at $U_1 = 2.66U_{mf}$ (Run #1)

Probe 1

Time [min]	m_{total} [g]	V_{EDTA} [ml]	m_{Ca} [mg]	$m_{tracers}$ [g]	% tracers
1	22.9	3.97	105.8	0.0	0.0
5	22.9	4.30	114.7	0.3	1.2
9	23.0	4.95	132.0	1.0	4.5
11	22.4	4.70	125.3	0.9	3.9
13	24.6	5.00	133.3	0.8	3.1
15	24.6	5.05	134.7	0.8	3.3
17	23.8	4.90	130.7	0.8	3.4
19	23.1	4.85	129.3	0.9	3.9
21	24.0	4.90	130.7	0.8	3.2
23	23.2	4.75	126.7	0.8	3.2
25	23.7	4.80	128.0	0.7	3.0
27	21.3	4.60	122.7	1.0	4.6
29	23.6	4.80	128.0	0.7	3.1
33	26.3	5.10	136.0	0.5	1.9
37	23.3	4.80	128.0	0.8	3.4
43	24.7	5.00	133.3	0.7	3.0
53	24.0	4.90	130.7	0.8	3.2
63	22.9	4.85	129.3	0.9	4.1

Calculation was done similarly as in the baffle-free trial (Appendix C-1), except the neutral resin was holding 4.754 mg calcium per gram resin, thus:

$$m_{tracer} = \frac{m_{Ca} - 4.754 * m_{total}}{25.4430 - 4.754}$$

Time and %tracer – C are used to calculate time mean, variance.

t	C(t)	Δt	$C * \Delta t$	E(t)	$E(t) * t * \Delta t$	$(t-36.8)^2 * E * \Delta t$
1	0.0	3	0.0	0.000	0.00	0.00
5	1.2	4	4.7	0.005	0.11	22.26
9	4.5	3	13.6	0.021	0.58	49.62
11	3.9	2	7.7	0.018	0.40	24.33
13	3.1	2	6.1	0.014	0.38	16.39
15	3.3	2	6.6	0.016	0.47	14.87
17	3.4	2	6.8	0.016	0.54	12.54
19	3.9	2	7.8	0.018	0.70	11.63
21	3.2	2	6.3	0.015	0.63	7.49
23	3.2	2	6.5	0.015	0.70	5.84
25	3.0	2	5.9	0.014	0.70	3.92
27	4.6	2	9.2	0.022	1.18	4.20

29	3.1	3	9.2	0.015	1.27	2.66
33	1.9	4	7.7	0.009	1.20	0.52
37	3.4	5	17.0	0.016	2.97	0.00
43	3.0	8	23.7	0.014	4.81	4.29
53	3.2	10	31.7	0.015	7.95	39.31
63	4.1	10	41.1	0.019	12.23	133.15
Σ		68	221.6		36.8	353.0

Probe 2

Time [min]	m_{total} [g]	V_{EDTA} [ml]	m_{Ca} [mg]	m_{tracers} [g]	% tracers
2	24.9	4.45	118.7	0.0	0.1
10	22.2	4.70	125.3	0.9	4.1
18	21.5	4.45	118.7	0.8	3.5
22	23.5	4.75	126.7	0.7	2.9
30	21.8	4.55	121.3	0.8	3.7
34	22.1	4.55	121.3	0.7	3.4
38	21.8	4.65	124.0	0.9	4.3
42	22.9	4.80	128.0	0.9	3.8
49	23.1	4.85	129.3	0.9	3.9
52	23.4	4.85	129.3	0.8	3.6
57	23.9	4.90	130.7	0.8	3.3
65	21.4	4.55	121.3	0.9	4.2
69	22.6	4.55	121.3	0.6	2.8
74	24.6	4.90	130.7	0.6	2.6
80	24.1	4.90	130.7	0.7	3.1
98	23.1	4.80	128.0	0.8	3.6
108	23.9	4.85	129.3	0.7	3.0

These data were then used to calculate the time mean and the variance as follow:

t	C(t)	Δt	$C * \Delta t$	E(t)	$E(t) * t * \Delta t$	$(t-55.6)^2 * E * \Delta t$
2	0.1	6	0.3	0.000	0.00	2.62
10	4.1	8	32.8	0.012	0.92	191.86
18	3.5	6	21.1	0.010	1.07	83.99
22	2.9	6	17.5	0.008	1.09	55.74
30	3.7	6	22.4	0.010	1.89	41.31
34	3.4	4	13.5	0.010	1.29	17.78
38	4.3	4	17.2	0.012	1.84	14.99
42	3.8	5.5	21.1	0.011	2.49	11.01
49	3.9	5	19.4	0.011	2.68	2.39
52	3.6	4	14.2	0.010	2.08	0.52
57	3.3	6.5	21.3	0.009	3.42	0.11
65	4.2	6	25.2	0.012	4.62	6.26
69	2.8	4.5	12.7	0.008	2.47	6.41
74	2.6	5.5	14.1	0.007	2.93	13.40

80	3.1	12	36.8	0.009	8.29	61.60
98	3.6	14	50.6	0.010	13.96	255.90
108	3.0	5	15.1	0.008	4.59	116.60
Σ		108	355.4		55.6	882.5

Using the time means and the variances from probe 1 and probe 2 data, the Peclet number and the mixing coefficient were calculated.

$$\bar{t} = \bar{t}_2 - \bar{t}_1 = 18.8 \text{ min}$$

$$\delta^2 = \delta^2_2 - \delta^2_1 = 529.4 \text{ min}^2$$

$$\bar{\delta}^2 = \frac{529.4}{18.8^2} = 1.50$$

$$\frac{1}{Pe} = \frac{1}{8} * (\sqrt{8 * 1.50 + 1} - 1) = 0.325 \rightarrow Pe = \frac{1}{0.325} = 3.07$$

$$D_{ax} = \frac{U_s H}{Pe} = \frac{1.85 \text{ cm/min} * 92.0 \text{ cm}}{3.07} = 55.4 \text{ cm}^2/\text{min}$$

Appendix C-6: Data for the baffle-free trial at $U_1 = 2.66U_{mf}$ (Run #2)

Probe 1

Time [min]	m_{total} [g]	V_{EDTA} [ml]	m_{Ca} [mg]	$m_{tracers}$ [g]	% tracers
1	30.9	5.45	145.3	0.0	0.0
5	28.9	5.50	146.7	0.0	0.0
9	25.0	5.65	150.7	0.9	3.7
11	26.4	6.00	160.0	1.0	3.8
13	22.6	5.40	144.0	1.2	5.3
15	23.0	5.25	140.0	0.9	4.0
17	24.5	5.55	148.0	0.9	3.7
21	21.8	5.05	134.7	1.0	4.4
25	24.8	5.40	144.0	0.7	2.6
29	23.2	5.20	138.7	0.8	3.4
37	24.0	5.30	141.3	0.7	3.0
43	24.8	5.40	144.0	0.7	2.6
53	26.0	5.55	148.0	0.5	2.1
68	22.5	5.05	134.7	0.8	3.5

Calculation was done similarly as in the baffle-free trial (Appendix C-1), except the neutral resin was holding 5.243 mg calcium per gram resin, thus:

$$m_{tracer} = \frac{m_{Ca} - 5.243 * m_{total}}{25.4430 - 5.243}$$

Time and %tracer – C are used to calculate time mean, variance.

t	C(t)	Δt	$C * \Delta t$	E(t)	$E(t) * t * \Delta t$	$(t-35.0)^2 * E * \Delta t$
1	0.0	3.0	0.0	0.000	0.00	0.00
5	0.0	4.0	0.0	0.000	0.00	0.00
9	3.7	3.0	11.0	0.019	0.52	38.95
11	3.8	2.0	7.7	0.020	0.44	23.09
13	5.3	2.0	10.6	0.028	0.72	26.79
15	4.0	2.0	7.9	0.021	0.62	16.56
17	3.7	3.0	11.2	0.019	0.99	19.03
21	4.4	4.0	17.6	0.023	1.92	18.00
25	2.6	4.0	10.6	0.014	1.38	5.55
29	3.4	6.0	20.7	0.018	3.12	3.93
37	3.0	7.0	21.2	0.016	4.09	0.42
43	2.6	8.0	21.2	0.014	4.74	6.97
53	2.1	12.5	26.4	0.011	7.27	44.25
68	3.5	7.5	26.2	0.018	9.25	147.72
Σ		68	192.4		35.0	351.3

Probe 2

Time [min]	m _{total} [g]	V _{EDTA} [ml]	m _{Ca} [mg]	m _{tracers} [g]	% tracers
2	34.5	5.90	157.3	0.0	0.0
10	22.3	5.30	141.3	1.1	5.1
18	21.9	5.10	136.0	1.0	4.5
26	23.1	5.15	137.3	0.8	3.3
34	22.6	5.15	137.3	0.9	3.9
42	21.4	4.90	130.7	0.9	4.1
48	23.3	5.25	140.0	0.8	3.6
57	22.3	5.05	134.7	0.8	3.7
65	22.9	5.15	137.3	0.8	3.5
74	22.2	5.05	134.7	0.9	3.9
80	22.5	5.05	134.7	0.8	3.5
89	21.8	5.00	133.3	0.9	4.1
98	25.4	5.55	148.0	0.7	2.7
108	23.4	5.20	138.7	0.8	3.2

These data were then used to calculate the time mean and the variance as follow:

t	C(t)	Δt	C * Δt	E(t)	E(t) * t * Δt	$(t-54.0)^2 * E * \Delta t$
2	0.0	6.0	0.0	0.000	0.00	0.00
10	5.1	8.0	41.2	0.013	1.06	206.15
18	4.5	8.0	36.4	0.012	1.69	121.91
26	3.3	8.0	26.4	0.009	1.77	53.56
34	3.9	8.0	31.3	0.010	2.76	32.45
42	4.1	7.0	28.4	0.010	3.08	10.59
48	3.6	7.5	27.0	0.009	3.35	2.52
57	3.7	8.5	31.8	0.010	4.69	0.73
65	3.5	8.5	30.1	0.009	5.06	9.40
74	3.9	7.5	29.0	0.010	5.55	29.97
80	3.5	7.5	26.2	0.009	5.41	45.68
89	4.1	9.0	36.9	0.011	8.50	116.90
98	2.7	9.5	26.1	0.007	6.60	130.39
108	3.2	5.0	16.0	0.008	4.48	120.94
Σ		108	386.8		54.0	881.2

Using the time means and the variances from probe 1 and probe 2 data, the Peclet number and the mixing coefficient were calculated.

$$\bar{t} = \bar{t}_2 - \bar{t}_1 = 19.0 \text{ min}$$

$$\delta^2 = \delta^2_2 - \delta^2_1 = 529.9 \text{ min}^2$$

$$\bar{\delta}^2 = \frac{529.9}{19.0^2} = 1.47$$

$$\frac{1}{Pe} = \frac{1}{8} * (\sqrt{8 * 1.47 + 1} - 1) = 0.322 \rightarrow Pe = \frac{1}{0.322} = 3.11$$

$$D_{ax} = \frac{U_s H}{Pe} = \frac{1.85 \text{ cm/min} * 92.0 \text{ cm}}{3.11} = 54.8 \text{ cm}^2/\text{min}$$

Appendix C-7: Data for the louver trial at $U_1 = 2.66U_{mf}$

Probe 1

Time [min]	m_{total} [g]	V_{EDTA} [ml]	m_{Ca} [mg]	$m_{tracers}$ [g]	% tracers
1	25.6	5.00	133.3	0.1	0.2
5	21.9	5.20	138.7	1.2	5.5
9	25.6	6.45	172.0	1.9	7.3
13	23.6	5.80	154.7	1.5	6.5
15	23.0	5.80	154.7	1.7	7.3
23	22.5	5.30	141.3	1.2	5.3
27	26.1	5.75	153.3	0.9	3.4
34	22.8	5.20	138.7	1.0	4.3
42	31.3	6.10	162.7	0.1	0.2
52	24.9	5.30	141.3	0.6	2.4
64	26.7	5.00	133.3	0.0	0.0
74	23.3	5.20	138.7	0.9	3.7
87	24.5	5.30	141.3	0.7	2.9
101	22.9	5.20	138.7	1.0	4.2
119	21.8	4.95	132.0	0.9	4.2

Calculation was done similarly as in the baffle-free trial (Appendix C-1), except the neutral resin was holding 4.794 mg calcium per gram resin, thus:

$$m_{tracer} = \frac{m_{Ca} - 4.794 * m_{total}}{25.4430 - 4.794}$$

Time and %tracer – C are used to calculate time mean, variance.

t	C(t)	Δt	$C * \Delta t$	E(t)	$E(t) * t * \Delta t$	$(t-22.7)^2 * E * \Delta t$
1	0.2	3.0	0.7	0.001	0.00	1.49
5	5.5	4.0	22.0	0.025	0.50	31.30
9	7.3	4.0	29.2	0.033	1.20	24.90
13	6.5	3.0	19.6	0.030	1.16	8.35
15	7.3	5.0	36.6	0.034	2.51	9.82
23	5.3	6.0	31.5	0.024	3.32	0.02
27	3.4	5.5	18.4	0.015	2.28	1.59
34	4.3	7.5	32.4	0.020	5.04	19.08
42	0.2	9.0	1.6	0.001	0.31	2.74
52	2.4	11.0	26.6	0.011	6.33	104.85
64	0.0	10.0	0.0	0.000	0.00	0.00
Σ		68	218.7		22.7	204.1

Probe 2

Time [min]	m _{total} [g]	V _{EDTA} [ml]	m _{Ca} [mg]	m _{tracers} [g]	% tracers
2	24.1	4.75	126.7	0.1	0.5
14	24.9	5.80	154.7	1.2	4.9
20	22.8	5.70	152.0	1.6	7.1
26	20.8	5.20	138.7	1.5	7.1
36	20.7	5.00	133.3	1.2	6.0
44	22.8	5.10	136.0	0.9	3.8
51	20.8	4.80	128.0	1.0	4.7
55	21.2	4.90	130.7	1.0	4.7
59	24.0	5.30	141.3	0.8	3.4
63	20.4	4.80	128.0	1.1	5.2
68	20.2	4.80	128.0	1.1	5.5
73	20.0	4.75	126.7	1.1	5.5
77	21.3	4.95	132.0	1.0	4.9
86	22.4	4.90	130.7	0.7	3.2
99	22.6	5.10	136.0	0.9	4.0
106	22.0	4.05	108.0	0.0	0.0

These data were then used to calculate the time mean and the variance as follow:

t	C(t)	Δt	C * Δt	E(t)	E(t) * t * Δt	$(t-46.3)^2 * E * \Delta t$
2	0.5	8.0	3.6	0.001	0.02	18.38
14	4.9	9.0	44.3	0.010	1.32	127.73
20	7.1	6.0	42.3	0.015	1.80	85.42
26	7.1	8.0	56.5	0.015	3.13	73.82
36	6.0	9.0	54.0	0.013	4.14	25.12
44	3.8	7.5	28.3	0.008	2.65	2.77
51	4.7	5.5	25.6	0.010	2.78	0.00
55	4.7	4.0	18.8	0.010	2.20	0.72
59	3.4	4.0	13.7	0.007	1.72	1.97
63	5.2	4.5	23.5	0.011	3.15	7.48
68	5.5	5.0	27.6	0.012	3.99	17.42
73	5.5	4.5	24.7	0.012	3.85	26.03
77	4.9	6.5	31.6	0.010	5.18	46.27
86	3.2	11.0	34.7	0.007	6.36	91.77
99	4.0	10.0	40.2	0.009	8.48	199.12
106	0.0	5.5	0.0	0.000	0.00	0.00
Σ		108	469.5		50.8	724.0

Using the time means and the variances from probe 1 and probe 2 data, the Peclet number and the mixing coefficient were calculated.

$$\bar{t} = \bar{t}_2 - \bar{t}_1 = 28.1 \text{ min}$$

$$\delta^2 = \delta^2_2 - \delta^2_1 = 519.9 \text{ min}^2$$

$$\bar{\delta}^2 = \frac{519.9}{28.1^2} = 0.657$$

$$\frac{1}{Pe} = \frac{1}{8} * (\sqrt{8 * 0.657 + 1} - 1) = 0.188 \rightarrow Pe = \frac{1}{0.188} = 5.33$$

$$D_{ax} = \frac{U_s H}{Pe} = \frac{1.85 \text{ cm/min} * 92.0 \text{ cm}}{5.33} = 32.0 \text{ cm}^2/\text{min}$$

Appendix C-8: Data for the mesh trial at $U_1 = 2.66U_{mf}$

Probe 1

Time [min]	m_{total} [g]	V_{EDTA} [ml]	m_{Ca} [mg]	$m_{tracers}$ [g]	% tracers
1	26.5	4.50	120.0	0.0	0.0
5	26.0	5.60	149.3	1.1	4.4
9	21.5	5.10	136.0	1.5	7.0
13	25.0	5.35	142.7	1.1	4.2
15	25.0	5.30	141.3	1.0	4.0
23	21.8	4.80	128.0	1.1	5.0
27	21.6	4.60	122.7	0.9	4.1
34	21.2	4.40	117.3	0.7	3.4
42	25.4	4.95	132.0	0.5	1.9
52	22.0	4.45	118.7	0.6	2.8
64	22.1	4.50	120.0	0.6	2.9
81	22.3	4.60	122.7	0.7	3.3
101	21.9	4.50	120.0	0.7	3.2
119	27.3	5.25	140.0	0.4	1.5

Calculation was done similarly as in the baffle-free trial (Appendix C-1), except the neutral resin was holding 4.794 mg calcium per gram resin, thus:

$$m_{tracer} = \frac{m_{Ca} - 4.794 * m_{total}}{25.4430 - 4.794}$$

Time and %tracer – C are used to calculate time mean, variance.

t	C(t)	Δt	$C * \Delta t$	E(t)	$E(t) * t * \Delta t$	$(t-30.6)^2 * E * \Delta t$
1	0.0	3.0	0.0	0.000	0.00	0.00
5	4.4	4.0	17.5	0.019	0.38	49.54
9	7.0	4.0	28.2	0.030	1.09	56.93
13	4.2	3.0	12.6	0.018	0.71	16.91
15	4.0	5.0	19.8	0.017	1.28	20.86
23	5.0	6.0	29.8	0.021	2.95	7.50
27	4.1	5.5	22.4	0.018	2.61	1.28
34	3.4	7.5	25.6	0.015	3.74	1.24
42	1.9	9.0	16.7	0.008	3.02	9.27
52	2.8	11.0	30.4	0.012	6.80	59.66
64	2.9	10.0	29.3	0.013	8.07	140.26
Σ		68	232.1		30.6	363.4

Probe 2

Time [min]	m _{total} [g]	V _{EDTA} [ml]	m _{Ca} [mg]	m _{tracers} [g]	% tracers
2	29.4	4.85	129.3	0.0	0.0
14	22.9	5.00	133.3	1.1	4.7
20	20.9	4.70	125.3	1.2	5.5
26	21.4	4.60	122.7	0.9	4.3
36	21.7	4.55	121.3	0.8	3.7
51	22.2	4.65	124.0	0.8	3.6
55	22.1	4.60	122.7	0.8	3.5
59	24.3	4.80	128.0	0.5	2.2
63	21.2	4.40	117.3	0.7	3.4
68	20.9	4.40	117.3	0.8	3.8
73	21.4	4.50	120.0	0.8	3.7
77	24.3	4.75	126.7	0.5	1.9
86	22.2	4.55	121.3	0.7	3.1
99	24.9	4.95	132.0	0.6	2.3
120	25.2	4.95	132.0	0.5	2.0

These data were then used to calculate the time mean and the variance as follow:

t	C(t)	Δt	C * Δt	E(t)	E(t) * t * Δt	(t-51.3) ² *E* Δt
2	0.0	8.0	0.0	0.000	0.00	0.00
14	4.7	9.0	42.6	0.014	1.72	170.46
20	5.5	6.0	33.2	0.016	1.91	93.57
26	4.3	8.0	34.5	0.012	2.59	63.55
36	3.7	12.5	45.9	0.011	4.76	30.83
51	3.6	9.5	34.6	0.010	5.08	0.01
55	3.5	4.0	13.9	0.010	2.21	0.56
59	2.2	4.0	8.7	0.006	1.48	1.50
63	3.4	4.5	15.3	0.010	2.78	6.07
68	3.8	5.0	18.9	0.011	3.70	15.20
73	3.7	4.5	16.8	0.011	3.54	22.90
77	1.9	6.5	12.5	0.006	2.78	23.87
86	3.1	11.0	34.0	0.009	8.42	118.04
99	2.3	15.5	36.2	0.007	10.32	237.33
Σ		108	347.3		51.3	783.9

Using the time means and the variances from probe 1 and probe 2 data, the Peclet number and the mixing coefficient were calculated.

$$\bar{t} = \bar{t}_2 - \bar{t}_1 = 20.6 \text{ min}$$

$$\delta^2 = \delta^2_2 - \delta^2_1 = 420.4 \text{ min}^2$$

$$\bar{\delta}^2 = \frac{420.4}{20.6^2} = 0.988$$

$$\frac{1}{Pe} = \frac{1}{8} * (\sqrt{8 * 0.988 + 1} - 1) = 0.248 \rightarrow Pe = \frac{1}{0.248} = 4.03$$

$$D_{ax} = \frac{U_s H}{Pe} = \frac{1.85 \text{ cm/min} * 92.0 \text{ cm}}{4.03} = 42.2 \text{ cm}^2/\text{min}$$

Appendix C-9: Data for the vertical plane trial at $U_1 = 2.66U_{mf}$

Probe 1

Time [min]	m_{total} [g]	V_{EDTA} [ml]	m_{Ca} [mg]	$m_{tracers}$ [g]	% tracers
1	26.6	5.10	136.0	0.0	0.0
8	23.0	5.40	144.0	0.8	3.4
11	22.7	5.25	140.0	0.7	2.9
14	20.5	5.00	133.3	0.9	4.5
16	22.6	5.35	142.7	0.8	3.6
18	22.1	5.25	140.0	0.8	3.7
22	22.8	5.20	138.7	0.6	2.5
26	25.0	5.50	146.7	0.4	1.5
31	25.2	5.50	146.7	0.3	1.3
37	25.6	5.60	149.3	0.3	1.3
46	23.3	5.25	140.0	0.5	2.1
57	23.2	5.30	141.3	0.6	2.5
71	23.3	5.20	138.7	0.4	1.9
97	21.8	4.95	132.0	0.5	2.4
115	23.3	5.30	141.3	0.6	2.4

Calculation was done similarly as in the baffle-free trial (Appendix C-1), except the neutral resin was holding 5.558 mg calcium per gram resin, thus:

$$m_{tracer} = \frac{m_{Ca} - 5.558 * m_{total}}{25.4430 - 5.558}$$

Time and %tracer – C are used to calculate time mean, variance.

t	C(t)	Δt	$C * \Delta t$	E(t)	$E(t) * t * \Delta t$	$(t-33.4)^2 * E * \Delta t$
1	0.0	4.5	0.0	0.000	0.00	0.0
8	3.4	5.0	16.8	0.022	0.90	72.5
11	2.9	3.0	8.7	0.019	0.64	29.3
14	4.5	2.5	11.3	0.030	1.06	28.5
16	3.6	2.0	7.2	0.024	0.77	14.6
18	3.7	3.0	11.1	0.025	1.34	17.7
22	2.5	4.0	10.0	0.017	1.47	8.7
26	1.5	4.5	6.6	0.010	1.15	2.4
31	1.3	5.5	6.9	0.008	1.43	0.3
37	1.3	7.5	9.9	0.009	2.44	0.9
46	2.1	10.0	21.5	0.014	6.62	22.8
57	2.5	12.5	31.8	0.017	12.16	118.7
68	1.9	4.0	7.5	0.013	3.42	60.2
Σ		68	149.3		33.4	376.6

Probe 2

Time [min]	m _{total} [g]	V _{EDTA} [ml]	m _{Ca} [mg]	m _{tracers} [g]	% tracers
2	28.0	5.40	144.0	0.0	0.0
9	22.4	5.10	136.0	0.5	2.4
15	21.4	5.15	137.3	0.9	4.1
25	22.1	5.00	133.3	0.5	2.3
35	22.8	5.15	137.3	0.5	2.2
45	21.7	4.95	132.0	0.5	2.5
52	23.1	5.20	138.7	0.5	2.1
56	22.7	5.10	136.0	0.5	2.1
60	22.2	5.00	133.3	0.5	2.1
64	21.4	5.00	133.3	0.7	3.2
68	22.0	5.10	136.0	0.7	3.0
72	23.1	5.20	138.7	0.5	2.1
76	22.1	5.25	140.0	0.8	3.7
83	22.6	5.10	136.0	0.5	2.2
91	22.1	5.05	134.7	0.6	2.6
102	21.3	5.00	133.3	0.7	3.3
110	20.4	4.80	128.0	0.7	3.4
119	22.6	5.15	137.3	0.6	2.5

These data were then used to calculate the time mean and the variance as follow:

t	C(t)	Δt	C * Δt	E(t)	E(t) * t * Δt	(t-54.7) ² *E*Δt
2	0.0	5.5	0.0	0.000	0.00	0.0
9	2.4	6.5	15.9	0.009	0.52	115.4
15	4.1	8.0	32.8	0.015	1.78	178.2
25	2.3	10.0	22.7	0.008	2.05	67.8
35	2.2	10.0	22.2	0.008	2.81	28.2
45	2.5	8.5	21.3	0.009	3.47	5.9
52	2.1	5.5	11.7	0.008	2.20	0.1
56	2.1	4.0	8.3	0.007	1.68	0.2
60	2.1	4.0	8.5	0.008	1.86	1.2
64	3.2	4.0	12.8	0.012	2.97	4.9
68	3.0	4.0	11.9	0.011	2.93	8.7
72	2.1	4.0	8.5	0.008	2.21	10.2
76	3.7	5.5	20.4	0.013	5.61	36.5
83	2.2	7.5	16.4	0.008	4.94	50.9
91	2.6	9.5	24.3	0.009	7.99	121.9
102	3.3	9.5	31.8	0.012	11.74	268.0
108	3.4	2.0	6.8	0.012	2.67	72.8
Σ		108	276.3		54.7	898.2

Using the time means and the variances from probe 1 and probe 2 data, the Peclet number and the mixing coefficient were calculated.

$$\bar{t} = \bar{t}_2 - \bar{t}_1 = 21.3 \text{ min}$$

$$\delta^2 = \delta^2_2 - \delta^2_1 = 521.6 \text{ min}^2$$

$$\bar{\delta}^2 = \frac{521.6}{21.3^2} = 1.15$$

$$\frac{1}{Pe} = \frac{1}{8} * (\sqrt{8 * 1.15 + 1} - 1) = 0.274 \rightarrow Pe = \frac{1}{0.274} = 3.66$$

$$D_{ax} = \frac{U_s H}{Pe} = \frac{1.85 \text{ cm/min} * 92.0 \text{ cm}}{3.66} = 46.6 \text{ cm}^2/\text{min}$$

Appendix C-10: Data for the baffle-free trial at $U_1 = 3.86U_{mf}$

Probe 1

Time [min]	m_{total} [g]	V_{EDTA} [ml]	m_{Ca} [mg]	$m_{tracers}$ [g]	% tracers
1	22.3	0.80	64	0.5	2.2
4	23.8	0.80	64	0.3	1.5
7	23.0	1.35	108	2.2	9.6
10	24.7	1.40	112	2.2	8.9
13	23.7	1.30	104	2.0	8.3
17	28.5	1.40	112	1.8	6.5
21	27.0	1.20	96	1.3	5.0
25	27.5	1.20	96	1.3	4.7
27	25.8	1.20	96	1.5	5.6
29	24.9	1.25	100	1.7	6.8
35	26.0	1.20	96	1.4	5.5
43	29.4	1.30	104	1.4	4.9
57	29.5	1.35	108	1.6	5.4
74	31.5	1.30	104	1.2	3.9
95	34.6	1.30	104	0.9	2.7

Calculation was done similarly as in the baffle-free trial (Appendix C-1), except the neutral resin was holding 2.331 mg calcium per gram resin, thus:

$$m_{tracer} = \frac{m_{Ca} - 2.331 * m_{total}}{27.24 - 2.331}$$

Time and %tracer – C are used to calculated time mean, variance.

t	C(t)	Δt	$C * \Delta t$	E(t)	$E(t) * t * \Delta t$	$(t-35.0)^2 * E * \Delta t$
1	2.2	2.5	5.5	0.005	0.01	15.7
4	1.5	3.0	4.4	0.004	0.04	10.4
7	9.6	3.0	28.8	0.024	0.50	56.0
10	8.9	3.0	26.8	0.022	0.67	41.6
13	8.3	3.5	29.2	0.021	0.94	35.1
17	6.5	4.0	25.9	0.016	1.10	20.8
21	5.0	4.0	19.9	0.012	1.04	9.7
25	4.7	3.0	14.1	0.012	0.88	3.5
27	5.6	2.0	11.3	0.014	0.76	1.8
29	6.8	4.0	27.3	0.017	1.97	2.4
35	5.5	7.0	38.7	0.014	3.36	0.0
43	4.9	11.0	53.8	0.012	5.75	8.6
57	5.4	15.5	83.6	0.013	11.84	100.6
74	3.9	8.5	33.5	0.010	6.15	126.5
Σ		74	402.8		35.0	432.5

Probe 2

Time [min]	m _{total} [g]	V _{EDTA} [ml]	m _{Ca} [mg]	m _{tracers} [g]	% tracers
2	16.1	0.60	48	0.4	2.6
8	19.0	0.90	72	1.1	5.9
16	21.8	1.10	88	1.5	6.9
24	25.6	1.20	96	1.5	5.8
33	25.3	1.10	88	1.2	4.7
38	23.0	1.05	84	1.2	5.4
44	22.3	0.90	72	0.8	3.6
50	25.9	1.15	92	1.3	5.0
56	26.5	1.15	92	1.2	4.6
62	25.1	1.15	92	1.4	5.4
68	25.0	1.00	80	0.9	3.5
72	23.5	1.20	96	1.7	7.1
78	27.5	1.30	104	1.6	5.9
82	27.7	1.30	104	1.6	5.8
91	29.6	1.30	104	1.4	4.8

These data were then used to calculate the time mean and the variance as follow:

t	C(t)	Δt	C * Δt	E(t)	E(t) * t * Δt	(t-45.8) ² *E*Δt
2	2.6	5.0	13.2	0.006	0.06	53.3
8	5.9	7.0	41.4	0.012	0.70	124.6
16	6.9	8.0	55.4	0.015	1.87	103.5
24	5.8	8.5	48.9	0.012	2.47	48.9
33	4.7	7.0	32.6	0.010	2.27	11.2
38	5.4	5.5	29.5	0.011	2.36	3.8
44	3.6	6.0	21.9	0.008	2.03	0.1
50	5.0	6.0	29.7	0.010	3.13	1.1
56	4.6	6.0	27.8	0.010	3.28	6.1
62	5.4	6.0	32.5	0.011	4.24	18.0
68	3.5	5.0	17.6	0.007	2.53	18.3
72	7.1	5.0	35.6	0.015	5.40	51.5
78	5.9	5.0	29.4	0.012	4.84	64.4
82	5.8	6.5	37.5	0.012	6.49	103.7
91	4.8	4.5	21.6	0.010	4.14	93.0
Σ		91	474.6		45.8	701.6

Using the time means and the variances from probe 1 and probe 2 data, the Peclet number and the mixing coefficient were calculated.

$$\bar{t} = \bar{t}_2 - \bar{t}_1 = 10.8 \text{ min}$$

$$\delta^2 = \delta^2_2 - \delta^2_1 = 269.1 \text{ min}^2$$

$$\bar{\delta}^2 = \frac{269.1}{10.8^2} = 2.31$$

$$\frac{1}{Pe} = \frac{1}{8} * (\sqrt{8 * 2.31 + 1} - 1) = 0.426 \rightarrow Pe = \frac{1}{0.426} = 2.34$$

$$D_{ax} = \frac{U_s H}{Pe} = \frac{1.85 \text{ cm/min} * 92.0 \text{ cm}}{2.34} = 72.6 \text{ cm}^2/\text{min}$$

Appendix C-11: Data for the louver trial at $U_1 = 3.86U_{mf}$

Probe 1

Time [min]	m_{total} [g]	V_{EDTA} [ml]	m_{Ca} [mg]	$m_{tracers}$ [g]	% tracers
1	25.9	5.10	136.0	0.0	0.0
9	24.3	5.80	154.7	1.1	4.4
12	22.3	5.70	152.0	1.4	6.5
14	28.2	6.35	169.3	0.8	2.7
18	22.7	5.05	134.7	0.5	2.4
22	23.3	5.50	146.7	0.9	4.1
26	21.5	4.60	122.7	0.3	1.4
33	24.2	5.50	146.7	0.7	3.0
41	21.8	4.80	128.0	0.5	2.1
54	24.9	5.30	141.3	0.3	1.2
86	27.9	5.80	154.7	0.2	0.6
105	27.8	5.05	134.7	0.0	0.0
113	27.4	5.80	154.7	0.3	1.1

Calculation was done similarly as in the baffle-free trial (Appendix C-1), except the neutral resin was holding 5.412 mg calcium per gram resin, thus:

$$m_{tracer} = \frac{m_{Ca} - 5.412 * m_{total}}{27.24 - 5.412}$$

Time and %tracer – C are used to calculate time mean, variance.

t	C(t)	Δt	$C * \Delta t$	E(t)	$E(t) * t * \Delta t$	$(t-29.2)^2 * E * \Delta t$
1	0.0	5.0	0.0	0.000	0.00	0.0
9	4.4	5.5	24.2	0.028	1.39	62.9
12	6.5	2.5	16.2	0.041	1.24	30.5
14	2.7	3.0	8.2	0.017	0.73	12.1
18	2.4	4.0	9.6	0.015	1.10	7.7
22	4.1	4.0	16.3	0.026	2.29	5.4
26	1.4	5.5	7.4	0.009	1.24	0.5
33	3.0	7.5	22.4	0.019	4.73	2.1
41	2.1	10.5	22.3	0.014	5.83	19.9
54	1.2	22.5	27.4	0.008	9.46	108.0
74	0.6	4.0	2.4	0.004	1.15	31.2
Σ		74	156.4		29.2	280.2

Probe 2

Time [min]	m _{total} [g]	V _{EDTA} [ml]	m _{Ca} [mg]	m _{tracers} [g]	% tracers
2	21.7	4.05	108.0	0.0	0.0
10	28.1	5.40	144.0	0.0	0.0
17	23.5	5.75	153.3	1.2	5.1
23	22.2	5.30	141.3	1.0	4.4
30	19.8	4.50	120.0	0.6	3.0
42	19.8	4.60	122.7	0.7	3.6
51	24.0	5.45	145.3	0.7	3.0
55	22.8	5.15	137.3	0.6	2.8
59	23.4	5.30	141.3	0.7	2.9
63	22.5	5.15	137.3	0.7	3.2
68	17.3	4.10	109.3	0.7	4.2
74	21.8	5.10	136.0	0.8	3.8
90	22.9	5.20	138.7	0.7	3.0
96	20.7	4.85	129.3	0.8	3.9
114	21.2	5.00	133.3	0.9	4.0

These data were then used to calculate the time mean and the variance as follow:

t	C(t)	Δt	C * Δt	E(t)	E(t) * t * Δt	(t-50.4) ² *E* Δt
2	0.0	6.0	0.0	0.000	0.00	0.0
10	0.0	7.5	0.0	0.000	0.00	0.0
17	5.1	6.5	33.4	0.019	2.05	134.6
23	4.4	6.5	28.6	0.016	2.38	77.7
30	3.0	9.5	28.4	0.011	3.08	42.8
42	3.6	10.5	37.9	0.013	5.76	9.7
51	3.0	6.5	19.3	0.011	3.56	0.0
55	2.8	4.0	11.3	0.010	2.24	0.9
59	2.9	4.0	11.6	0.010	2.47	3.1
63	3.2	4.5	14.4	0.012	3.27	8.2
68	4.2	5.5	23.0	0.015	5.66	25.8
74	3.8	11.0	41.9	0.014	11.22	84.5
90	3.0	9.0	26.7	0.011	8.69	151.5
Σ		91	276.5		50.4	538.7

Using the time means and the variances from probe 1 and probe 2 data, the Peclet number and the mixing coefficient were calculated.

$$\bar{t} = \bar{t}_2 - \bar{t}_1 = 21.2 \text{ min}$$

$$\delta^2 = \delta^2_2 - \delta^2_1 = 258.5 \text{ min}^2$$

$$\bar{\delta}^2 = \frac{258.5}{21.2^2} = 0.574$$

$$\frac{1}{Pe} = \frac{1}{8} * (\sqrt{8 * 0.574 + 1} - 1) = 0.171 \rightarrow Pe = \frac{1}{0.171} = 5.86$$

$$D_{ax} = \frac{U_s H}{Pe} = \frac{1.85 \text{ cm/min} * 92.0 \text{ cm}}{5.86} = 29.0 \text{ cm}^2/\text{min}$$

Appendix C-12: Data for the mesh trial at $U_1 = 3.86U_{mf}$

Probe 1

Time [min]	m_{total} [g]	V_{EDTA} [ml]	m_{Ca} [mg]	$m_{tracers}$ [g]	% tracers
1	27.3	5.10	136.0	0.0	0.0
5	21.3	5.55	148.0	1.8	8.7
9	21.9	5.70	152.0	1.9	8.6
12	23.4	5.50	146.7	1.3	5.5
14	21.6	5.30	141.3	1.5	6.8
18	30.5	6.35	169.3	0.7	2.2
22	21.3	5.00	133.3	1.2	5.5
26	21.9	4.90	130.7	0.9	4.1
33	21.2	4.80	128.0	0.9	4.4
42	22.5	5.00	133.3	0.9	3.9
53	24.5	5.30	141.3	0.8	3.2
65	23.3	5.20	138.7	0.9	4.0
79	21.2	4.85	129.3	1.0	4.7
98	25.4	5.30	141.3	0.6	2.2
118	24.0	5.20	138.7	0.8	3.2

Calculation was done similarly as in the baffle-free trial (Appendix C-1), except the neutral resin was holding 5.089 mg calcium per gram resin, thus:

$$m_{tracer} = \frac{m_{Ca} - 5.089 * m_{total}}{25.443 - 5.089}$$

Time and %tracer – C are used to calculate time mean, variance.

t	C(t)	Δt	$C * \Delta t$	E(t)	$E(t) * t * \Delta t$	$(t-33.7)^2 * E * \Delta t$
1	0.0	3.0	0.0	0.000	0.00	0.0
5	8.7	4.0	34.7	0.027	0.53	88.3
9	8.6	3.5	30.2	0.027	0.84	57.0
12	5.5	2.5	13.8	0.017	0.51	20.0
14	6.8	3.0	20.4	0.021	0.88	24.4
18	2.2	4.0	8.6	0.007	0.48	6.6
22	5.5	4.0	21.9	0.017	1.48	9.3
26	4.1	5.5	22.5	0.013	1.80	4.2
33	4.4	8.0	35.4	0.014	3.60	0.1
42	3.9	10.0	39.1	0.012	5.05	8.2
53	3.2	11.5	36.5	0.010	5.95	41.6
65	4.0	13.0	52.3	0.012	10.47	157.4
74	4.7	2.0	9.4	0.015	2.15	47.1
Σ		74	324.8		33.7	464.2

Probe 2

Time [min]	m _{total} [g]	V _{EDTA} [ml]	m _{Ca} [mg]	m _{tracers} [g]	% tracers
2	24.9	4.70	125.3	0.0	0.0
8	25.0	5.30	141.3	0.7	2.6
13	21.2	5.20	138.7	1.4	6.8
19	21.4	5.10	136.0	1.3	5.9
25	22.9	5.15	137.3	1.0	4.2
34	20.5	4.75	126.7	1.0	5.1
46	22.2	4.80	128.0	0.7	3.2
50	21.2	4.85	129.3	1.0	4.7
54	22.7	5.00	133.3	0.8	3.7
58	21.4	4.75	126.7	0.8	3.9
62	20.6	4.80	128.0	1.1	5.2
66	23.1	5.20	138.7	1.0	4.3
70	20.5	4.70	125.3	1.0	4.8
77	23.3	5.30	141.3	1.1	4.6
87	21.5	4.95	132.0	1.1	4.9
99	21.0	4.70	125.3	0.9	4.1
119	21.7	4.80	128.0	0.8	3.8

These data were then used to calculate the time mean and the variance as follow:

t	C(t)	Δt	C * Δt	E(t)	E(t) * t * Δt	(t-47.7) ² *E*Δt
2	0.0	5.0	0.0	0.000	0.00	0.0
8	2.6	5.5	14.5	0.007	0.29	57.8
13	6.8	5.5	37.3	0.017	1.23	113.6
19	5.9	6.0	35.4	0.015	1.71	73.9
25	4.2	7.5	31.8	0.011	2.02	41.4
34	5.1	10.5	53.4	0.013	4.61	25.3
46	3.2	8.0	25.3	0.008	2.95	0.2
50	4.7	4.0	18.9	0.012	2.40	0.3
54	3.7	4.0	14.6	0.009	2.01	1.5
58	3.9	4.0	15.5	0.010	2.28	4.2
62	5.2	4.0	21.0	0.013	3.30	11.0
66	4.3	4.0	17.1	0.011	2.86	14.6
70	4.8	5.5	26.3	0.012	4.67	33.3
77	4.6	8.5	38.7	0.012	7.57	84.7
87	4.9	9.0	44.1	0.012	9.75	173.4
Σ		91	393.0		47.7	635.2

Using the time means and the variances from probe 1 and probe 2 data, the Peclet number and the mixing coefficient were calculated.

$$\bar{t} = \bar{t}_2 - \bar{t}_1 = 13.9 \text{ min}$$

$$\delta^2 = \delta^2_2 - \delta^2_1 = 171.0 \text{ min}^2$$

$$\bar{\delta}^2 = \frac{171.0}{13.9^2} = 0.884$$

$$\frac{1}{Pe} = \frac{1}{8} * (\sqrt{8 * 0.884 + 1} - 1) = 0.230 \rightarrow Pe = \frac{1}{0.230} = 4.35$$

$$D_{ax} = \frac{U_s H}{Pe} = \frac{1.85 \text{ cm/min} * 92.0 \text{ cm}}{4.35} = 39.2 \text{ cm}^2/\text{min}$$

Appendix C-13: Data for the vertical plane trial at $U_1 = 3.86U_{mf}$

Probe 1

Time [min]	m_{total} [g]	V_{EDTA} [ml]	m_{Ca} [mg]	$m_{tracers}$ [g]	% tracers
1	26.7	5.15	137.3	0.0	0.0
5	24.4	5.50	146.7	0.8	3.4
9	22.6	5.60	149.3	1.4	6.3
12	22.5	5.50	146.7	1.3	5.8
14	23.3	5.60	149.3	1.2	5.3
19	20.8	5.20	138.7	1.4	6.5
23	22.1	5.30	141.3	1.2	5.3
27	24.5	5.60	149.3	0.9	3.8
33	24.6	5.55	148.0	0.9	3.5
41	22.6	5.30	141.3	1.0	4.6
51	22.8	5.40	144.0	1.1	4.9
63	22.9	5.35	142.7	1.0	4.5
79	21.9	5.20	138.7	1.1	5.0
95	23.9	5.50	146.7	1.0	4.0

Calculation was done similarly as in the baffle-free trial (Appendix C-1), except the neutral resin was holding 5.279 mg calcium per gram resin, thus:

$$m_{tracer} = \frac{m_{Ca} - 5.279 * m_{total}}{25.443 - 5.279}$$

Time and %tracer – C are used to calculate time mean, variance.

t	C(t)	Δt	$C * \Delta t$	E(t)	$E(t) * t * \Delta t$	$(t-37.4)^2 * E * \Delta t$
1	0.0	3.0	0.0	0.000	0.00	0.0
5	3.4	4.0	13.8	0.010	0.21	43.2
9	6.3	3.5	21.9	0.019	0.59	52.7
12	5.8	2.5	14.6	0.017	0.52	28.1
14	5.3	3.5	18.6	0.016	0.78	30.4
19	6.5	4.5	29.4	0.019	1.67	29.7
23	5.3	2.0	10.5	0.016	0.72	6.5
23	5.3	2.0	10.5	0.016	0.72	6.5
27	3.8	5.0	19.2	0.011	1.55	6.2
33	3.5	7.0	24.3	0.010	2.39	1.4
41	4.6	9.0	41.3	0.014	5.05	1.6
51	4.9	11.0	53.7	0.015	8.17	29.6
63	4.5	14.0	62.7	0.013	11.78	122.4
74	5.0	3.0	14.9	0.015	3.28	59.4
Σ		74	335.4		37.4	417.6

Probe 2

Time [min]	m _{total} [g]	V _{EDTA} [ml]	m _{Ca} [mg]	m _{tracers} [g]	% tracers
2	23.3	4.60	122.7	0.0	0.0
8	22.6	5.10	136.0	0.8	3.5
22	22.9	5.30	141.3	1.0	4.2
30	21.2	4.90	130.7	0.9	4.2
38	20.0	4.75	126.7	1.0	5.0
46	20.5	4.80	128.0	0.9	4.5
50	21.4	4.95	132.0	0.9	4.2
54	22.9	5.25	140.0	0.9	3.9
58	21.5	4.90	130.7	0.8	3.8
62	23.2	5.30	141.3	0.9	3.8
64	22.5	5.25	140.0	1.0	4.4
66	23.0	5.75	153.3	1.5	6.5
69	20.9	4.95	132.0	1.0	4.9
72	21.4	5.00	133.3	1.0	4.5
82	21.7	5.00	133.3	0.9	4.1
88	21.1	4.95	132.0	1.0	4.6
102	22.2	5.05	134.7	0.8	3.7

These data were then used to calculate the time mean and the variance as follow:

t	C(t)	Δt	C * Δt	E(t)	E(t) * t * Δt	(t-49.2) ² *E*Δt
2	0.0	5.0	0.0	0.000	0.00	0.0
8	3.5	10.0	34.8	0.009	0.75	159.9
22	4.2	11.0	46.2	0.011	2.75	92.7
30	4.2	8.0	33.3	0.011	2.71	33.3
38	5.0	8.0	39.7	0.013	4.08	13.5
46	4.5	6.0	27.3	0.012	3.39	0.8
50	4.2	4.0	16.7	0.011	2.27	0.0
54	3.9	4.0	15.7	0.011	2.30	1.0
58	3.8	4.0	15.0	0.010	2.36	3.1
62	3.8	3.0	11.5	0.010	1.93	5.1
64	4.4	2.0	8.9	0.012	1.54	5.3
66	6.5	2.5	16.3	0.018	2.92	12.5
69	4.9	3.0	14.6	0.013	2.73	15.5
72	4.5	6.5	29.1	0.012	5.67	40.9
82	4.1	8.0	32.6	0.011	7.23	94.8
88	4.6	6.0	27.6	0.012	6.57	112.4
Σ		91	369.4		49.2	590.7

Using the time means and the variances from probe 1 and probe 2 data, the Peclet number and the mixing coefficient were calculated.

$$\bar{t} = \bar{t}_2 - \bar{t}_1 = 11.8 \text{ min}$$

$$\delta^2 = \delta^2_2 - \delta^2_1 = 173.1 \text{ min}^2$$

$$\bar{\delta}^2 = \frac{173.1}{11.8^2} = 1.24$$

$$\frac{1}{Pe} = \frac{1}{8} * (\sqrt{8 * 1.24 + 1} - 1) = 0.288 \rightarrow Pe = \frac{1}{0.288} = 3.47$$

$$D_{ax} = \frac{U_s H}{Pe} = \frac{1.85 \text{ cm/min} * 92.0 \text{ cm}}{3.47} = 49.1 \text{ cm}^2/\text{min}$$

Curriculum Vitae

Name: Ha Doan

Post-secondary Education and Degrees: University of Western Ontario
London, Ontario, Canada
2008-2012 B.Sci.
Graduate with Distinction

Honours and Awards: Tom Ng Engineering Award
2011

Second place in Green Fuel competition
2011

Related Work Experience

Intern
Renix Inc
2012-2014

Teaching Assistant
The University of Western Ontario
2013-2014

CBE Graduate Seminar Committee
2013-2014

CBE departmental Union Steward
2013-2014